THESIS

FINDING WATER MANAGEMENT PRACTICES TO REDUCE SELENIUM AND NITRATE CONCENTRATIONS IN THE IRRIGATED STREAM-AQUIFER SYSTEM ALONG THE LOWER REACH OF COLORADO'S ARKANSAS RIVER VALLEY

Submitted by

Ibraheem A. Qurban

Department of Civil and Environmental Engineering

In partial fulfillment of the requirements

For the Degree of Master of Science

Colorado State University

Fort Collins, Colorado

Summer 2018

Master's Committee:

Advisor: Ryan T. Bailey
Co Advisor: Timothy K. Gates

Jordan F. Suter

ABSTRACT

FINDING WATER MANAGEMENT PRACTICES TO REDUCE SELENIUM AND NITRATE CONCENTRATIONS IN THE IRRIGATED STREAM-AQUIFER SYSTEM ALONG THE LOWER REACH OF COLORADO'S ARKANSAS RIVER VALLEY

Agricultural productivity in the Lower Arkansas River Valley (LARV) in southeastern Colorado has been high over the last 100 years due to extensive irrigation practices. In the face of this high productivity, however, the LARV currently face many issues as a result of the long period of irrigation, including waterlogging and soil salinization, leading to a decline in crops yields and high concentrations of nutrients and trace elements. In particular, irrigation practices have led to high concentrations of selenium (Se) and nitrate (NO_3) in groundwater, surface water, and soils, similar to other semi-arid irrigated watersheds worldwide. Environmental concerns due to these high concentrations include human health, health of fish and waterfowl, and eutrophication of surface water bodies.

The objective of this thesis is to identify water management strategies that can lead to a decrease in the concentrations of Se and NO_3 in groundwater and surface water in the LARV by evaluating the three-water management BMPs which is reduced irrigation (RI), lease fallowing of irrigated land (LF), and canal sealing (CS). This is accomplished by constructing and testing a computational model that simulates the fate and transport of Se and NO_3 in a coupled irrigated stream-aquifer system, and then applying the model to evaluate selected best management practices (BMPs) to decrease the concentration of Se and NO_3 to comply with Colorado water quality regulations. The modeling system consists of MODFLOW, which simulates groundwater

and stream flow, and RT3D-OTIS, which simulates the reactive transport of the principal Se and nitrogen (N) species in groundwater and a connected stream network. RT3D-OTIS uses simulated flows from MODFLOW to exchange Se and N species' mass between streams and the aquifer on a daily time step.

The coupled flow and reactive transport model is applied to an approximately 552 km² study region in the LARV between Lamar, Colorado and the Colorado-Kansas border. The model is tested against Se and NO_3 concentrations measured in a network of groundwater monitoring wells and stream sampling site, and against return flows and mass loads to the river estimated from the mass balance. Model calibration was performed manually and by using PEST software tool, and the effects BMPs on Se and NO_3 concentrations in groundwater, streams, and groundwater mass loadings to the Arkansas River within the stream-aquifer system are quantified. Three BMPs are considered RI, LF, and CS, which are simulated for a 40-year period and then compared to a baseline ("do nothing") scenario.

The results indicate that implementation of the CS scenario might lead to lower groundwater concentrations of Se and NO_3 by 40% and 38%, respectively, a reduction in groundwater mass loading to the Arkansas River by 100% and 60% for Se and NO_3, and a reduction in stream concentrations of Se and NO_3 by 30% and 40%, respectively. In contrast, the RI and LF scenario, while lowering the water table and in consequence the rate of groundwater return flow to the Arkansas River, leads to elevated groundwater concentrations of both Se and NO_3 in the riparian areas, resulting in an overall increase in groundwater mass loading to the river. This may be due to changes in the rate of groundwater flow due to lower hydraulic gradients leading to longer residence times of NO_3 in the aquifer, increasing the potential for the release of Se from the bedrock shale through oxidation processes. Also, lowering the water table

due to reduced recharge from irrigation reduces the size of the saturated zone, perhaps contributing to a higher concentration of Se and NO_3. Moreover, changes in water and mass flux between the saturated and unsaturated zone occur under RI and LF scenarios. As a consequence of these altered processes, the RI and LF scenarios do not decrease the in-stream concentrations of Se and NO_3 in the Arkansas River, with values for Se and NO_3 increasing by 15% and 8%, respectively under the RI scenario, and by 10% and 10.5% for the LF scenario. Further, the results are compared with results obtained from a modeling study in the Upstream Study Region of the Lower Arkansas River Valley, to determine the similarity and differences of BMP implementation in the two regions. Further assessment of localized BMPs should be performed to determine key regions where they should be implemented for the largest impact on Se and NO_3. Combined water management BMPs and land management BMPs, like reduced fertilizer application and enhanced riparian buffers, should also be evaluated.

ACKNOWLEDGMENTS

I would like to express my appreciation to all the people who helped me to complete this research. My sincere gratitude goes to Dr. Ryan T. Bailey; for his constant guidance, encouragement, support, without which this work would have not been completed, and for giving me the opportunity to work with him especially on the Lower Arkansas River Valley. Also, I would like to thank my committee, Co Advisor Prof. Timothy K. Gates and Prof. Jordan F. Suter, for their assistance and advice.

A special and generous thanks to my father, my mother, and all my family members for their continuous support. I am fully indebted to my beloved wife Ghofran Hamoh and my lovely son Abdulaziz for their patience, help, and encouragement.

Finally, it is a pleasure to acknowledge my thanks to the Saudi government and King Abdulaziz University for their financial support and cooperation for affording me the privilege of pursuing a Master of Science degree in the Civil and Environmental Engineering Department at Colorado State University.

TABLE OF CONTENTS

LIST OF TABLES

LIST OF TABLES

CHAPTER 1: INTRODUCTION

1.1 Overview

Today, around 250 million hectares are irrigated worldwide, an area that is approximately five times more than during the start of the 20th century (Rosegrant, Cai, & Cline, 2002) . Moreover, around 70% of water use for irrigation and agriculture globally (UNESCO-WWAP, 2003). Therefore, irrigation is one of the important sources for a sustainable food chain, especially with the potential for the spread of irrigated land in the future. Furthermore, the world population is still increasing and is expected to reach 9.7 billion people by 2050 (Rosegrant et al., 2002).

Long-term irrigation practices in semi-arid regions, however, typically lead to waterlogging and soil salinization, soil acidification, and a reduction of water quality, all which lead to a reduction in crop yield (Gates et al., 2006)(Colaizzi et al., 2009)(Musick et al., 1990) (Gates et al., 2008)(Dougherty, Hall, & Food and Agriculture Organization of the United Nations., 1995)(De Pascale & Barbieri, 1995). In addition, fertilizer, pesticides, and nutrients (e.g. nitrogen) are applied to the cropland to achieve high yields, each of which can lead to polluted groundwater sources which then can be transported to surface water (lakes, streams). Trace elements [e.g. selenium, molybdenum, and boron] are considered another source of water contamination. (Hoffman, Evans, Jensen, Martin, & Elliott, n.d.). High concentration of the trace elements are usually found in irrigation regions, which are related to different factors, such as arid and semi-arid climate, open basins versus closed topography, and geological source of the trace element (Presser et al., 1994).

For example, due to natural processes, selenium (Se) is present in the earth's crust, complex geological areas, and sedimentary rock, particularly Cretaceous marine shale. Since Se is found mainly in the geological area, it occurs by oxidative weathering of pyrite in bedrock and outcrop shale areas, leading to the release of dissolved Se in the groundwater (Large et al., 2014) through the oxidation of dissolved oxygen (DO) and Nitrate (NO_3). In the western United States, the concentration of Se has spread widely in recent years, leading to water contamination and thus water quality issues. The most famous investigation about the Se effect was at the early 1980s in the Kesterson National Wildlife Refuge in the San Joaquin Valley, California. Shorebirds were found dead and were being born with deformities due to the impact of a high concentration of toxic Se in the water (Hamilton, 2004). Many regions of the western United States are underlain by Cretaceous marine sedimentary rocks that contain Se (Presser et al., 1994; Seiler, 1995; Seiler et al., 1999), which is released to groundwater if the areas are irrigated. One of these regions is the Lower Arkansas Reviver Valley (LARV) in southern Colorado, which is the focus of this thesis. The next section describes this area in detail.

1.2 Study Area

The (LARV) is located in southern Colorado between the city of Pueblo in Colorado and the border between Colorado and Kansas. The climate of the study area is semi-arid, and the average annual precipitation is around 300 mm. The geology of the region consists of an alluvial aquifer underlain by a series of sedimentary formations of the late Cambrian to tertiary age (Darton, 1906). Soil types include clay loam, silty clay loam, loam, and sandy loam textural classes (Gates et al., 2008). The region has been studied by Colorado State University (CSU) over the last decade and has been divided into two study regions: the Upstream Study Region (USR) and the Downstream Study Region (DSR), the USR represent the upstream of John

Martin Reservoir and the DSR represent the downstream of John Martin Reservoir, as shown in Figure 1.A. Since agriculture practices have been heavily in last century, there has been around 109,00 ha of land that is irrigated from both groundwater and surface water. These lands need more than the amount of rainfall, so water has to come from local pumps to get the maximum crops yield production (Morway et al., 2013). The area has experienced irrigation on around 14,000 fields, and water supply is provided by 25 canals that transfer water from the river, in accordance with Colorado water law and from around 2,400 wells that pump from alluvial groundwater (Gates et al., 2008). Surface-irrigation methods are the most dominant method of the majority irrigated fields, and less than 5 % are irrigated with sprinklers (typically, center-pivot sprinklers) or drip line (Gates et al., 2008). The major crops that have been produced in the area are Alfalfa, corn, grass, wheat, and sorghum. The irrigation season states from mid-to-late-March and ends in the beginning of November. The water used for irrigation is either received from groundwater pumps or one of the eight main irrigated canals, which include the Amity, Buffalo, Fort Bent, Fort Lyon, Hyde Ditch, Lamar, South Side, and XY Graham. Thus, the extensive irrigation over the last century pose a number of issues and challenges related to a high-water table, salt concentration, salinization, waterlogging, and a decline in crop yields (Gates et al., 2008).

Water quality is one of the main concerns that challenge the area. Due to the extensive irrigation, the water has become salty and unusable. The river and its tributaries gain its water from the return flows that comes from evapotranspiration, canal seepage, and the high irrigation practices (Shultz et al., 2018). These return flows have a high concentration of nitrate (NO_3) and oxygen (O_2) that have been used for applied fertilizer and are in contact with weathering Cretaceous marine rocks, which are dissolved, generated, and returned with Se and sulfate salts

into the river (Bern & Stogner, 2017). A high concentration of NO_3 led to drinking water contaminations which were related to health problems, especially for infants because of the methemoglobinemia (Fan & Steinberg, 1996). Moreover, trace elements such as Se, U, and the salt ion, which is dissolved in irrigation water, led to health problems for livestock, fish and waterfowl, and humans. Thus, the observation data that have been collected in the LARV represented a high concentration level of Se that reach to 15 µg/L in stream and 30 µg/L in the tributary, with it exceeding the Colorado State chronic standards of 4.6 µg/L (Gates et al., 2009). Also, (Miller et al., 2010) shows similar result that high concentration of Se in the LARV. On the other hand, the NO_3, as nitrogen (NO_3-N) observed data that have been collected in the LARV, shows that the concentrations are temporarily under the state standard of 2.0 mg/L for total nitrogen (N) (Gates et al., 2009).

This thesis focuses on the DSR. The location of the DSR is shown in the Figure 1 (Tummalapenta, 2015), bounded by the city of Lamar on the west and the border of Colorado and Kansas on the east. There are four major towns in the area: Lamar, Granada, Holly, and Hartman, all located in Prowers County. In addition, Table (1) gives the 2017-2018 population of each city (List of Counties and cities in Colorado, 2018). The area of the DSR is around 55,200 ha (552 km^2) of which 60% is irrigated from diverted river water or groundwater wells. The Arkansas River has four main tributaries in the DSR: Clay Creek, Big Sandy Creek, Buffalo Creek, and Wild Horse Creek. These tributaries mainly gain water from groundwater return flow, which results from irrigation of croplands. From April 2003 to July 2008, water was sampled for salt ions, Se, and NO_3 from a network of 47 groundwater monitoring wells, 12 locations in tributaries, and 6 locations in the Arkansas River. (Gates et al., 2009). Sample was performed periodically from an additional 59 monitoring wells (Gates et al., 2009). The location of the

observation wells is shown in Figure 1.B. Figures 2 and 3 show the average Se (µg/L) and NO_3 (mg/L) concentration at the location of each observation well for the 2003-2008 sampling period. In addition, the total number of samples for Se and NO_3 are 1852 and 1282 samples, respectively. Also, the average concentrations are 61.31 µg/L for Se and 9.75 mg/L. where, the maximum and minimum concentrations for Se and NO_3 are 3760 µg/L and 0 µg/L, and respectively, and 685 mg/L and 0 mg/L, respectively. Furthermore, the maximum values of Se and NO_3 are way different than the standard deviation which is 315 for Se and 60.17 for NO_3.

Table 1: City Population in 2017-2018, (List of Counties and cities in Colorado, 2018)

City	Population
Lamar	7804
Granada,	517
Holly	802
Hartman	75

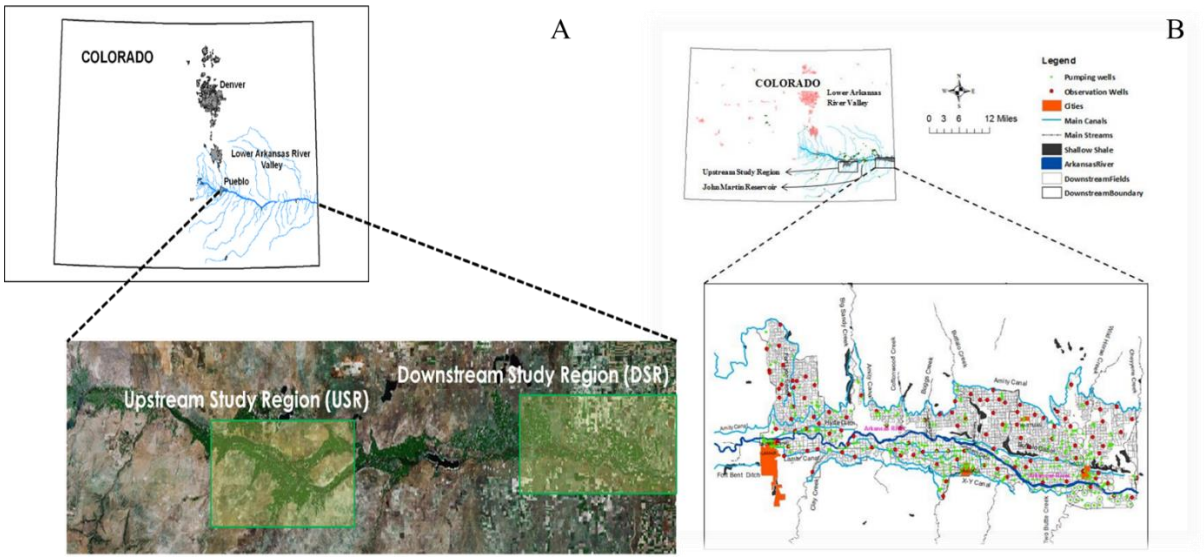

Figure 1 (1.A) Location of the USR and DSR and (1.B) Downstream Study Region, located in the Lower Arkansas River Valley, southern Colorado, USA.

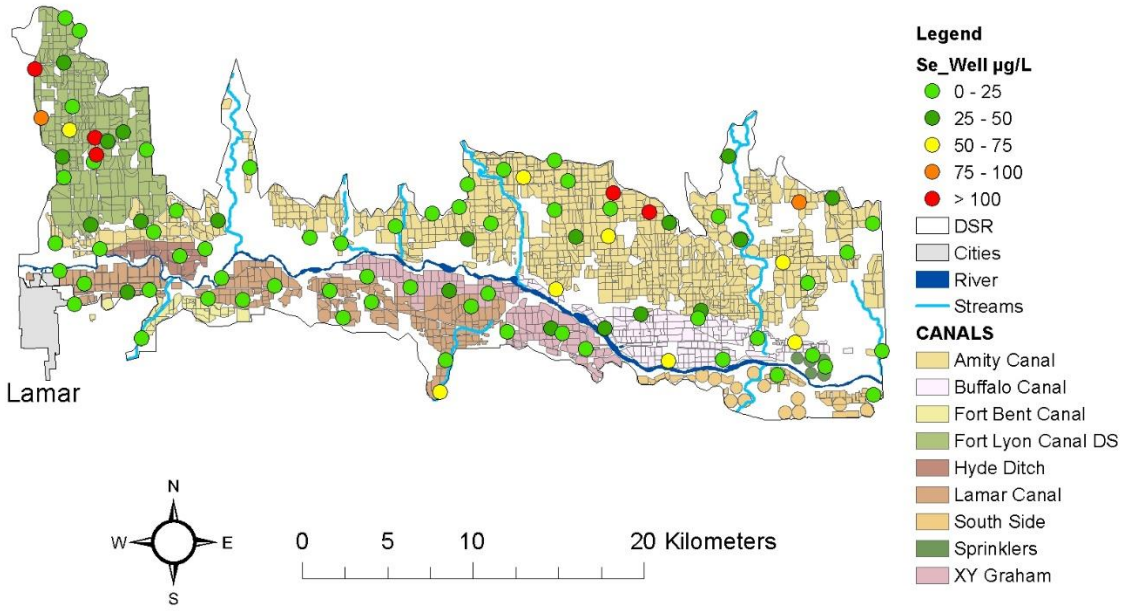

Figure 2: Average Se concentration (µg/L) in each observation well during the 2003-2008 time period.

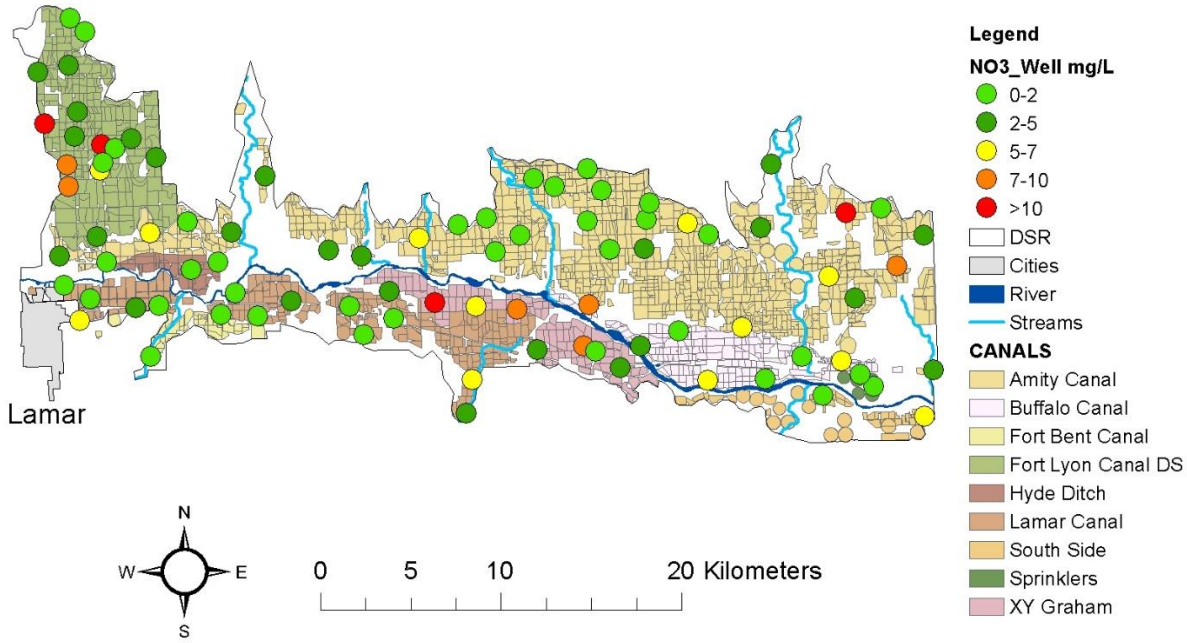

Figure 3 Average NO_3 concentration (mg/L) in each observation well during the 2003-2008 time period.

1.3 Objectives

There are several factors that make the area an ideal place for Se mitigation analysis: (i) the river is considered a seleniferous river basin (Seiler, 1995), (ii) the concentrations of Se and NO_3 exceed the CDPHE standard, (iii) the area has been studied and monitored by CSU during the last decade, yielding a vast collection of water sample data, and (iv) a groundwater model and simulated reactive transport model were construct and developed at the LARV for the upstream and the downstream study regions.

The overall objective of this research is to identify land and water management strategies that can assist in decreasing the contamination of Se and NO_3 in the stream-aquifer system of the DSR in the LARV. This goal will be achieved by the following tasks:

1. Evaluate water quality and contamination related to Se and NO_3 in the DSR, from previously collected water samples from observation wells and the Arkansas river network;
2. Construct a computational model that simulates the fate and transport of Se and NO_3 in a coupled irrigated stream-aquifer system;
3. Calibrate and test the stream-aquifer flow model (MODFLOW) and the reactive transport model (RT3D-OTIS) against the observed Se and NO_3 that have been measured in groundwater monitoring wells and streams; and
4. Apply the model to evaluate the best management practices (BMPs) for decreasing the groundwater and in-stream concentration of Se and NO_3 and the groundwater mass loadings to the Arkansas River. These BMPs include reducing applied irrigation volumes, land fallowing, and partially sealing earthen irrigation canals.

1.4 Thesis Organization

This thesis includes 5 chapters. Chapter 1 is an introduction that contains 3 main parts: (1) problem statement, (2) description of the study area, and (3) list of objectives of the thesis. Chapter 2 presents a literature review of previous studies of Se and NO_3 in stream-aquifer systems. Chapter 3 outlines the methodology that has been done this thesis, including model construction and model calibration and testing. Chapter 4 is describing the implementation of the BMPs. Chapter 5 provides a conclusion and a discussion of future work.

CHAPTER 2: LITERATURE REVIEW

2.1 Selenium Overview

Selenium (Se) is a micro-nutrient for humans and animals. However, at high concentrations Se can have a toxic effect (Kumar & Riyazuddin, 2011). The range of Se that separates it between a dietary deficiency and a toxic level for humans is 40 μg / day and 400 μg / day, respectively (Levander & Burk, 2006). The elevated level of Se has occur in several locations, such as the United States, Middle East, Asia, and western Europe (Gates et al., 2009; Hudak, 2010; Seiler, 1995; Seiler et al., 1999) (Afzal et al., 2000) (Mizutani & Kanaya, 2001; Zhang et al., 2008) (Alfthan et al., 1995; Bye & Lund, 1982). The toxic levels can lead several diseases. For animals, the high concentration of Se can cause chronic poisoning, termed as alkali disease (Levander and Burk, 1994). Research in Keshan, China, showed that the low level of Se in soil leads to Keshan disease, which is defined as endemic cardiomyopathy with the myocardial inability (Chen, 2012). Moreover, Se concentration affects the human body in many ways, such as muscle pain, cancer, diabetes, cirrhosis, etc. (Navarro-Alarcón & López-Martínez, 2000). In northwestern India, the high level of Se was noticed in water samples and in the groundwater. This created a poisoning issue for human, animal, and plants (Dhillon & Dhillon, 2003). Furthermore, the seleniferous regions in Venezuela has reported a liver disease especially for children (Brätter et al., 1997).

In The United States, several locations have been discovered to have toxic levels of Se, mainly in the western United States due to the geologic source and climate, which is arid and semi-arid (Feltz et al., 1990). North Dakota, Idaho, California, Wyoming, Colorado, and some other areas were reported to have elevated Se levels during the last decades. Initial investigation

into the Se toxicity in the United States was done in 1856 at Fort Randall, South Dakota (Boon, 1989). The most highly publicized Se toxicity study was done in the early 1980s in the Kesterson National Wildlife Refuge in the San Joaquin Valley, California, where shorebirds were found either dead or born with deformities due toxic Se concentrations (Ohlendorf, 2002) (Seiler, 1995) (Hamilton, 2004). Furthermore, in the Colorado River, the population of various types kinds of fishes were in decline due to the Se pollution (Hamilton & Weston, 2005). Finally, an investigation that had been done by (Seiler et al., 1999) showed the location of Se contamination in the western U.S, as shown in Figure 4. Areas with a high evaporative index, and thus irrigation, in which the landscape is underlain by Cretacious marine sedimentary rock, often leads to Se contamination. Notice that the LARV in southeastern Colorado is one of the areas highlighted in Figure 4.

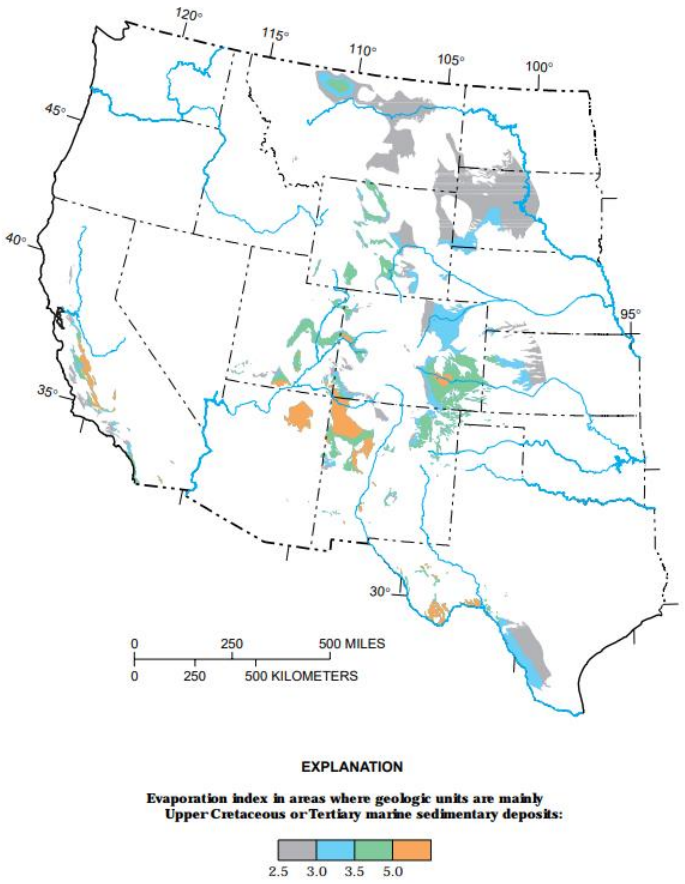

Figure 4 locations of Se contamination in the western United States (R. Seiler et al., 1999)**.**

Se contamination is mainly found in semi-arid climates, geological marine shales, areas with volcanic activities, weathering rocks and soils, groundwater leaching, chemical or bacterial reductions and oxidations, and plant uptake (Jacobs, McNeal, & Balistrieri, 1989; R. L. Seiler, 1995). In addition, Se occurs in groundwater and other water bodies in four different forms: selenate (SeO_4^{-2}), selenite (SeO_3^{-2}), elemental Se (Se^0), and Selenide (Se^{-2}). SeO_4^{-2} is a weak sorbent and a very soluble species of Se, and it is the most toxic species of Se (Severson et al. 1992). Also, its derivative from Se and it is easily taken up by plants (Jacobs et al., 1989). SeO_3^{-2} has strong affinity for adsorption and soluble mobile species of Se. Se^0 is naturally resistant and idle to oxidation and very insoluble in the water system (Jacobs et al., 1989). Se^{-2} is insoluble in the water system, appears as Organic-Selenomethionine (SeMet), and is a product of the

volatilization of SeMet. Moreover, Se is present in the earth's crust, cretaceous sediments complex geological area, and sedimentary rock (Seiler, 1995), which can be released due to oxidative weathering. Typically, this occurs through the chemical reduction of dissolved oxygen (DO) and Nitrate (NO_3) in the groundwater.

2.2 Nitrate Overview

The presence of nitrate (NO_3) in groundwater and surface water can lead to freshwater eutrophication and potability issues (Elrashidi et al., 2009). In addition, a high concentration of NO_3 in drinking water can lead to health problems, namely methemoglobinemia, in infants (Johnson et al., 1987). Also, as NO_3 is an essential food for algae , its presence in surface water can lead to a lowering in oxygen level that leads to fish dying and interfering with recreational uses (Lorenzen, 1979; Mueller et al., 1995). Over-application of fertilizer is typically the main source of NO_3 in agricultural groundwater systems.

To combat rising NO_3 levels, the USEPA has set a maximum contamination level of 10 mg/L (NO_3-N) for drinking water (Fan & Steinberg, 1996). In the United States, groundwater contamination by NO_3 has been noticed in the Central Great Plains, the Palouse and Columbia Basin in Washington, southwest Arizona, Kansas, and California. Furthermore, west Texas, southern Arizona, and Kansas have the highest NO_3 concentration (Nielsen & Lee, 1987). Figure 5 shows the contamination levels in agricultural groundwater areas in the late 1980s (Nielsen & Lee, 1987), with areas of high NO_3 typically associated with areas of intensive agricultural practices. Note that one area of high NO_3 is southeastern Colorado along the Arkansas River.

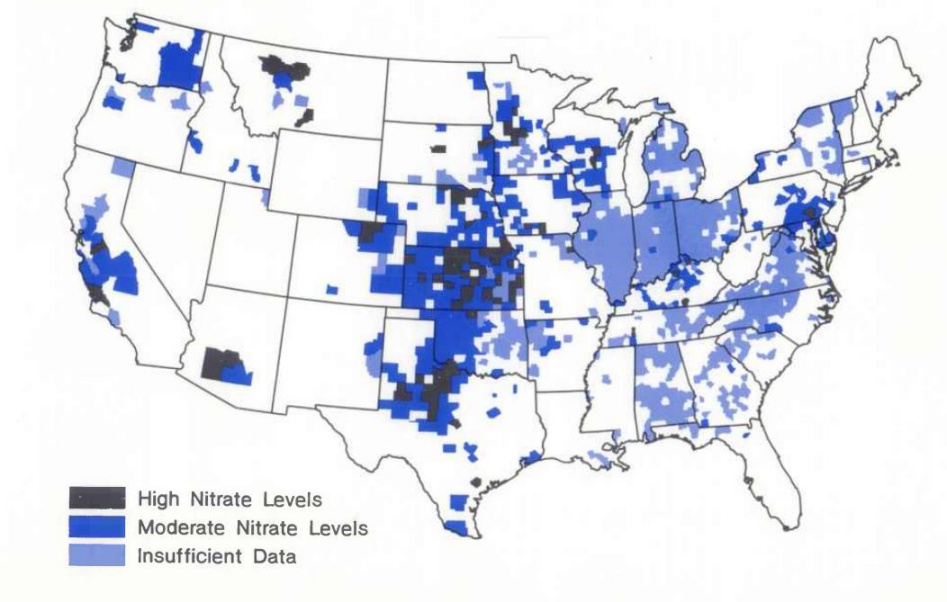

Figure 5 Nitrate-Nitrogen distribution in groundwater in the agriculture areas (Nielsen & Lee, 1987)

2.3 Influence of O_2 and NO_3 on Se in Groundwater Systems

Field and laboratory studies have demonstrated that the presence of O_2 and NO_3 in soil and groundwater effects Se species in two principal ways: 1) preventing SeO_4 chemical reduction to SeO_3, and undergoing autotrophic reduction in the presence of pyrite (FeS_2) and seleno-pyrite ($FeSe_2$) that oxidizes residual Se into mobile SeO_4 and SeO_3 ((Weres et al., 1990; (Oremland et al., 1990; Sposito et al., 1991)(Bailey et al., 2012; Fernández-Martínez & Charlet, 2009; Stillings & Amacher, 2010) . This occurs when O_2 infiltrates into groundwater and soil water, as well as the NO_3-laden water from the applied fertilization over the cultivated irrigation area (Bailey et al., 2013a) (Bailey et al., 2013b). Thus, studying the fate and transport of Se should include the fate and transport of NO_3 and O_2.

2.4 Modeling Se Transport in Stream-Aquifer Systems

Several studies have shown the analysis and result for numerical models of Se in soils and groundwater. (Alemi et al., 1988) constructed a one-dimension model with vertical movement that simulates the transport of SeO_4 in steady state condition for the saturated zone by

using DYNAMIX. Another study by (Alemi et al., 1991) simulated the 1D model for the unsaturated zone for the SeO_3 and SeO_4 species. In addition, (Tayfur et al., 2010) constructed and developed a two-dimension numerical model to solve for the Se by using the finite element method for the saturated and the unsaturated zones. The model considers adsorption, desorption, oxidation, reduction, volatilization, and chemical and biological transformation. (Myers, 2013) used a MODFLOW-2000 linked with MT3D, in order to simulate the flow and Se transport, respectively. However, the reactive transport of Se was not included. (Bailey et al., 2013b) constructed a 3D reactive transport model RT3D, which was linked with the unsaturated zone (UZF1) and MODFLOW, which is known as UZF-RT3D (Bailey et al., 2013b). In addition, the UZF-RT3D model was amended to include Se cycling due to agriculture practices in the soil-crop-water system, oxidation-reduction, and included the NO_3 cycle (Bailey et al., 2013a). As such, the model solves for different species of Se and NO_3, such as NH_4-N, NO_3-N, SeO_4-Se, and SeO_3-Se as a dissolved phase, along with the organic litter, humus, and manure.

2.5 Best Management Practices for Se Mitigation in Stream-Aquifer Systems

Several studies done in the past have found the best management practices for Se and NO_3. Some strategies have been used in San Joaquin Valley, CA to decrease the concentration of Se. These include controlling the fertilizer that is applied in the irrigation areas to decrease deep percolation, recycling the drainage water and applying it as irrigation water, and isolating the lands that have a shallow groundwater and contain high levels of Se concentration (Ohlendorf, 2011). Another study showed that when ten wetland cells were used and tested in California, it had a high impact in the reduction of Se from drainage water by an average of 69.2%, mainly by retaining Se in sediments and volatilization (Lin & Terry, 2003). On the other hand, studies have been done to show the best strategies for the reduction of NO_3 concentrations. Reducing the

amount of fertilizer that is applied in the irrigation region is the principal NO_3 remediation strategy (Kramer et al., 2006) (Yang & Wang, 2011). In addition, constructing and creating wetlands or bio-filters can also reduce the amount of NO_3 (Dinnes et al., 2002) in groundwater and drainage water. Reduction of the irrigation practices (Yang & Wang, 2011), and the acidification and nitrification in the forested areas will reduce the amount of NO_3, as the forest sunshade will circulate the atmosphere from any pollution (Calder, Reid, Nisbet, & Green, 2003) (Allen & Chapman, 2001).

In the LARV, the linked MODFLOW/RT3D-OTIS modeling system has been applied to the Upstream Study Region (see Figure 1) to determine strategies for mitigating Se and NO_3 concentrations in groundwater and surface water. Using the MODFLOW groundwater flow model developed by (Morway et al., 2013), Bailey et al. (2014) tested the UZF-RT3D model for Se and NO_3, and subsequently used the model to determine the effect of BMPs for NO_3 (Bailey et al., 2015a) and Se (Bailey et al., 2015b). Specific BMPs investigated include reduced irrigation, sealing earthen canals, rotational fallowing of cultivated land, reduced fertilizer, and enhancing riparian buffer zones. Investigating single and combined BMPs, model results indicated that NO_3 groundwater concentration can be lowered by 40% and the mass loading decreased by 70% to the Arkansas River Valley over a four-decade span (Bailey et al., 2015a). The most effective BMPs are reducing fertilizer loading and sealing irrigated canals. The most effective combined BMP are reduce fertilizer, reduce irrigation application, canal sealing, and enhanced riparian buffer zones (Bailey et al., 2015a). They also found that land fallowing implementation by 25% leads to decrease the NO_3 groundwater loading to streams by 15%. Another study indicates that Se mass loading from groundwater to the River can be decreased by 14% (Bailey et al,. 2015b)

More recently, Shultz et al. (2018) amended the USR model system to include streamflow routing and surface water transport, with model results tested against both groundwater and in-stream concentrations of Se and NO_3. An additional study applied the coupled groundwater/surface water model to investigate the influence of BMPs. Model results indicate that the groundwater concentrations can be lowered by 23% for Se and 40% for NO_3, and the steam concentrations lowered by 57% for Se and 33% for NO_3 (Shultz, 2017). Shultz, (2017) reports that the most effective water management BMP is canal sealing, and the most effective land management is enhancing the riparian buffer zone with organic material.

For the DSR, (Tummalapenta, 2015) applied the MODFLOW/UZF-RT3D model to investigate the effect of BMPs. The results show significant reduction in SeO_4 and NO_3 mass loading by 22.7% and 34.7%, respectively, especially under the combinations of BMPs. Also, under the single scenario the reduced irrigation has high decrease for SeO_4 and NO_3 in mass loading by 13.4% and 30%, respectively. This thesis extends the work of Tummalapenta (2015) by coupling the groundwater models with surface water flow and reactive transport, thereby allowing model results to indicate the influence of BMPs on in-stream concentrations of Se and NO_3.

CHAPTER 3: METHODOLOGY

This chapters describes the methods for assessing the effectiveness of BMPs (reduced irrigation, land fallowing, canal sealing) on Se and N concentrations and loadings within the stream-aquifer system of the DSR. The groundwater flow model (MODFLOW) and reactive transport model (RT3D-OTIS) described, along with calibration and testing procedures, followed by a description of the baseline and BMP simulations for the LARV, DSR.

3.1 Groundwater Flow Model for the Downstream Study Region

3.1.1 MODFLOW Model of Morway et al. (2013)

Morway et al. (2013) constructed and tested a MODFLOW model for the LARV, DSR. Although several numerical models have been provided to solve the groundwater equation, such as FEFLOW (Yamagata et al., 2012), SUTRA (Voss & Provost, 2010), and HydroGeoSphere (Brunner & Simmons, 2011), MODFLOW is used most frequently . MODFLOW solves the 3D groundwater flow equation using the finite difference method, with hydraulic head h solved for at the centroid of each finite difference cell at each time step of the groundwater flow simulation.

MODFLOW is used for solving the groundwater flow equation and head in each grid cell (i,j,k) in the 3D model domain. MODFLOW-NWT is a Newton formulation of MODFLOW-2005 and solves the nonlinear unconfined groundwater flow equation (Niswonger et al., 2011). Also, it is a version that aims for a linearization that creates an asymmetric matrix, instead of solving for the symmetric matrix that is used in the MODFLOW-2005 version (Niswonger et al., 2011). In addition, MODFLOW has many modular packages that allow for the simulation of various sources and sinks of groundwater. Some of these packages include the Well package, River package, Evaporation package, Streamflow-Routing (SFR2) Package, and the Unsaturated

Zone Flow (UZF) package. The SFR package routes water through a stream network and quantifies the interaction between stream water and groundwater based on the head in the river, the head in the aquifer, and the conductivity of the streambed layer. The UZF1 package simulates 1D flow in a homogeneous soil profile (Niswonger et al., 2006).

In the DSR the MODFLOW model was constructed, described, and applied by (Morway et al., 2013). MODFLOW-NWT was used, coupled with the Well package, UZF1 package, and River package for groundwater-surface water interactions, to solve the groundwater flow equation. In addition, in order to solve the 3D numerical method (MODFLOW) certain steps need to be done, these steps are 1. Discretize the domain into a finite number of calculation points (grid cells); 2. Identify the linear equation of each cell; and 3. Solve the system equation for each cell to obtain the hydraulic head and the volumetric flow rate between grid cells. As such, the domain of the study area was discretized into 22,134 cells that contained 9312 active cells and 12822 inactive cells (i.e. cells outside the domain). The grid cells were identified by 102 rows and 217 column, and the uniform areal dimension of each grid cell was 250 m x 250 m horizontally, which would be the average area of typical irrigation fields in the study region. The finite difference grid is shown in Figure 6.

Pumping data and river stage at various points along the Arkansas River and tributaries (Timpas Creek, Crooked Arroyo) were provided by Colorado Division of Water Resources data bases. Applied irrigation rates to each cultivated field during the growing season were based on weekly diversions into the irrigation canals, with water apportioned to fields based on a hierarchy of crop type. The observation database of groundwater and surface water was available for 5.5 years, from the period of 2002 to 2007. The alluvial aquifer was divided into two layers, with each layer having a depth of around 5 m, and the 3rd layer (bedrock shale) started right

below layer two. More than 7200 water table measurements from 118 monitoring wells were used to calibrate and test the model (Morway et al., 2013). The model was also tested against groundwater return flows to the Arkansas River, canal seepage rates, and ET rates. Table 2 represents stream aquifer properties, such as hydraulic conductivity, specific storage, and water content (Morway et al., 2013).

Table 2: Aquifer Properties of the DSR

Number	Model parameter	Range value
1	Layer 1 K_H	0.3-160 m/d
2	Layer 1 K_S/K_H	$7x10^{-5}$–$2.9x10^{-2}$
3	Layer 2 K_H	1.4-75 m/d
4	Layer 2 K_V/ K_H	0.1
5	Layer 1 Sy	0.01-0.33
6	Layer 2 Sy	0.01-0.34
7	Layer 1and 2 Ss	$1.7x10^{-5}$
8	Canal conductance	$1.7x10^{-3}$-8.6 m^2/d/m
9	Saturated K in UZF1	$1.1x10^{-2}$-0.26 m/d
10	ε (Brooks-Corey exponent)	3.5
11	θs (UZF1)	0.18-0.39
12	Extinction depth	1.3-4.5 m

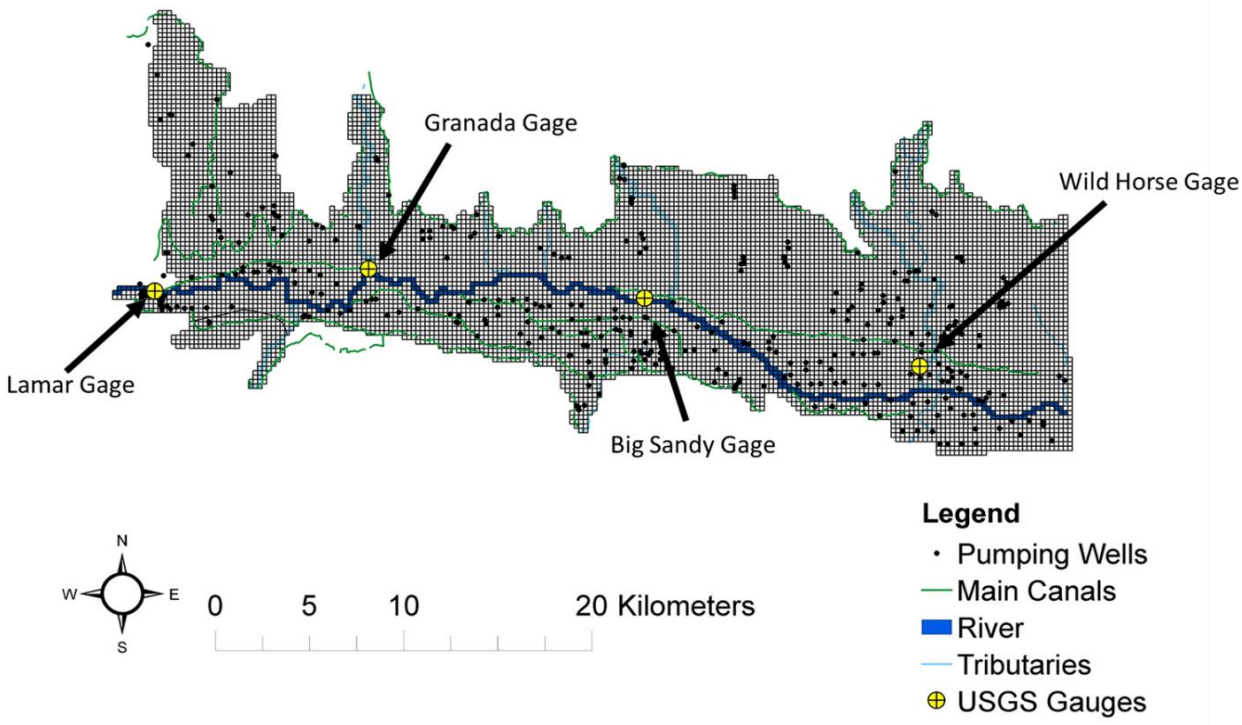

Figure 6 Discretize the model into grid cells in the DSR.

In addition, the time domain (2002 to 2007) was divided into weekly stress periods and weekly time steps. As such, the total number of the weekly time steps was 291 (Morway et al., 2013). Also, the number of stress periods has been increased from 261 to 2085 stress periods, which was to match the 40 years spin up simulation, and the original baseline input files that were done by (Morway et al., 2013) were changed. In addition, several packages were changed in the MODFLOW initial conditions. These included the discretization file (dis), name file (mfn), basic file (bas), output control (oc), well package (wel), river package (riv), unsaturated zone flow package (uzf), and stream routing package (sfr) (Niswonger et al., 2011). All these packages have been edited and its stress periods were increased from 252 to 261 and then looped for 40 years. The flow had changed as well from a steady state to a transient as the initial

condition had changed, thus entailing that the flow condition had to be changed. Figures 7 and 8 below show the average groundwater head and the depth to the water table.

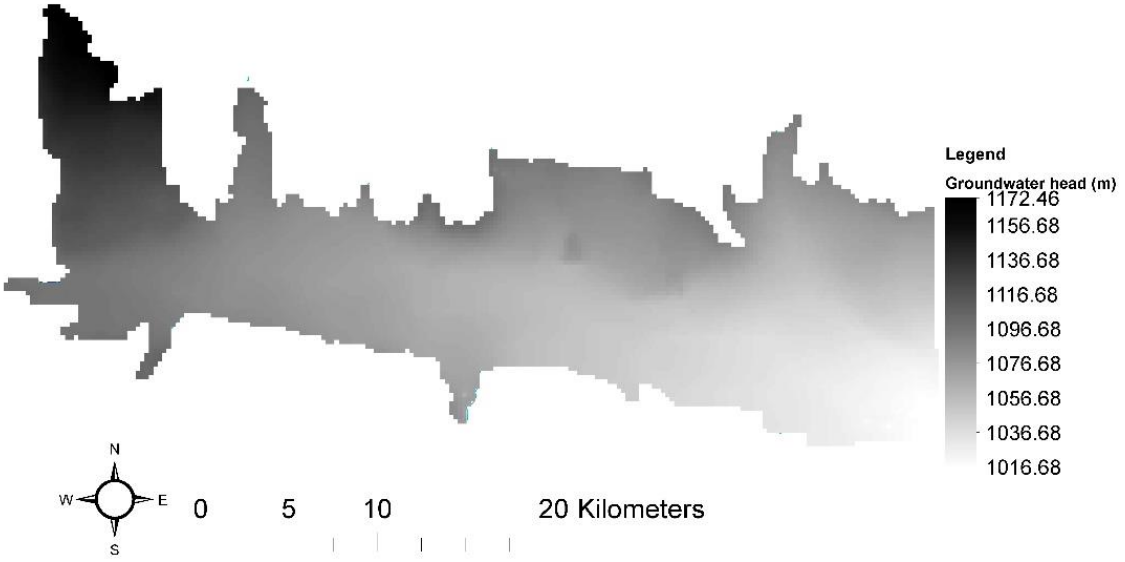

Figure 7 Average simulated groundwater head in the DSR.

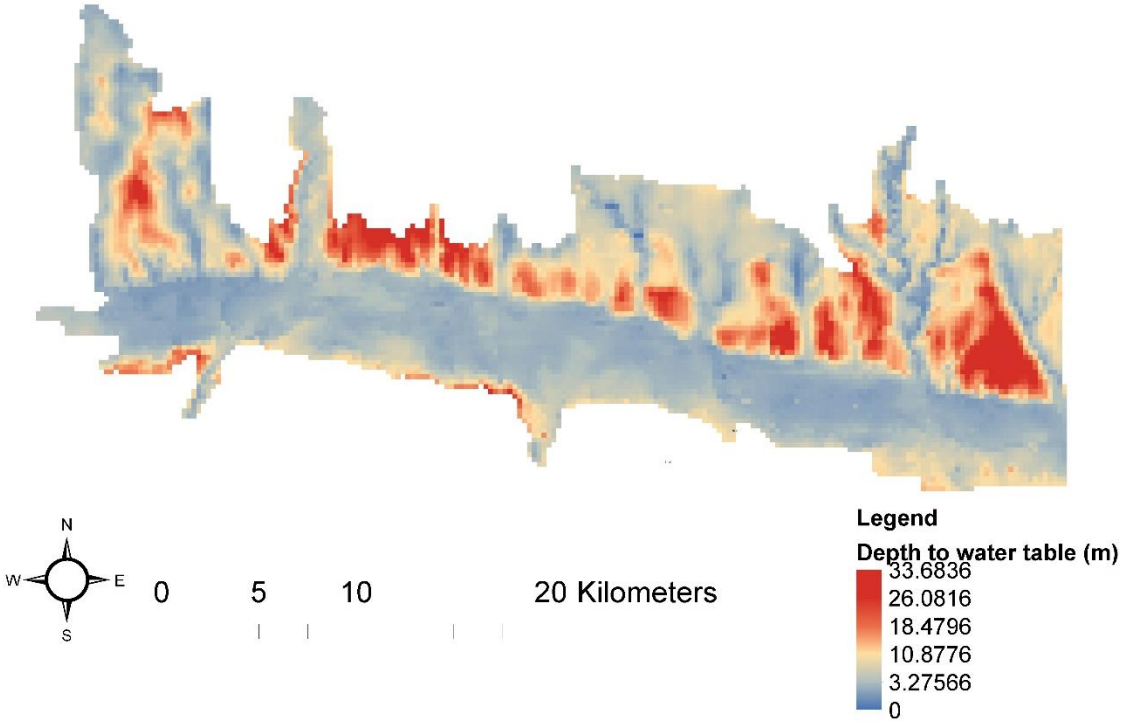

Figure 8 Average simulated depth to water table in the DSR.

3.1.2 Modification of MODFLOW Model to simulate Streamflow Routing

The model of Morway et al. (2013) is amended for the current study by including the SFR2 package to simulate streamflow and groundwater-surface water interactions into Morway et al. (2013) MODFLOW model. This was performed to allow the simulation of streamflow and stream stage in the stream-aquifer system, which is required to simulate Se and N surface water transport, as described in Section 3.3. Morway et al. (2013) used the River package for the DSR, which requires the user to specify stream stage for each model stress period and does not simulate streamflow. The SFR2 package routes water from the upstream to downstream of the river and it is tributaries, with Darcy's Law used to quantify water exchange rates between each SFR2 cell and adjacent aquifer cells. To implement the SFR2 package in the grid shown in Figure 6, the Arkansas River stream network was divided the streams into 488 reaches (= cells)

The modified MODFLOW model, with the SFR2 package, is tested against observed streamflow at several gauges within the stream network. The observation data that is available to be used as a baseline for the model is from the period of 2003 to 2007. Moreover, MODFLOW simulated 292 stress periods from May 2002 to August 2007. In the end, the gauges include four different gages in the Arkansas River (Lamar gage; ARKLAMCO, Granada gage; ARKGRACO, Big Sandy Creek; BIGLAMCO, and Wild Horse Creek; WILDHOCO). The observations data have been collected in 15-min intervals, with flow data aggregated to compare with the weekly MODFLOW streamflow output.

3.3 Se and N Reactive Transport Model for the Downstream Study Region

3.3.1 Conceptual Model of Se and N Reactive Transport

Se is abundant in numerous inorganic and biochemical processes globally (Tummalapenta, 2015). Since the sulfur (S) and Se are similar in the geochemistry properties, the selenide form of Se can occur in the geological formation as seleno-pyrite ($FeSe_xS_{2-x}$). This is by changing the S in pyrite (FeS_2) (Bye & Lund, 1982). SeO_4^{-2} is the most dominate species of Se, with about 90-95% of the Se in agriculture waters, and its main objectives is to remediate the contamination of SeO_4^{-2} in the system. SeO_4^{-2} is found as pyrite at the shale bedrock and oxidized by dissolved oxygen (O_2) of nitrate (NO_3) in the irrigation systems (Wright, 1999). The following equations illustrate the release of SeO_4^{-2}:

$$2FeSe_2 + 7O_2 + 2H_2O \longrightarrow 2Fe^{2+} + 4SeO_4^{-2} + 4H^+ \qquad \text{EQ.1}$$

$$5FeSe_2 + 14NO_3^- + 4H^+ \longrightarrow 5Fe^{2+} + 10SeO_4^{-2} + 7N_2 + 2H_2O \qquad \text{EQ.2}$$

Se transport and fate in irrigated alluvial stream aquifer system often is significant due to the presence of Se-bearing geological formations, especially marine shale (Kulp & Pratt, 2004; Neitsch et al., 2005), either as outcrops or as bedrock underneath the alluvial aquifer material. The residual Se in bedrock shale or outcrop can be oxidized by the O_2 that infiltrates into groundwater and soil water, as well as the NO_3-laden water that comes from leaching of applied N fertilizer load over the cultivated irrigation area (Bailey et al., 2013a) (Bailey et al., 2013b). The reduction of redox which has been described of both O_2 and NO_3 are demonstrated by the following equations:

$$CH_2O + O_2 \longrightarrow CO_2 + H_2O \qquad \text{EQ.3}$$

$$3CH_2O + 2NO_3 \longrightarrow 3CO_3 + 3H_2O + N_2 \qquad \text{EQ.4}$$

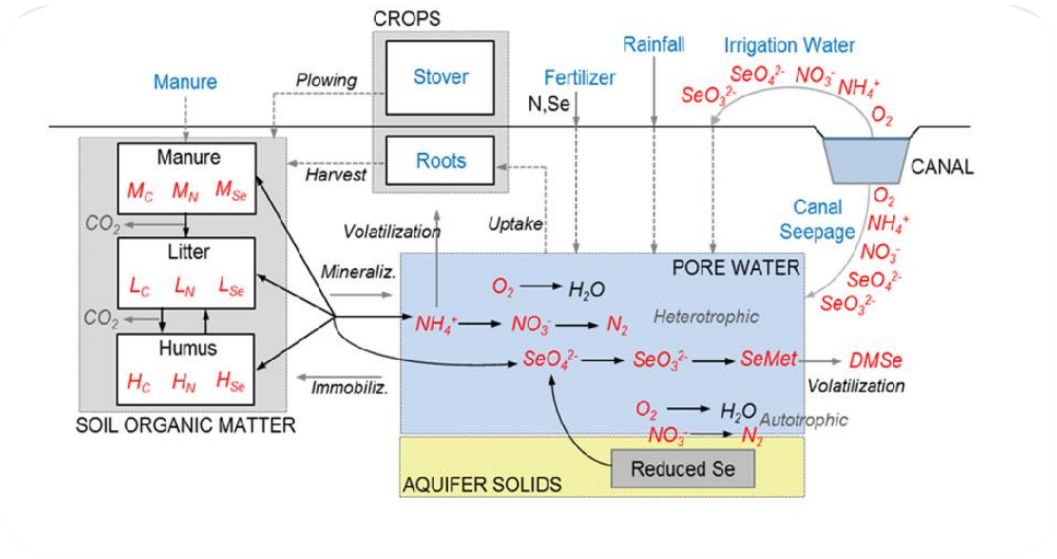

Figure 9 Conceptual model for the root zones and chemical reactions and transformations (Bailey, Gates, & Ahmadi, 2014)**.**

Figure (9) illustrates the cycling of Se and NO_3 in such an irrigated agriculture area. N and Se mass can be introduced into the subsurface via fertilizer and irrigation water (surface water irrigation or groundwater irrigation), and also canal seepage water. N and Se species can be taken up by crop roots, and then plowed into the soil at the end of the harvest period. There are three immobile species and six mobile species that represent the organic soil matter. The immobile species are humus (H) (slow-decomposing), litter (L) (fast-decomposing), and manure (M), and the mobile species represents the solid phase, which is, O_2, NH_4-N, NO_3-N, SeO_4-Se, SeO_3-Se, and SeMet. In order to simplify the symbols, NH_4-N, NO_3-N, SeO_4-Se, and SeO_3-Se will be written as NH_4, NO_3, SeO_4, and SeO_3 during the remainder of the text. The organic Se and N are combined with the dead root mass of the crop that occurs in the harvest season, and it is combined at the litter pool. The organic matter can be mineralized to mobile SeO_4, SeO_3, and NO_3, which then can undergo chemical redox reactions. The presence of both O_2 and NO_3 can inhibit the reduction of SeO_4 to SeO_3. Also, Residual Se in the marine shale can be oxidized to SeO_4 via O_2 and NO_3 autotrophic reduction.

3.3.2 RT3D Model of Tummalapenta (2015)

Using the RT3D modeling code, Tummalapenta (2015) constructed a Se and N reactive transport groundwater model for the DSR. RT3D is a FORTRAN code that solves the advection-dispersion-reaction (ADR) mass balance equation for multiple reactive chemical species using the finite difference method:

$$\frac{\partial(C_k\theta)}{\partial t}R_k = \frac{\partial(\theta v_i C_k)}{\partial x_i} + \frac{\partial}{\partial x_i}\left[\theta D_{ij}\frac{\partial C_k}{\partial x_i}\right] + q_f C_{fk} + \theta r_f \qquad k = 1,2,\dots m \quad \text{EQ.5}$$

$$\frac{\partial(C_l\,\varepsilon)}{\partial t} = \alpha_l P_s + \varepsilon r_s \quad l = 1,2,\dots m \qquad \text{EQ.6}$$

Where:

m and n: are the total number of dissolved and solid phase respectively.

C_k: dissolved phase concentration of k^{th} species (M_f/L_f^3).

C_L: solid phase concentration of L^{th} species (M_f/L_f^3).

f denotes the fluid phase.

D_{ij}: hydrodynamic dispersion coefficient (L^2/T).

υ: pore viscosity (L_b/T).

b denotes the bulk phase.

θ: volumetric water content (L_f^3/L_b^3).

ε: volumetric solid content (L_f^3/L_b^3).

q_f: volumetric flux of water representing sources and sinks ($L_f^3/T/ L_b^3$).

C_{fk}: concentration of the source or sink (M_f/L_f^3)

P_s: mass application rate for the L^{th} solid phase sources (M_s/ L_b^3).

α_l: fraction of P_s attributed to species *l*.

r_f: rate of all reactions that occur in the dissolved ($M_f\ L_f^3/T$).

r_s: rate of all reactions that occur in the solid phase ($M_s\ L_s^3/T$).

R_k: retardation factor for the k^{th} dissolved-phase species, equal to $1+ (\rho_b + k_{d,k})/\theta$

ρ_b: bulk density of the porous media (M_b/L_b^3)

$k_{d,k}$: partitioning coefficient for the kth species (L_f^3/M_b). $_{SeO4}$

To solve the ADR equation, the flow rates between cells and the water content for each cell is required. This is provided by the MODFLOW-NWT model, as described in Section 3.1. Thus, both RT3D and MODFLOW can be linked and connected to each other, and the RT3D has been selected as the baseline code as it has been constructed by combining the Se and N reactions modules of UZF-RT3D (Bailey et al., 2013b), which is connected to the MODFLOW-NWT with the UZF1 package (Niswonger et al., 2011) that has been described at section 3.2. Since RT3D solves for advection and dispersion equations, UZF-RT3D solves for the same reaction equation (ADR) and removes the diffusive term in Richard's equation. (Bailey et al., 2013b), by using the numerical strategy method, which is known as of operator-split (OS), finds a solution for deference transport equations (Clement, 1997).

For Se dissolved phase species, the following equations are used to represent the fate and transport model in Figure (9):

$$\frac{\partial(C_{SeO4}\theta)}{\partial t}R_{SeO4} = -\frac{\partial(\theta viC_{SeO4})}{\partial x_i} + \frac{\partial}{\partial x_i}\left[\theta\, Dij\, \frac{\partial C_{SeO4}}{\partial xi}\right] + q_f C_{fSeO4} + F_{SeO4} - U_{SeO4} + \varepsilon\left(r_{s,se}^{min} - r_{s,se}^{imm}\right) + \theta\,(r_{f_{SeO4}}^{auto} - r_{f_{SeO4}}^{het}) \qquad \text{EQ.7}$$

$$\frac{\partial(C_{SeO3}\theta)}{\partial t}R_{SeO3} = -\frac{\partial(\theta viC_{SeO3})}{\partial x_i} + \frac{\partial}{\partial x_i}\left[\theta\, Dij\, \frac{\partial C_{SeO3}}{\partial xi}\right] + q_f C_{fSeO3} + F_{SeO3} - U_{SeO3} + \varepsilon\left(r_{s,se}^{min} - r_{s,se}^{imm}\right) + \theta\,(r_{f_{SeO4}}^{het} - r_{f_{SeO3}}^{het(Se_S)} - r_{f_{SeO3}}^{het(SeMet)}) \qquad \text{EQ.8}$$

$$\frac{\partial(C_{SeMet}\theta)}{\partial t}R_{SeO4} = -\frac{\partial(\theta viC_{SeMet})}{\partial x_i} + \frac{\partial}{\partial x_i}\left[\theta\, Dij\, \frac{\partial C_{SeMet}}{\partial xi}\right] + q_f C_{fSeMet} + F_{SeMet} - U_{SeMet} + \theta\,(r_{f_{SeO3}}^{het(SeMet)} - r_{f_{SeMet}}^{het}) \qquad \text{EQ.9}$$

Where

min and *imm*: mineralization and immobilization, respectively.

Auto and *het*: autotrophic and heterotrophic chemical reduction, respectively.

The following equations represent the NH_4, NO_3, and O_2, *nit*, which is identified as nitrification, and is similar to the pervious Se equations.

$$\frac{\partial(C_{NH4}\theta)}{\partial t}R_{NH4} = -\frac{\partial(\theta viC_{NH4})}{\partial x_i} + \frac{\partial}{\partial x_i}\left[\theta\, Dij\, \frac{\partial C_{NH4}}{\partial xi}\right] + q_f C_{fNH4} + F_{NH4} - U_{NH4} + \varepsilon\left(r_{s,N}^{min} - r_{s,N}^{imm}\right) + \theta\,(-r_f^{nit} - r_f^{vol}) \quad \text{EQ.10}$$

$$\frac{\partial(C_{NO3}\theta)}{\partial t}R_{NO3} = -\frac{\partial(\theta viC_{NO3})}{\partial x_i} + \frac{\partial}{\partial x_i}\left[\theta\, Dij\, \frac{\partial C_{NO3}}{\partial xi}\right] + q_f C_{fNO3} + F_{NO3} - U_{NO3} + \theta\,(r_f^{nit} - r_{f,NO3}^{het} - r_{f,NO3}^{auto}) \quad \text{EQ.11}$$

$$\frac{\partial(C_{O2}\theta)}{\partial t} = -\frac{\partial(\theta viC_{O2})}{\partial x_i} + \frac{\partial}{\partial x_i}\left[\theta\, Dij\, \frac{\partial C_{O2}}{\partial xi}\right] + q_f C_{fO2} + \theta\,(-r_{f,O2}^{het} - r_{f,O2}^{auto}) \quad \text{EQ.12}$$

The first-order kinetics is applied for decomposition, mineralization, and immobilization. Moreover, for all the UZF-RT3D chemical species that have been used, first-order Mond terms are applied as (Bailey et al., 2013a) states. Thus, the following equations represent the chemical heterotrophic reduction for all species:

$$r^{het}_{f,O2} = \lambda^{het}_{O2} C_{O2}\left(\frac{CO2}{KO2+CO2}\right)\left(\frac{CO2.prod}{KCO2+CO2.prod}\right)E \quad \text{EQ.13}$$

$$r^{het}_{f,NO3} = \lambda^{het}_{NO3}\, C_{NO3}\left(\frac{CNO3}{KNO3+CNO3}\right)\left(\frac{CO2.prod}{KCO2+CO2.prod}\right)\left(\frac{IO2}{IO2+CO2}\right)E \quad \text{EQ.14}$$

$$r^{het}_{f,SeO4} = \lambda^{het}_{SeO4}\, C_{SeO4}\left(\frac{CO2.prod}{KCO2+CO2.prod}\right)\left(\frac{IO2}{IO2+CO2}\right)\left(\frac{INO3}{INO3+CNO3}\right)E \quad \text{EQ.15}$$

Where

λj: constant rate for each species *j* (1/T).

K*j*: Monod half-saturation constant for each species *j* (M_f/L_f^3).

I_{O2} and I_{NO3}: inhabitation constant for O_2 and NO_3, respectively, (M_f/L_f^3). This implies that the concentration species effect reaches the higher-redox species.

$CO_{2.prod}$: total mass of CO_2 during the organic matter decomposition.

E [-]: environmental reduction factor for soil moisture and soil temperature.

For all other species, it is described in (Bailey, Morway, et al., 2013) and (Bailey, Gates, et al., 2013).

3.3.3 Modification of RT3D Model to simulate Stream Reactive Transport

One of the goals of modeling in this thesis is to determine the effect of BMPs on in-stream concentrations of Se and NO_3. As such, the model needs to have the capability of simulating these in-stream concentrations. To do so, the RT3D model of Tummalapenta (2015) is coupled with the OTIS (Runkel, 1998) modeling code to allow for both groundwater and surface water chemical reactive transport, with chemical mass exchange between streams and the aquifer based on the exchange flow rates simulated by the SFR2 package of MODFLOW. This section describes the implementation of the new RT3D-OTIS coupled code (Shultz et al., 2018) for the DSR. Only the basic linkage process is described here. For more details, refer to Shultz (2017) and Shultz et al. (2018).

RT3D-OTIS is a single FORTRAN code that couples the OTIS model with UZF-RT3D. OTIS solves for 1D chemical transport of species in streamflow. The model solves for advection, dispersion, lateral inflow, transient storage, and first order decay (Runkel & Broshears, 1991) (Figure 11). The following equations of stream and storage zone represent the basic differential equation, which illustrates the concept of the conservation of mass (Runkel & Broshears, 1991):

$$\frac{\partial C}{\partial t} = -\frac{Q}{A}\frac{\partial C}{\partial x} + \frac{1}{A}\frac{\partial}{\partial x}\left(\mathrm{AD}\,\frac{\partial C}{\partial x}\right) + \frac{qLIN}{A}\,(CL - C) + \alpha\,(Cs - C) - \lambda c \qquad \text{EQ.16}$$

$$\frac{\partial Cs}{\partial t} = \alpha\frac{A}{As}\,(C - Cs) - \lambda c\,Cs \qquad \text{EQ.17}$$

Where

A: cross-sectional area of stream channel (L^2).

As: cross-sectional area of storage zone (L^2).

C: solute concentration in stream (M/L^3).

C_L: solute concentration in lateral flow (M/L^3).

C_S: storage zone solute concentration (M/L^3).

D: dispersion coefficient (L^2/T).

Q: volumetric flowrate (L^3/T).

q_{LIN}: lateral inflow rate (L^3/T L).

t: time (T)

x: distance (L)

α: storage zone exchange coefficient (1/T).

λ: first order decay, in stream (1/T).

λs: first order decay, storage zone (1/T).

The original OTIS code was modified to include QUAL2E chemical reactions for O_2 and N cycling, with Se cycling equations added (Shultz et al., 2018). The main reactions of QUAL2E are N cycling, O_2 fate and transport, algal growth, and algal uptake. Furthermore, the model solves for some other species, such as O_2, N, ammonia NH_3, nitrite NO_2, NO_3, and algae (Shultz

et al., 2018). For this study, the relationship between the C_{DO} and de-nitrification that has been added as a first-order kinetic reaction is an inverse relationship.

OTIS was modified to allow for multiple stream segments, thereby allowing simulation for the Arkansas River and connecting tributaries. Diversion canals also can be included. The finite difference grid for OTIS is the same as for the MODFLOW SFR2 package grid cells, although each SFR2 grid cell is divided into 5 OTIS computational cells. The flow rate, stream stage, and cross-sectional flow area for each SFR2 cell is provided to OTIS for surface water transport. At each transport time step, mass exchange between RT3D cells and OTIS cells are calculated for all Se and N species.

The full coupled reactive transport system is shown in Figure 10 (Shultz et al., 2018). The blue text illustrates the MODFLOW process which include the irrigation from canals and groundwater, evapotranspiration, tailwater runoff, percolation, canal seepage, 3D groundwater flow in the saturated zone, and surface water interaction. In addition, the red text shows the UZF-RT3D process that include simulate the Se and N in the root zone, leaching of Se and N in the vadose zone, advection, dispersion, and chemical reactions for Se and N transport in the saturated zone, and release of SeO_4 from bedrock near surface layer. Finally, the green text indicates the OTIS model that include the simulation of in stream chemical transport.

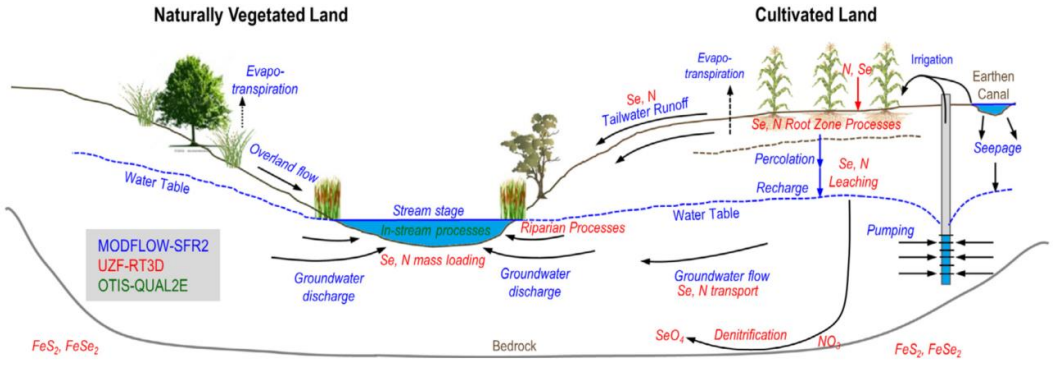

Figure 10 Conceptual flow modet, reactiver trasnport model, and OTID model, (Shultz et al., 2018)

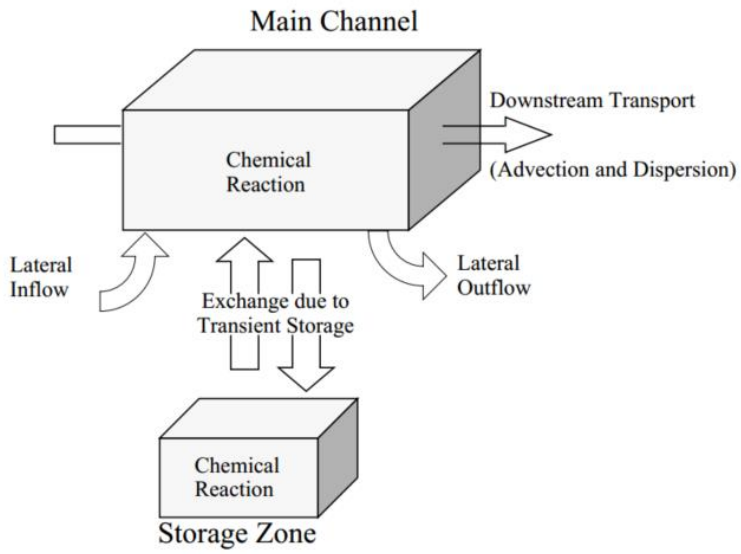

Figure 11 Conceptual model of the OTIS model (Runkel, 1998)

Figure 12 describes the data flow within the RT3D-OTIS modeling code (Shultz et al., 2018). At the beginning of each stress period, the MODFLOW results are read in for both groundwater and surface water systems. Advection, dispersion, and source/sink mixing is calculated for each chemical species in groundwater, followed by groundwater chemical reactions and then surface water transport using OTIS.

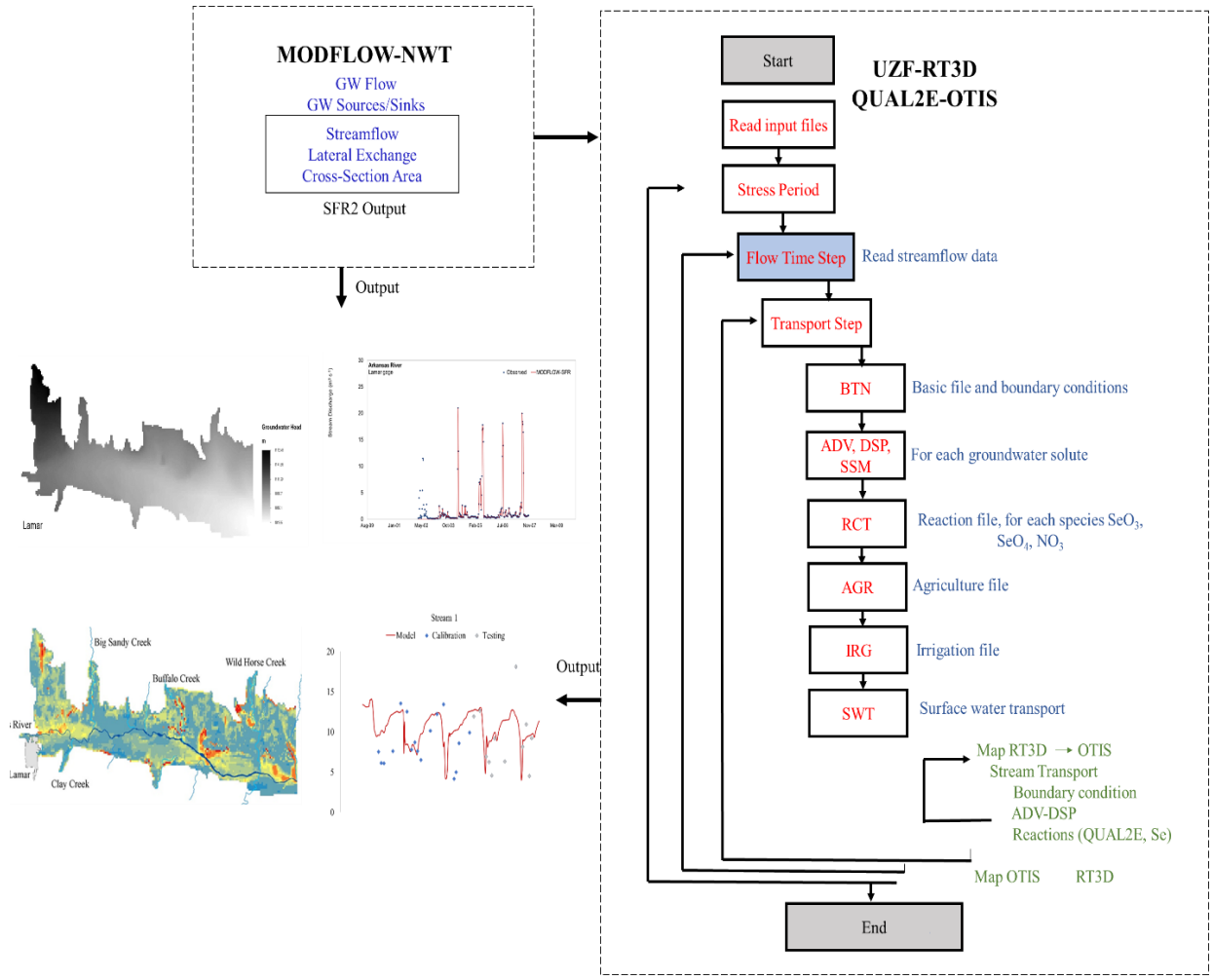

Figure 12 Work flow of coupled models flows and transport model.

For application to the DSR, UZF-RT3D was run on a daily time step and OTIS is run on an hourly time step, in order to solve the QUAL2E reactions. The same finite difference grid is used, although the 2 layers of MODFLOW are divided into 6 layers for RT3D, as in Figure (13). The stream network was divided into 9 streams, 5 representing segments of the Arkansas River and 4 representing the tributaries.

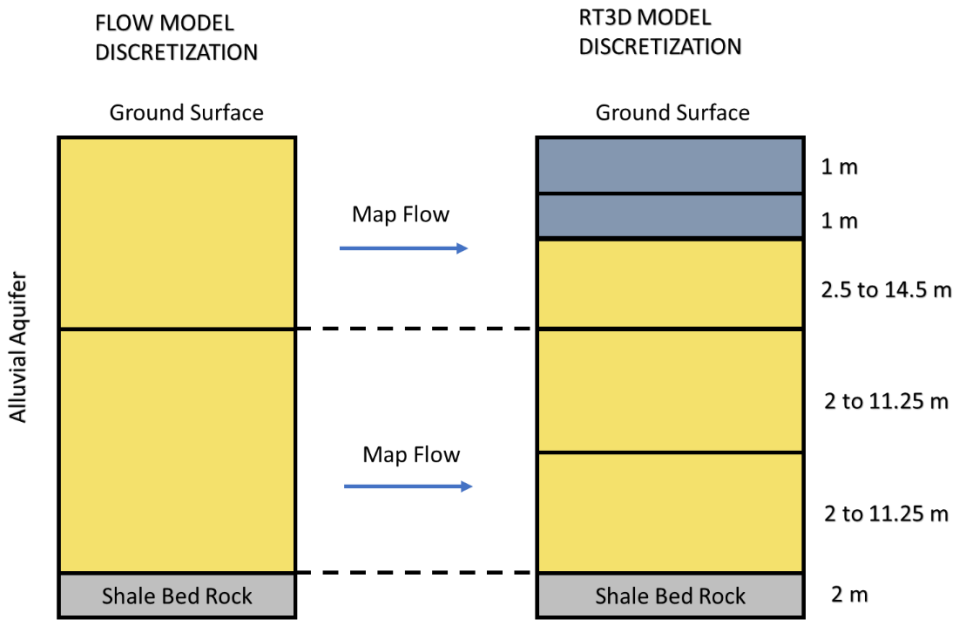

Figure 13 MODFLOW and RT3D layers depth for alluvial aquifer.

RT3D-OTIS was calibrated and tested against observation data in the DSR. The observation data that is available to be used as a baseline for the model are from the period of 2003 to 2007 and is divided into two periods. These are the calibration period from 2003 to 2005, and testing period from 2006 to 2007. Moreover, the RT3D simulated 252 stress periods from June 2003 to August 2007. Thus, many packages and initial conditions have been changed in The RT3D. The RT3D has been calibrated manually and automatically against historical observations data. Observation data consist of groundwater samples from the 118 monitoring wells (see Figure 14) and surface water samples from sites along the Arkansas River and the tributaries.

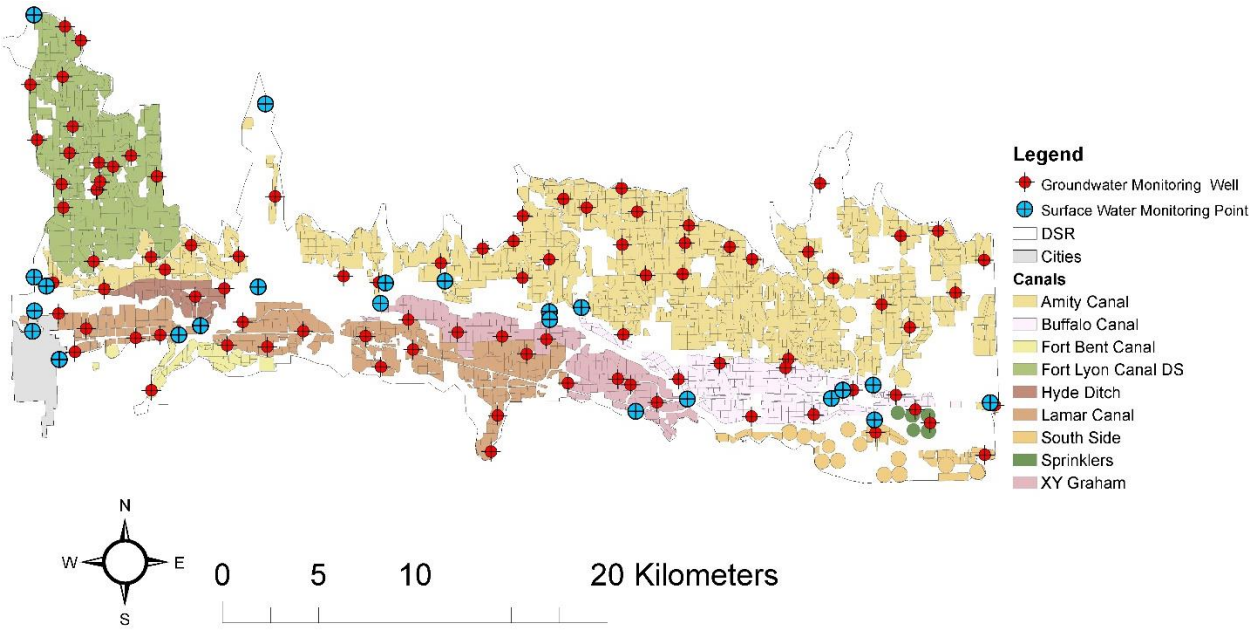

Figure 14 Location of the surface water sampling site and the groundwater monitoring well.

The calibration and adjustment of the RT3D-OTIS model for both the groundwater chemical reaction and the stream chemical reaction were done by quantifying selected the groundwater reactive transport parameters (Bailey et al., 2014). As such, the calibration is important to ensure that the simulation data and the observation data are matched and fit adequately to each other in the DSR. Two main processes were used to calibrate the model. These were the manual calibration and automated calibration by using the Parameter Estimation (PEST) software (Doherty 2016). Similar to the MODFLOW calibration that was discussed in section 3.1, the original RT3D stress period was 252 and it was extended to 261 stress periods, with the model being subsequently spun up for 40 years.

In addition, there are five main input files have been changed and modified from the initial condition. These included i. basic transport package (btn); maintaining the information of the initial and boundary conditions and the concentration of Se and NO_3, ii. Source-sink mixing (ssm); including the solute concentration of each species and the information of the source/sink,

iii. Irrigation files (irg); including the mass of species that enter the system through the surface water (pump, canal, rainfall), iv. Agriculture files (agr); determining the agriculture process due to source/sink, v. surface water transport (swt). Subsequently, each of these files has been modified as such:

I. BTN:

Increased the number of stress period (NPER) from 252 to 2085 weeks. The number of days has been changed as well, from 1764 to 14595 days, to match the stress period. Finally, the number of the stress period length was looped, and the number of flow time steps was increased 7 times to match the simulation spin up which is 40 years.

II. SSM:

The point of sources/sinks for each stress period has been extended from 252 to 261 weeks by match and repeats the same data in the file of weeks 201, 202, 203, 204, 205, 206, 207, 209 at year 2006. This step has been done in order to match the observed data, which is from Jan 2003 to December 2007. Finally, the source/sinks have been looped 7 times until it reached the stress period number of 2085 weeks.

III. IRG:

The initial list of irrigation canals has been changed, along with the NPER and the sampling data from the sampling event from 29 to 240. This is based off the assumption that the number of sampling data has been changed from 29 sample dates to 240 sample dates. This data has been taken from the observation filed from the period of 2003 to 2007 (i.e. day 115, 149, etc.). This was in order to match the data with the 40 years spin up. Finally, the infiltrated portions for each grid cell have been looped 7 times in order to achieve the 40 years spin up.

IV. AGR:

The number of years of the simulation has been increased from 5 years to 40 years, so that the number is increased until year 2042. The Cell crop information has been increased, firstly from 252 stress periods to 261 stress periods, and is similarly the case with step iii, after that the data has been looped for 40 years. The temperature data at the year before beginning of simulation (2002) has been looped 7 times, as well as the step iii.

V. SWT:

The number of observation times has been changed from 252 to 2085 weeks. The time of general concentration output has been changed and as it is in hours, the total number of hours has been increased to 350280 hours. This is by adding units of 168 hours, which is equivalent to one week. The total timing information was 42336 hours and it was changed to be 350280 hours. The number of stress period at the upstream boundary condition has changed similarly with step iii. and then the missing data was completed in the file to complete the total hours for the simulation. The daily temperature and daylight hours, and the hourly solar radiation has been increased in similarity with step iii. Finally, the algae concentrations are to be included with the groundwater mass discharge to the streams, and have been increased as per step iii, and subsequently looped till day 14595.

Moreover, based on the literature, there are reasonable ranges in the chemical parameter values to get the groundwater concentration, stream concentration, and mass loading to the Arkansas River, this match with the observations data of Se and NO_3. The domain area has been divided into 15 sub-regions, as seen in Figure (16), to get accurate results that match between the simulation and the field data. The criteria of dividing the area into sub-regions are based on

several factors which is (1) the geology of the area, since the LARV underline by the marine shale in the most of the area, so that it is divided base on the location of the geological formation, Figure (15.A), (2) the location of the main irrigated canals (Amity, Buffalo, Fort Lyon, Lamar) that effect the area, Figure (15.B), (3) location of each sub-basin that obtained from the largest LARV basin, Figure (15.C), (4) OTIS stream segments or cells along the modeled stream and the reaches of the Arkansas River, Figure (15.D), and (5) the location of the observation wells of Se and NO_3, Figure (15.E). Also, the stream divides into the main Arkansas River segments and the four main tributaries, which are Clay Creek, Big Sandy Creek, Buffalo Creek, and Wild Horse Creek.

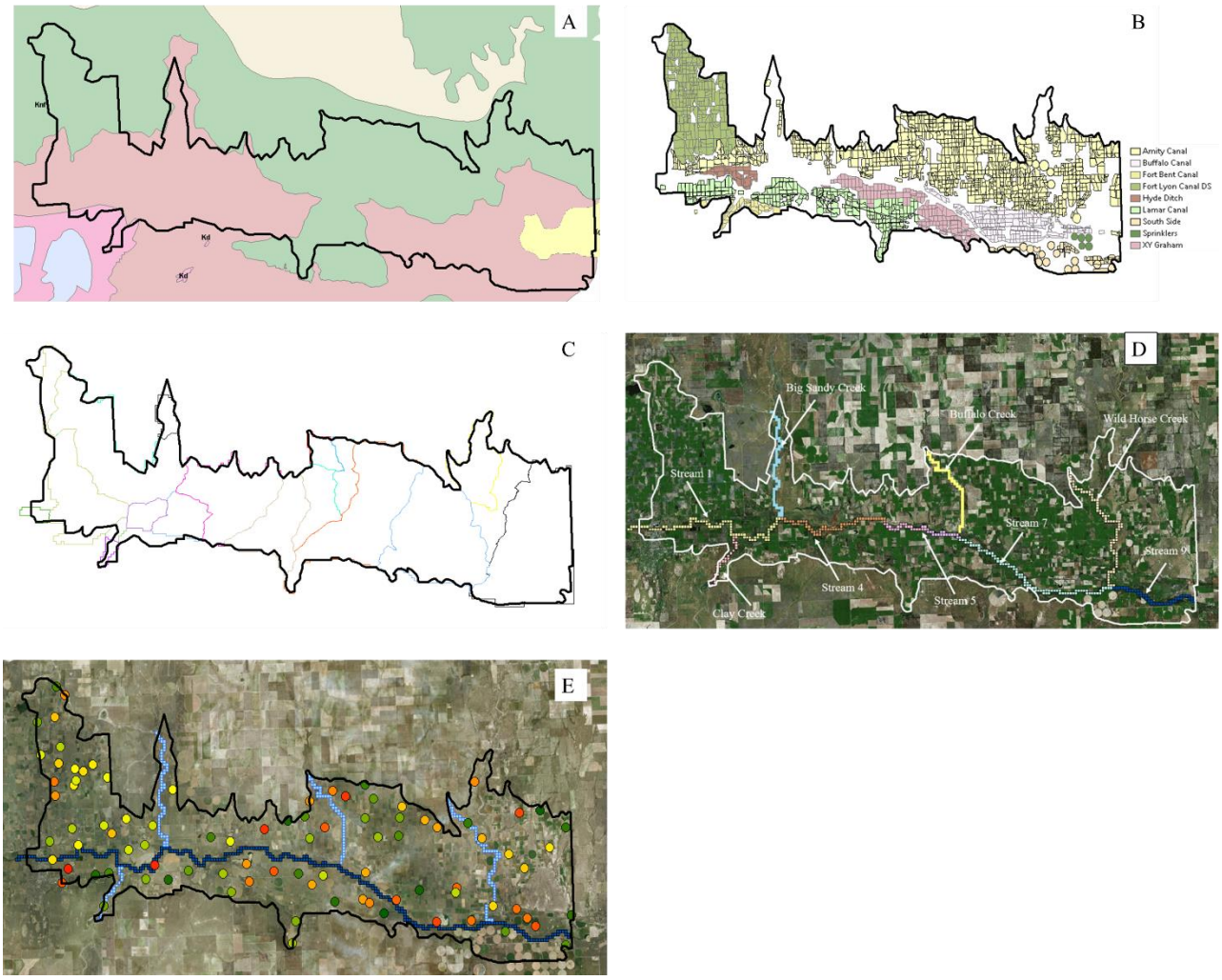

Figure 15: Criteria of dividing the area into sub-regions, (A) locations of geological formation, (B) irrigated fields, (C) sub basins, (D) stream segments for the river and it is tributaries, and (E) monitoring wells locations.

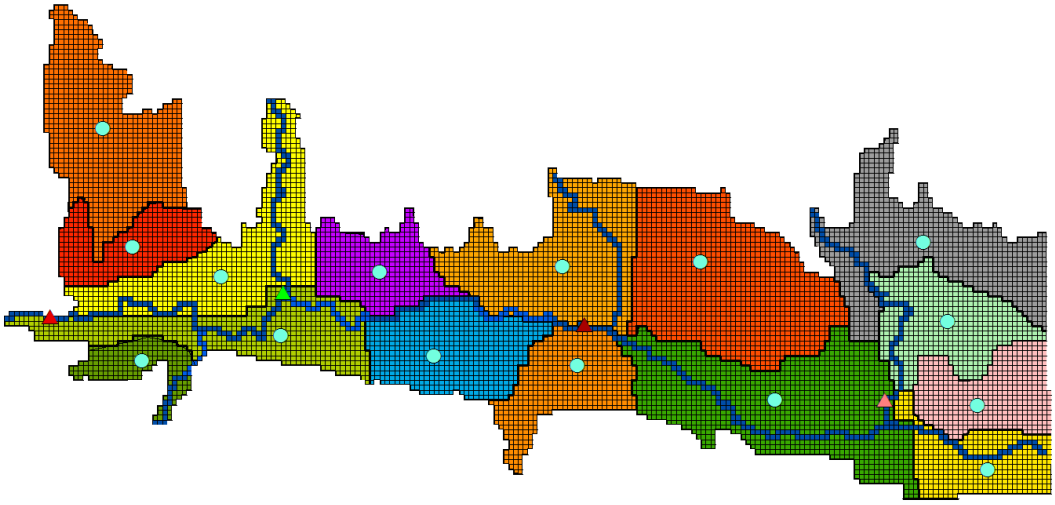

Figure 16 The 15 sub-regions in the DSR.

Furthermore, the manual calibration has been done for the groundwater parameter and surface water parameter separately. However, the automated calibration was divided into the calibration period and testing period. The calibration period is from January 1st, 2003 to December 31st, 2005, and the testing period was from January 1st, 2006 to December 31st,2007, as shown in the chart below.

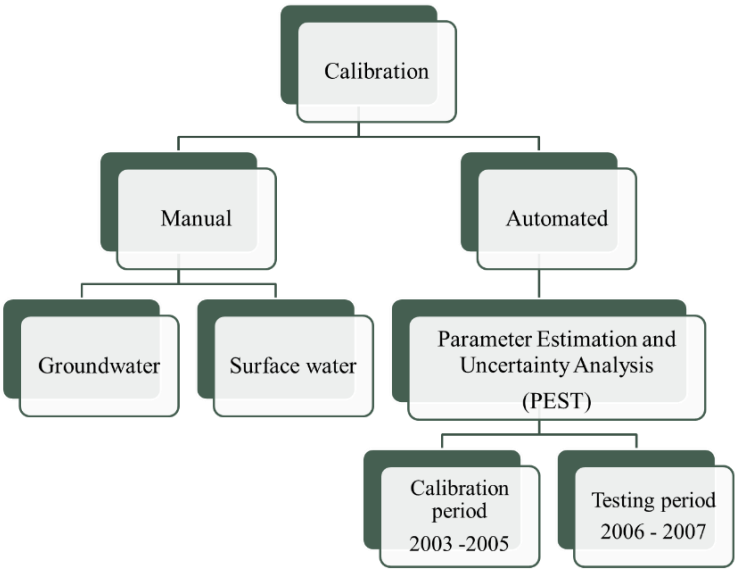

Figure 17 Calibration flow chart

The aims of this calibration are to ascertain: i. Average groundwater concentrations of each sub-region for Se and NO_3. ii. OTIS stream segments and the tributary concentrations for Se and NO_3. iii. Mass loading to the Arkansas River of Se and NO_3. Similar to (Shultz et al., 2018) a combination of manual and automated calibration has to be done in order to achieve the best match between the observation data and the model data. There are four calibration periods have been done in the USR by (Shultz et al., 2018), and these steps will used in the DSR as well. These are:

1. Different chemicals reactions rates in the RT3D-OTIS input files have been modified for groundwater, along with the Arkansas River and its tributaries. These chemical reactions rates are: the rate of heterotrophic reduction of SeO_4 and NO_3 in the presence shale $\lambda_{SeO_4}^{het}$ and $\lambda_{NO_3}^{het}$, ($KSeO_4$) and (KDENH); the rate of heterotrophic reduction SeO_3 to mobile SeMet $\lambda_{SeO_3}^{het}$ ($KSeO_3$); and the rate of Nitrification λ_{Nit} (KNIT). These are based off the previous studies that show that the heterotrophic has a main role in the riparian zones to control the reduction and solute transport of groundwater from the riparian zone (Hill, 1996) (Ranalli & Macalady, 2010) (Bailey et al., 2015b).
2. Using the manual calibration parameter and make it as initial values for PEST. PEST is used to minimize the uncertainty between the observation data and the model calibrated data. The equation below describes the way to minimize the residual that's found in the PEST user manual:

   $Min\ \Phi = \sum_{j=1}^{Ni}(wi\ ri)^2$ EQ.18

   Where,

   Φ: objective function, N_i: number of variable associated with the i^{th} calibration target, w_i: weight used to address the uncertainty in the variable associated with the i^{th} calibration

target, r_i: the residual between the observed value and simulated value for the j^{th} variable of the i^{th} calibration target. Also, PEST was calibrated for the 40 years spin up to reduce the uncertainty.

3. Using the final parameter that was obtained from the automated calibration, the model was run for the 40 years simulation and that built an initial groundwater concentration in the final baseline simulation.
4. The result that was obtained from PEST and compared with the observed value in the calibration period needed to ensure that its matched with the testing period of January 2006 to December 2007.

3.4 Assessing Effectiveness of BMPs to Mitigate Se and N in Groundwater and Stream

High concentrations of Se and NO_3 contain a toxic component that leads to a serious water quality issues for human, livestock, plants, and birds. Thus, one of the aims of the research is to find strategies to reduce the concentrations of Se and NO_3 through the application of best management practices (BMPs). Moreover, the BMPs are always applied after calibrating the model because it will use the calibrated model as a baseline that compares all the BMPs with it.

However, at the LARV DSR, this paper has modified the work done by (Bailey et al., 2015a; Bailey et al., 2015b), and the BMPs have been applied for the reactive transport model RT3D-OTIS meant for groundwater and surface water for Se and NO_3. The BMPs investigated herein are reduced applied irrigation (Reduced Irrigation = RI), land fallowing of agriculture land (Land Fallowing = LF), and the sealing of irrigation canals (Canal Sealing = CS). Results from BMP simulations are compared with results from a Baseline ("do nothing") scenario. The Baseline simulation is described in the next section.

3.4.1 Baseline Simulations

The MODFLOW-SFR model has been coupled with the RT3D-OTIS for application to the BMPs. A long multi-decadal simulation is used to determine the long-term effect of the BMPs on Se and NO_3 groundwater concentrations, groundwater return flow to the Arkansas River, mass loading of Se and NO_3 to the River, and in-stream concentrations of Se and NO_3. The long period of simulation is instituted done due to the slow rate of groundwater flow, and thus changes made to cultivated fields in the interior of the agricultural area may not have an impact on groundwater-to-river loadings and in-stream concentrations for several decades after the BMP is implemented. As such, the MODFLOW model was modified to increase the simulation period from 5 years to 40 years by repeating the MODFLOW simulation 7 times, using the final head of each simulation as initial head for the second simulation. Then, the output head from the MODFLOW-SFR was used in the RT3D-OTIS to run the baseline condition (calibrated model).

3.4.2 BMP Simulations

Three different BMPs were applied at the DSR in order to reduce the groundwater concentrations, surface water concentrations, return flow to river, and the mass loading. These BPMs were considered as water management and includes (1) reduced irrigation (IR), (2) lease fallowing of agriculture land, and (3) sealing of irrigation canals. In addition, there are 9 different scenarios, three BMPs level (basic, intermediate, aggressive) implementation, and the baseline condition. Table (3) illustrates the different BMPs scenarios with their level.

Table 3: BMPs scenarios

BMP level	Scenario	Reduced Irrigation, %	Lease Fallowing, %	Canal Sealing, %
	Baseline	0	0	0
Basic	1	10	0	0
Intermediate	2	20	0	0
Aggressive	3	30	0	0
Basic	4	0	10	0
Intermediate	5	0	20	0
Aggressive	6	0	30	0
Basic	7	0	0	10
Intermediate	8	0	0	50
Aggressive	9	0	0	90

Reduced irrigation means that improving the irrigation practices from the old methods, such as gravity irrigation, flood irrigation, pipe diverted water, to a new and more efficient method, which could be sprinklers or drip irrigation. This method is a more conservative method since it uses a lesser amount of irrigation water in the same filed. In this project, the reduction efficacy varies from 10 to 30 %. the input file for the UZF1 package is modified to include the reduction in applied irrigation water for designated fields (= grid cells) (Morway et al., 2013). Output (groundwater heads, groundwater flow rates, surface water flows and cross-sectional area) from the modified MODFLOW model is used in the RT3D-OTIS model.

Lease fallowing is mainly so farmers could lease their irrigation fields and their water right to municipalities instead of transferring the water outside the agriculture domain, especially at the dry season. The LF is applied in the area by the range from 10 to 30 %. As with the RI scenarios, the UZF1 input file is modified to institute the removal of irrigation water for fallowed fields, and ET was changed to reflect the absence of a crop demand.

Canal sealing is used to decrease the rate of seepage from the earthen irrigation canals in the model domain. Polyachrilamide is assumed to be placed along the length of each canal, sealing the canal to a certain degree (Morway et al., 2013). The canal sealing values range from 10 to 90 % of seepage reduction. Also, the RIV package input file, which simulated groundwater-canal interaction in the original MODFLOW model and in the modified MODFLOW model used in this thesis, is modified by changing canal bed conductance to induce the appropriate rate of canal seepage reduction during the 40-year BMP simulations.

Land management BMPs such as the enhanced riparian buffer (ERB) and reduced fertilizer (RF) are considered as a strategy that leads to reducing the contamination of high concentrations of Se and NO3 in groundwater and in the streams. As discussed in (Shultz, 2017), that the most effective land management BMPs was the ERB in the USR. In addition, a combination of BMPs are also considered in the USR by (Shultz, 2017). However, due to a limitation of time, only water management BMPs is used in this thesis.

CHAPTER 4 RESULTS AND DISCUSSION

4.1 Groundwater and Streamflow Results

First, MODFLOW model results are compared with observed groundwater head data. The results of the original MODFLOW model from Morway et al. (2013) are also provided for comparison. The (RSME) is used to calculate the difference between the simulated result and the observed data, and it is known to minimize the residual. Table 4 and Figure 22 show results. Figure 22 shows a 1:1 plot of observed vs. simulated head values from the 118 monitoring wells in the DSR.

Table 4: Root mean square error (RMSE) between the RIV and SFR

Simulation vs Observation						
	Min	Mean	Max	Std.S	**RMSE**	**SSR**
RIV	-11.124	0.327	7.020	1.683	**1.71**	**21051**
SFR (261)	-11.352	0.237	6.835	1.612	**1.63**	**19016**

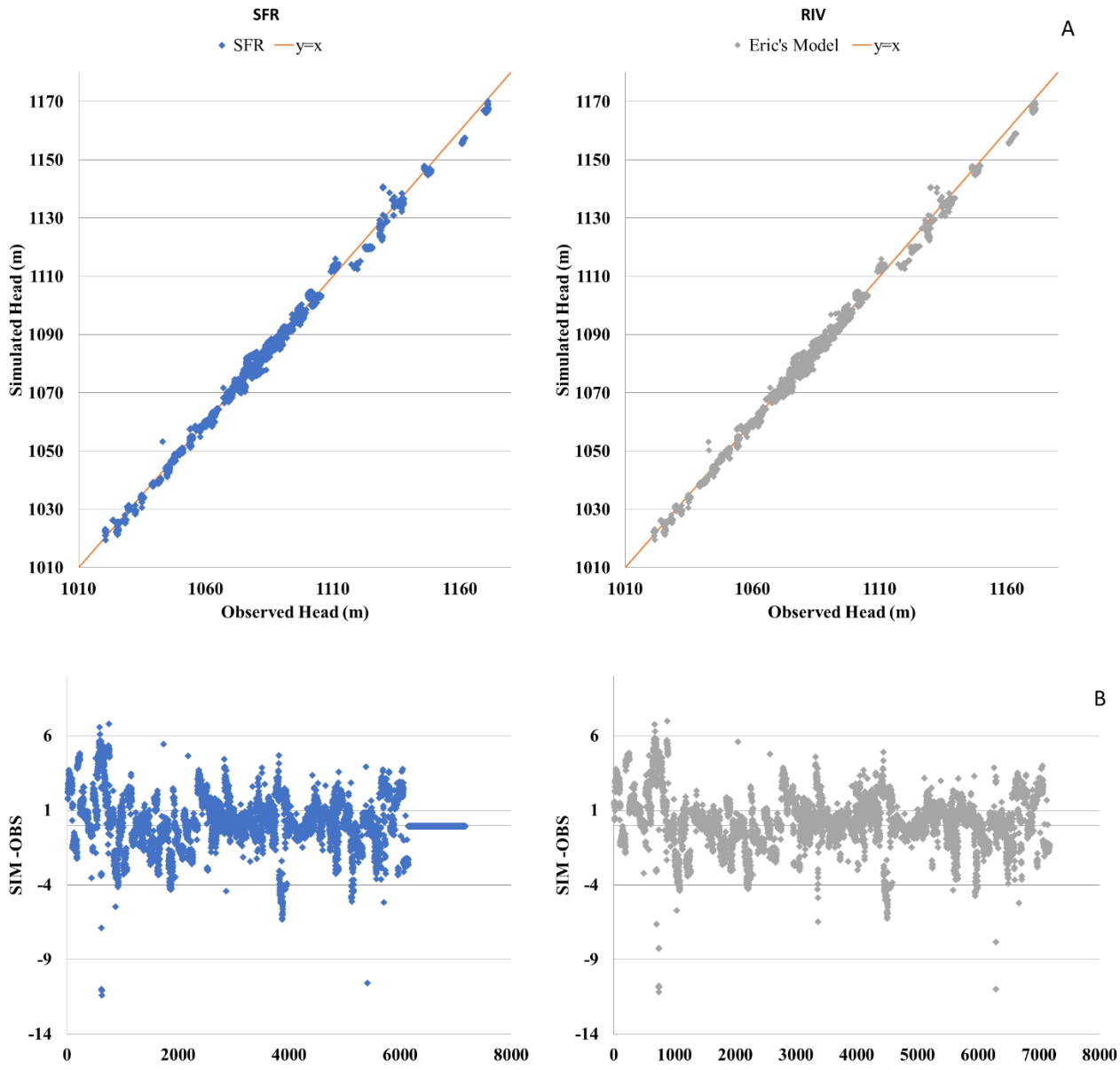

Figure 18 Compression between the RIV MODFLOW and SFR MODFLOW, (A) simulated head vs. observed, and (B) head difference

The table illustrate that the root mean square error of the original model had a value of 1.71 and the new model was 1.63, which was less than the original model In addition, the Figures showed matching results between the observation data and the simulations.

In the end, the model was tested and calibrated against the observation data that compared the streamflow at four different gages in the Arkansas River (Lamar gage; ARKLAMCO, Granada gage; ARKGRACO, Big Sandy Creek; BIGLAMCO, and Wild Horse Creek; WILDHOCO). The observations data have been collected in 15-min intervals and it was compared with the model as an average weekly time step. For the model, the output file contained a weekly time steps, stream flow, and stream depth, and was compared with the observation data. The results show that the model is match with the observation data especially, Lamar gage station and Granada gage station, however in the Big Sandy gage station the model show high prediction than the observation data, where, the Wild Horse gage station show high observation data than the simulated model. This poor match mainly due to the assumption that the inflow from the creek into the stream end from the outside domain of the study area is negligible. Table (5) shows the results within different methods to minimize the error which is the RMSE and the Nash-Sutcliffe Coefficient of Efficiency (NSCE) (Nash & Sutcliffe, 1970), the NSCE generally range from -∞ to 1, where 1 is perfect match, 0 mean the model predictions accurate with the mean observation data, and values less than 0 mean the observed average is a better than the model. As per the NSCE methods it is shows that Granada gauges is almost equal to one which is mean the observation data and the model are highly match, however, Big Sandy and Wild Horse gauges show poor match. The results of each stream gage are shown in Figure 23.

Table 5 Simulated data vs. observed data, compassion by RMSE and NSCE

Sim vs Obs							
	Min	Mean	Max	Std.S	**RMSE**	**NSCE**	**SUM**
Granada	-3.456	-0.248	4.593	0.890	**0.9226**	**0.9339**	**249**
Big Sandy	-0.874	-0.045	1.587	0.235	**0.2392**	**-0.8152**	**17**
Wild Horse	-1.541	-0.066	0.455	0.276	**0.2832**	**0.0355**	**23**

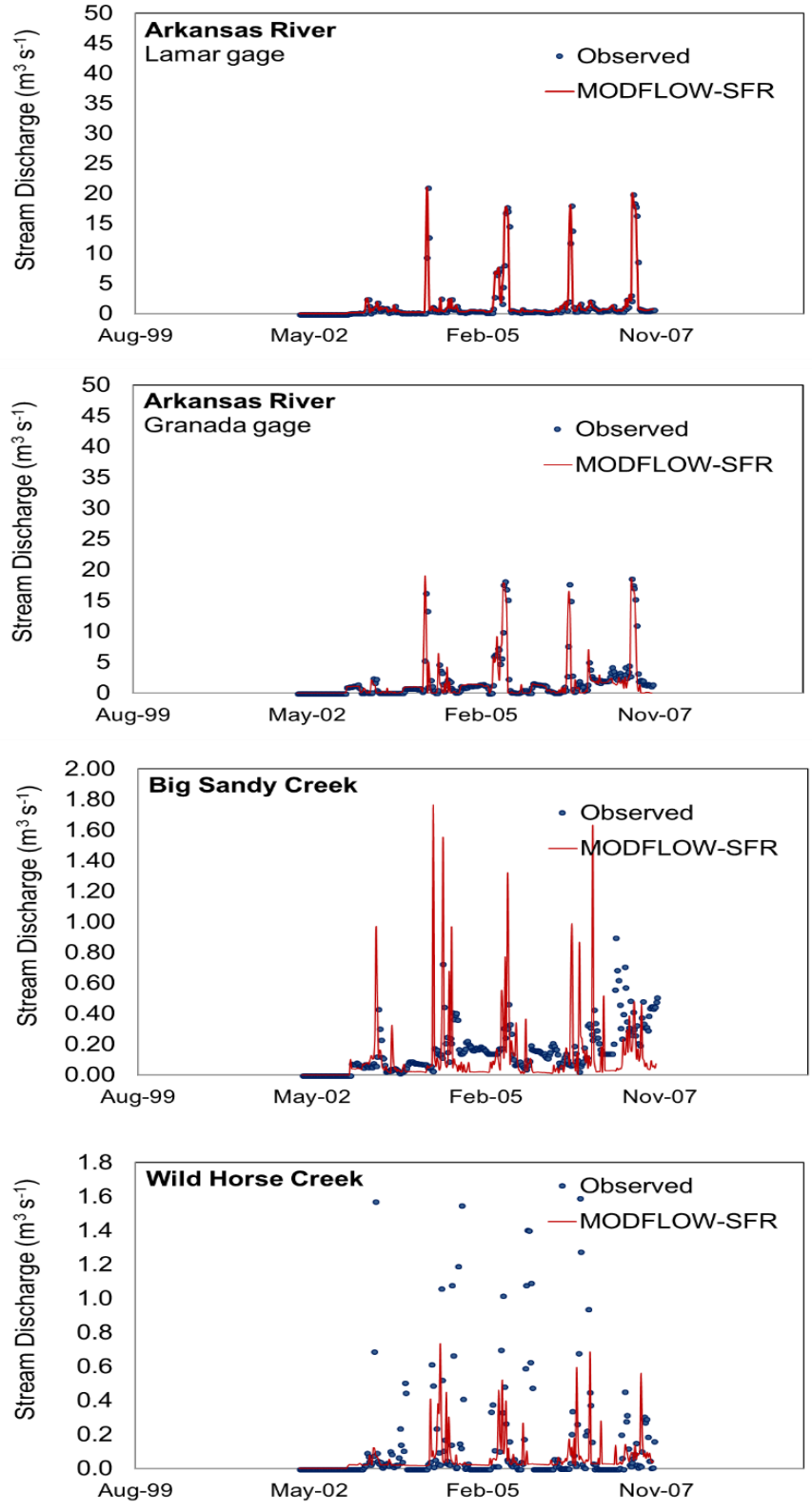

Figure 19 MODFLOW stream gage calibration

4.2 Se and N Reactive Transport Results

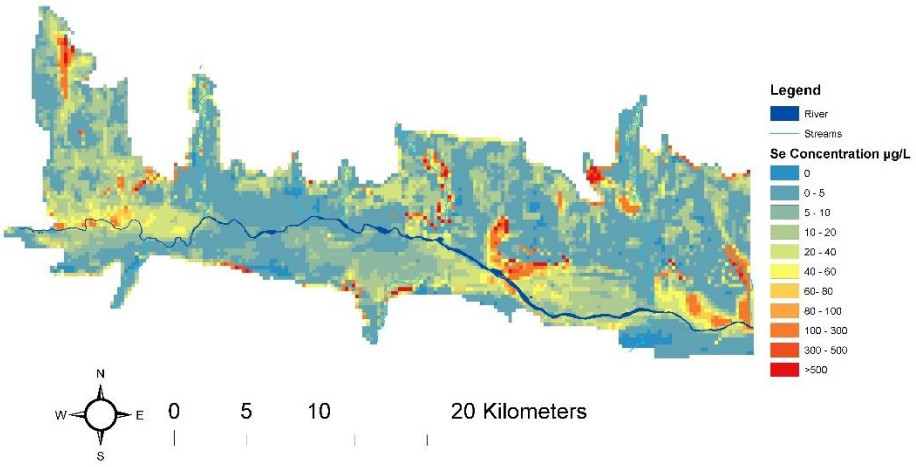

Figure 20 Average simulated Se groundwater concentration µg/L

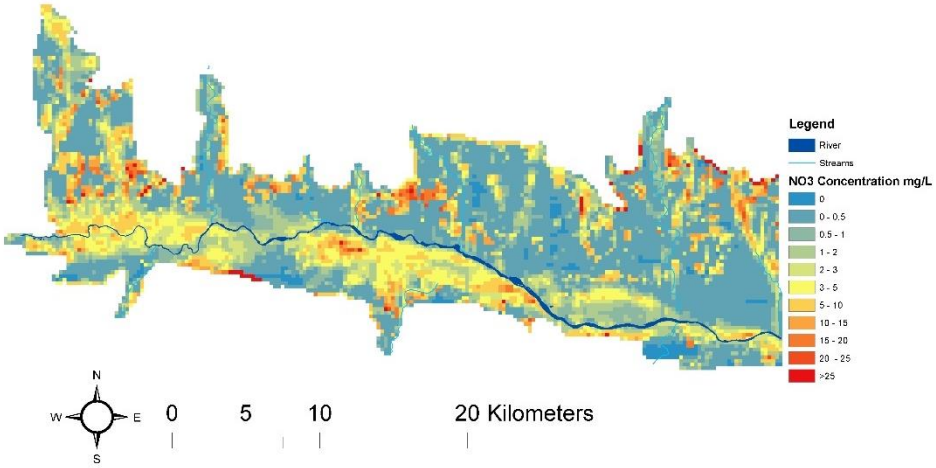

Figure 21 Average simulated NO_3 groundwater concentration mg/L

These Figures (20-21) illustrate the spatial map that shows the average groundwater concentrations of Se and NO_3. The average, maximum, minimum groundwater concentration of Se are, 26.9 µg/L, 3976.3 µg/L, and 0 µg/L, respectively. Where, the average, maximum, minimum groundwater concentration of NO_3 are, 2.6 mg/L, 84.6 mg/L, and 0 mg/L, respectively. Figure (20) shows the concentration of Se is high at the areas that the effected by the shale bedrock, near the Buffalo creek and the upstream that near to Buffalo irrigated canals and

downstream. However, there is a low concentration at the areas that far away from the shale bedrock, and that in middle of the stream. Figure (21) shows the concentration of NO_3 is high at the upstream and Fort Lyon irrigated canals. However, there is a low concentration at the downstream.

The final manual and automated results calibrated from the RT3D-OTIS for both groundwater and surface water parameters are shown in the following Table (6) and (7), respectively. Table (6) illustrates that the most valuable parameters which are $\boldsymbol{\lambda_{SeO_4}^{het}}$ and $\boldsymbol{\lambda_{NO_3}^{het}}$ that affect the simulated model in each sub region, however, other parameters that have similar USR values for all the region and it is used for the DSR. In addition, all of these values are within the range discussed in the literature.

Table 6: Final groundwater calibrated parameters

GW sub-region	$\boldsymbol{\lambda_{SeO_4}^{het}}$ (1/day)	$\boldsymbol{\lambda_{SeO_3}^{het}}$ (1/day)	$\boldsymbol{\lambda_{NO_3}^{het}}$ (1/day)	$\boldsymbol{\lambda_{NO_3}^{aut}}$ (1/day)	λ_{Nit} (1/day)
1	0.205	0.02	0.10	0.10	0.20
2	2.010	0.02	0.12	0.10	0.20
3	0.02	0.02	0.20	0.10	0.20
4	0.02	0.02	0.20	0.10	0.20
5	0.029	0.02	0.16	0.10	0.20
6	0.202	0.02	0.20	0.10	0.20
7	1	0.02	0.14	0.10	0.20
8	1	0.02	0.20	0.10	0.20
9	0.645	0.02	0.18	0.10	0.20
10	1	0.02	0.15	0.10	0.20
11	0.066	0.02	0.16	0.10	0.20
12	2.263	0.02	0.14	0.10	0.20

13	1	0.02	0.12	0.10	0.20
14	0.02	0.02	0.17	0.10	0.20
15	0.02	0.02	0.15	0.10	0.20

Table 7: Final surface water calibrated parameters

Parameters	
ρ (g/m^3)	4000
λ_{SeO4} (1/day)	1.50
$\lambda_{SeO_4}^{assim}$(1/day)	0.05
$\lambda_{SeO_4}^{vol}$(1/day)	0.05
DF_{NO3}	1

The comparison has been analyzed between the observation data and simulated results for the 40 years of simulation for Se and NO_3 concentrations within the 15 sub-regions for groundwater. The monitoring wells that were located in each sub-region have been averaged during the calibration periods and subsequently, the testing period, where the model results have been combined and averaged, then compared with observation data. The model result has been obtained as the last 5 years of simulation for layer number 4, since it's an approximate period that the model is simulating the data appropriately and the chemical reactions have been simulated for a long period. Also, the model data are obtained from the layer 4 since its modeled as the depth of the screen of the groundwater monitoring well. In addition, the shale marine layer is one of the key factors that affect and increase the concentration of Se, since it oxidizes with the O_2 at a specific location. Thus, by using the National Geologic Map Database from the U.S Geological survey that shows the location of the shale marine in the DSR and applying it within

the ArcGIS, the model can predict good results for both the Se and NO_3 concentrations. As seen below, Figure (22)) illustrate the shale marine location from the USGS and ArcGIS.

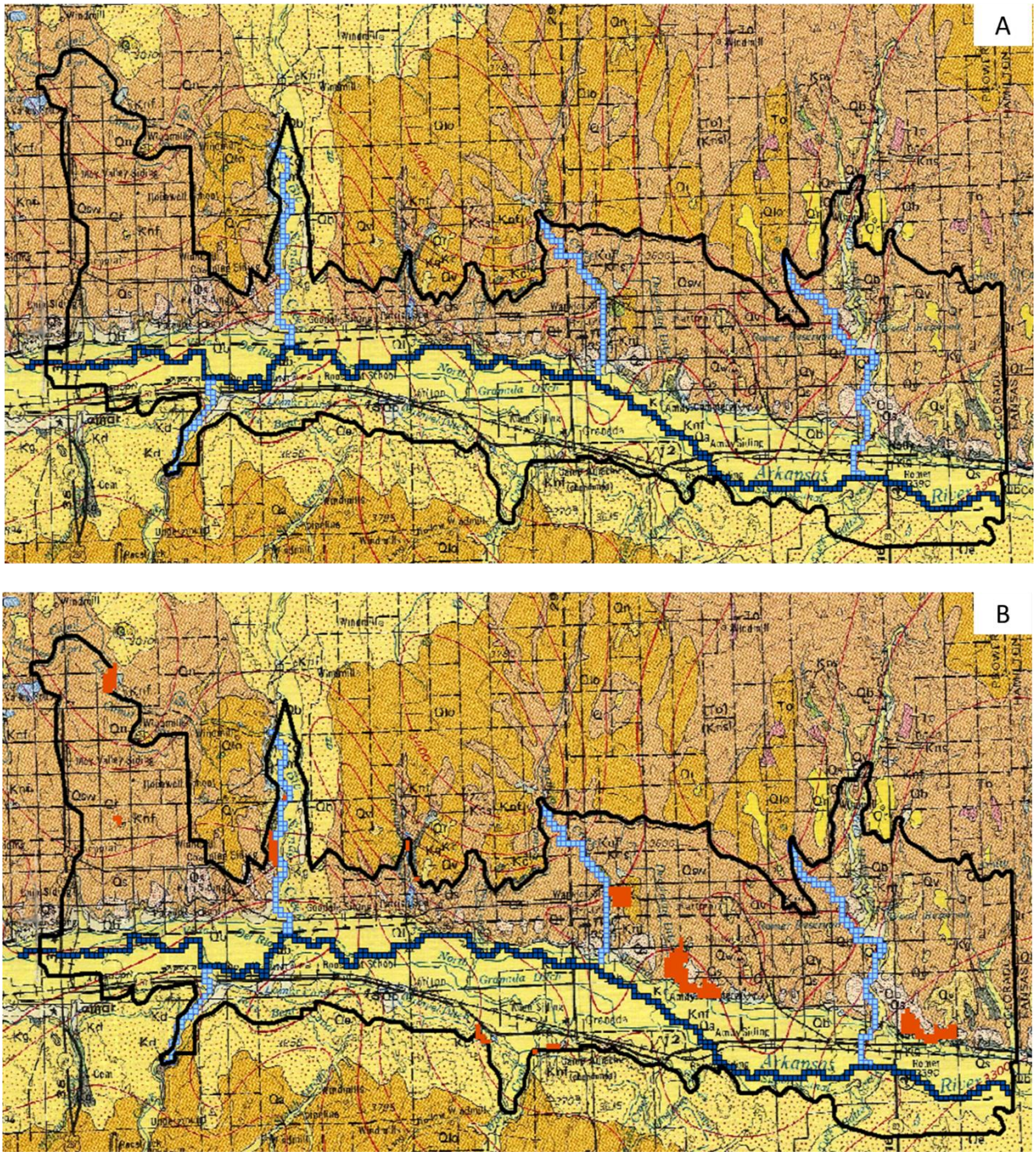

Figure 22 Shale bedrock, (Sharps, 1976)

As such, once the shale layer had been identified and modified in the DSR, the model simulated reasonable values for both Se and NO_3. Figure 23 shows the groundwater calibration and testing results for each sub-region. The uncertainty of the discrepancy scale that comes from the measurement error, and the whiskers that represented in Figure 23 for the observation values illustrate $\pm$ standard deviation of the observation data at each sub region. The average coefficient of variation (CV) of the electrical conductivity (EC) within each filed in the USR is equal to 0.42 for the USR (Bailey et al., 2014), and it is assumed the same CV in the DSR.

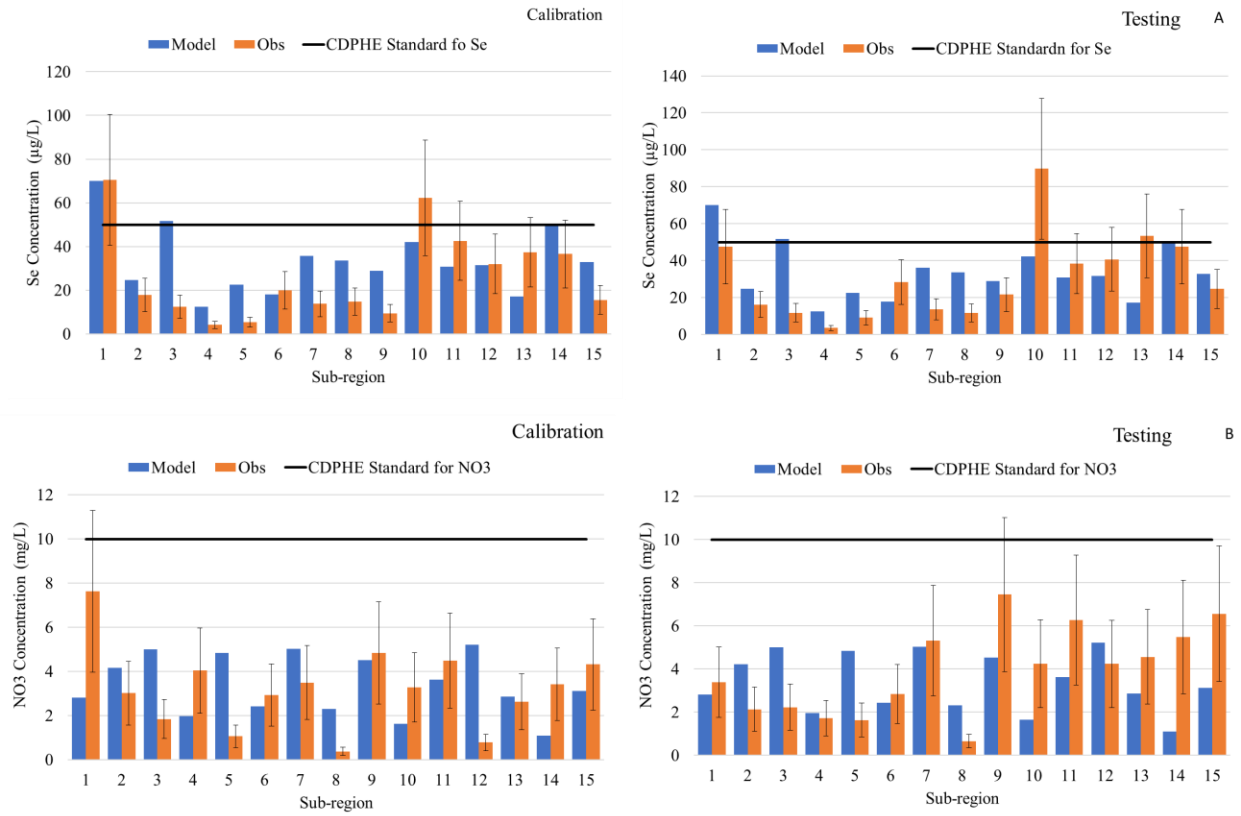

Figure 23 Groundwater calibration along with the CDPHE Standard for (A) Se and (B) NO_3

The results show that sub-regions 1,10, and 11 have a high concentration of Se, with the observations data valued at 70, 62.1, and 42.5 µg/L, respectively. This is due to the presence of the shale marine layer that is in contact with the aquifer. For the sub-region number one, there

was a monitoring well that had values from 2003 to 2004 and it had Se concentrations with a value of 3,760 µg/L which was notably a very high concentration of Se. Thus, this well has been removed since it was more than twice the standard deviation. Similarly, to the NO_3 concentrations at the sub-regions 1,9,11, the concentration was 7.6, 4.8, and 4.4 mg/L, with the same reasons being factored in. In addition, at the same region of the Se, the NO_3 has a high concentration with 685 mg/L. The model shows good matching with the observations values for the Se concentration. However, the model shows higher prediction at some regions, perhaps due to the flow and the concentration at the riparian zone decreased due to the denitrification, which is affected by the chemical reactions. Also, the observations values have few monitoring well in those regions. Furthermore, the measured values through the entire irrigation fields may not represent appropriate aquifer condition, also, point comparisons are not always good even if the model predict the major concentrations values of Se and NO_3, since the spatio-temporal averaging of the hydro chemical process (Shultz et al., 2018).

Finally, the model and the observations data show a good match at the calibration and testing periods. Similarly, this is the case with the NO_3 concentrations, and the matches between the model and the observation data. In conclusion, the uncertainty of the model can be described by the following Tables that shows the absolute difference between the simulated model and the observed values at each sub region and the total of all sub regions. These residuals occur due to several factors, such as lack of proper model parameterization, missing chemical processes in some of the model domain, and the coarseness of the finite difference grid. Therefore, matching between observed values and simulated values at a specific location is not the main objective of the calibration, rather to simulate the overall regional trends of solute contamination and transport. Table (8) represent the absolute difference between the model and the observed and

also it is compared against the pre-calibrated model, it is illustrated that the calibration model has better matching than the pre-calibrated model with difference around 38% of improvement. The total absolute difference in the calibrated model for calibration period and testing period are 216 and 266, respectively, compared with pre-calibrated model with total of 570.

For NO_3, the model shows that good prediction with the observation data and its mostly fall between the standard deviation bars that account for uncertainty due to measurement error and scale discrepancy that represent in Figure (23). The absolute difference between the model and the observed compared against the pre-calibrated model, it is showed that the calibration model has better matching than the pre-calibrated model with difference around 53% of improvement. The total absolute difference in the calibrated model for calibration period and testing period are 30 and 30, respectively, compared with pre-calibrated model with total of 57. So, that mean the model is calibrated and can be used as the baseline.

Table 8: Determine the uncertainty of groundwater calibration for Se

Se Concentration in groundwater	**Calibration Period (2003-2005)**	**Testing Period 2006-2007**	**Pre-Calibration**
Sub region	Absolute difference Model - Observed	Absolute difference Model - Observed	Absolute difference Model - Observed
1		22.6	145.4
2	6.9	8.6	3.3
3	39.3	39.9	50.5
4	8.5	9.0	0.3
5	17.1	13.3	14.3
6	2.0	10.5	5.0
7	21.8	22.5	46.5
8	18.8	22.0	98.7
9	19.5	7.3	13.2
10	20.1	47.5	8.8

11	11.7	7.5	6.7
12	0.5	9.1	7.0
13	20.2	36.1	5.7
14	12.7	1.9	125.6
15	17.3	8.2	39.7
Total	216.7	266.2	570.5

Table 9: Determine the uncertainty of groundwater calibration for NO_3

GW NO3	**Calibration Period (2003-2005)**	**Testing Period 2006-2007**	**Pre-Calibration**
Sub region	Absolute difference Model - Observed	Absolute difference Model - Observed	Absolute difference Model - Observed
1	4.8	0.6	39.7
2	1.2	2.1	1.7
3	3.1	2.8	1.6
4	2.1	0.3	0.6
5	3.8	3.2	3.0
6	0.5	0.4	0.5
7	1.5	0.3	2.0
8	1.9	1.7	1.5
9	0.3	2.9	1.1
10	1.6	2.6	0.4
11	0.9	2.6	0.8
12	4.4	1.0	0.1
13	0.2	1.7	1.9
14	2.3	4.4	1.9
15	1.2	3.4	0.2
Total	29.9	29.9	57.0

Figure (24) shows the simulated groundwater mass loading of Se and NO_3 (kg/day/km), compared with results from a stochastic surface water mass balance model and the solute rate for Se and NO_3. The mass balance model used a daily time step from October 1st, 2006 to September 30, 2010. So, the model tested against the data from 2006 – 2007 (the testing period), and the results shows that the model within the entire river reach. The mass loading that obtained from

the model it is generally between the 97.5 % and 2.5 % range of probability interval for Se and NO_3.

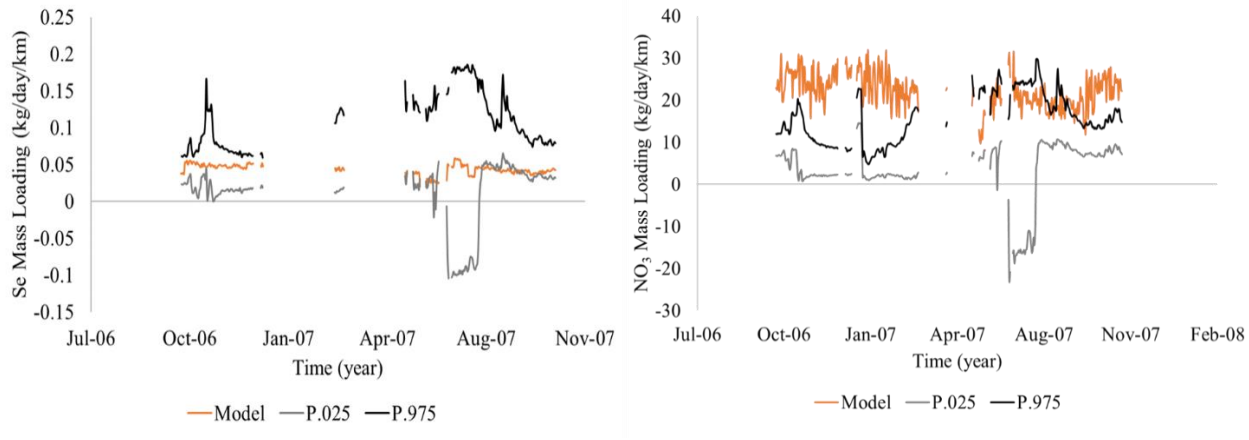

Figure 24 Mass loading to the Arkansas River (kg/day/km) (A) Se and (B) NO_3

In conclusion, the final groundwater calibration has been compared with the Colorado Department of Public Health and Environment (CDPHE) standard for Se and NO_3 in drinking water with values of 50 µg/L and 10 mg/L, respectively. Figure (23) shows the final calibration with the standard. Also, the results show that for the Se, it is mostly less than the CDPHE standard, except in some sub-regions where it is higher than the standard. For NO_3, it is interesting to note that both the model and observed values are less than the standard.

For stream calibration, the Arkansas River was divided into six stream segments and 4 main tributes and it was simulated for both Se and NO_3. Like the groundwater calibration, the stream calibration was done for two periods, the calibrated and testing periods. Furthermore, the model simulated a 40-year simulation and the data compared with the last 5 years of the simulation. The Figure below illustrates the stream concentration for Se and NO_3. The results show acceptable estimation and simulations between the observations and the model values, since it is match with the magnitude and spatiotemporal of the stream concentrations. Se concentrations that are represented in the Figure (25) mostly have good matches and predicted

values, except for some streams and tributaries such as stream 3 ,7, and 9, alongside the Big Sandy Creek and the Buffalo Creek, Figure (26). On the other hand, NO_3 concentrations show good matches in the streams, but was under predicted at Big Sandy and Buffalo Creeks, Figure (27-28). For both Se and NO3, the model is not predicting good results with the observation data, especially at the Big Sandy Creek and this due to the Creek were shortened in length since the flow was not predicted accurately, shale layer lies under this area, and the overflow in the irrigated ditch has been dumped into the Big Sandy Creek which makes a high fluctuation in the model. Big Sandy Creek will affect the stream number 3 since it is feed the stream directly, same with the Buffalo Creek that feed streams number 7 and 9.

Similarly, to the groundwater calibration uncertainty, the NCSH and the absolute difference have been used to determine stream uncertainty and that shows the calibration period for Se concentration in stream has acceptable results than the testing period, Table (10). For NO_3, both calibration period and testing period have an error less than zero which is mean that the average observed values is better than the simulated period, Table (11). The model shows spatial uncertainty for the stream concentrations and this might cause due to the assumption of averaging the observation data and compared them with average simulated model.

Table 10: Determine the uncertainty of streams calibration using NCSH for Se

Se Concentration in stream	**Calibration Period (2003-2005)**			**Testing Period (2006-2007)**		
Stream NO.	**Absolute difference Model - Observed**	NCSH	NCSH Over The area	**Absolute difference Model - Observed**	NCSH	NCSH Over The area
Stream 1	2.34	0.83	0.15	0.25	1.00	-0.06
Stream 3	4.59	0.33		3.71	-0.01	
Stream 5,1	0.71	0.98		9.60	-5.38	
Stream 5,2	1.75	0.76		2.63	-2.63	
Stream 7	4.92	-2.96		7.36	-8.42	
Stream 9	1.92	-3.58		2.26	-6.31	

Clay Creek	0.56	1.00		0.51	1.00
Big Sandy Creek	21.75	-0.95		22.10	-0.17
Buffalo Creek	9.51	0.70		4.26	0.72
Wild Horse Creek	3.83	-6.21		2.16	0.57

Table 11: Determine the uncertainty of groundwater calibration using NCSH for NO_3

NO_3 Concentration in stream	**Calibration Period (2003-2005)**			**Testing Period (2006-2007)**		
Stream NO.	**Absolute difference Model - Observed**	NCSH	NCSH Over The area	**Absolute difference Model - Observed**	NCSH	NCSH Over The area
Stream 1	0.37	0.74	-1.23	0.10	0.93	-1.56
Stream 3	0.73	-3.76		0.64	-8.83	
Stream 5,1	0.33	-2.14		0.62	-6.11	
Stream 5,2	0.23	-1.23		0.06	0.81	
Stream 7	0.44	-5.37		0.33	0.10	
Stream 9	0.02	0.96		0.05	0.97	
Clay Creek	0.33	0.87		0.45	0.80	
Big Sandy Creek	3.53	-1.42		1.90	-3.42	
Buffalo Creek	1.46	-4.06		1.14	-6.12	
Wild Horse Creek	0.22	0.79		0.28	0.39	

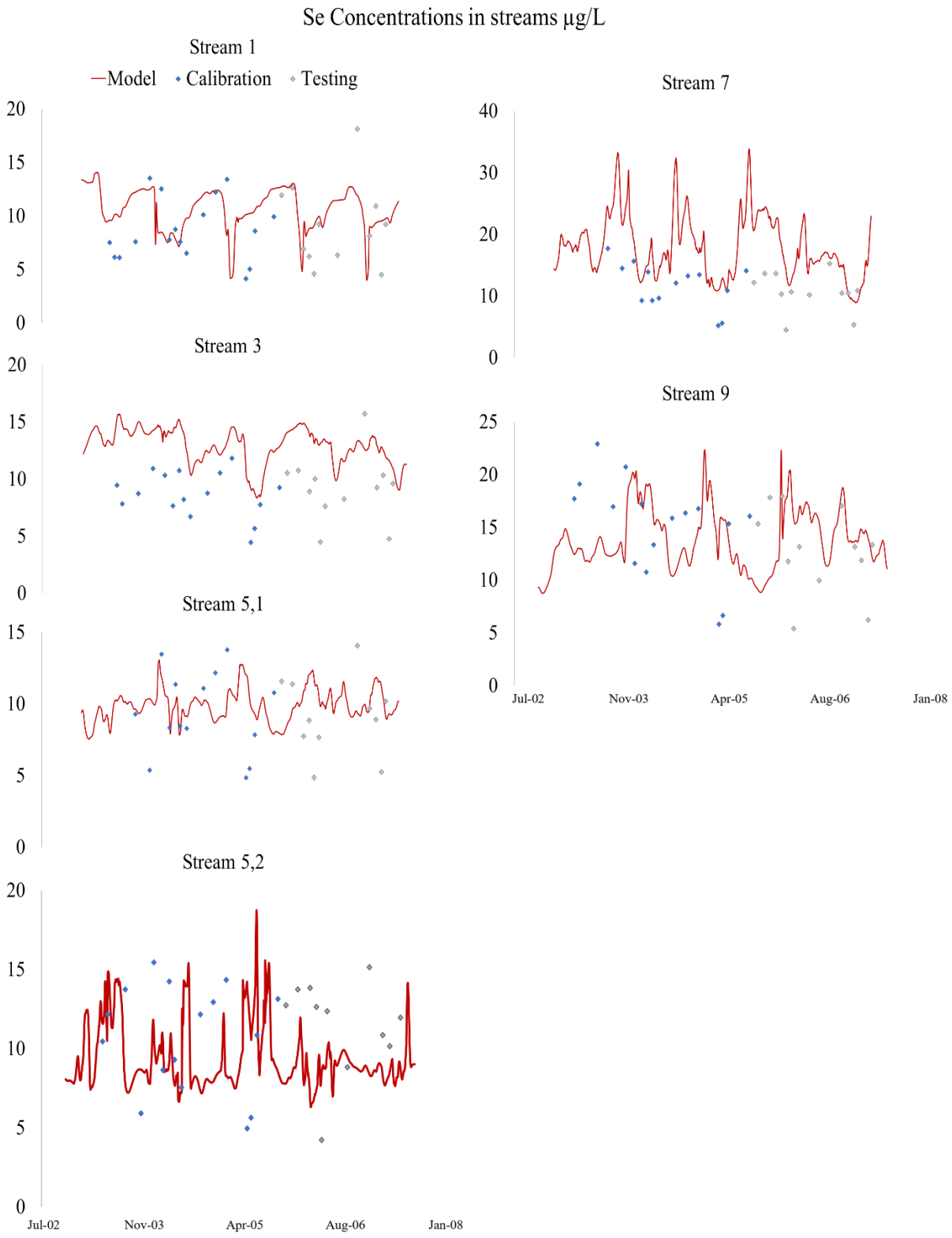

Figure 25 Simulated in streams calibration for Se

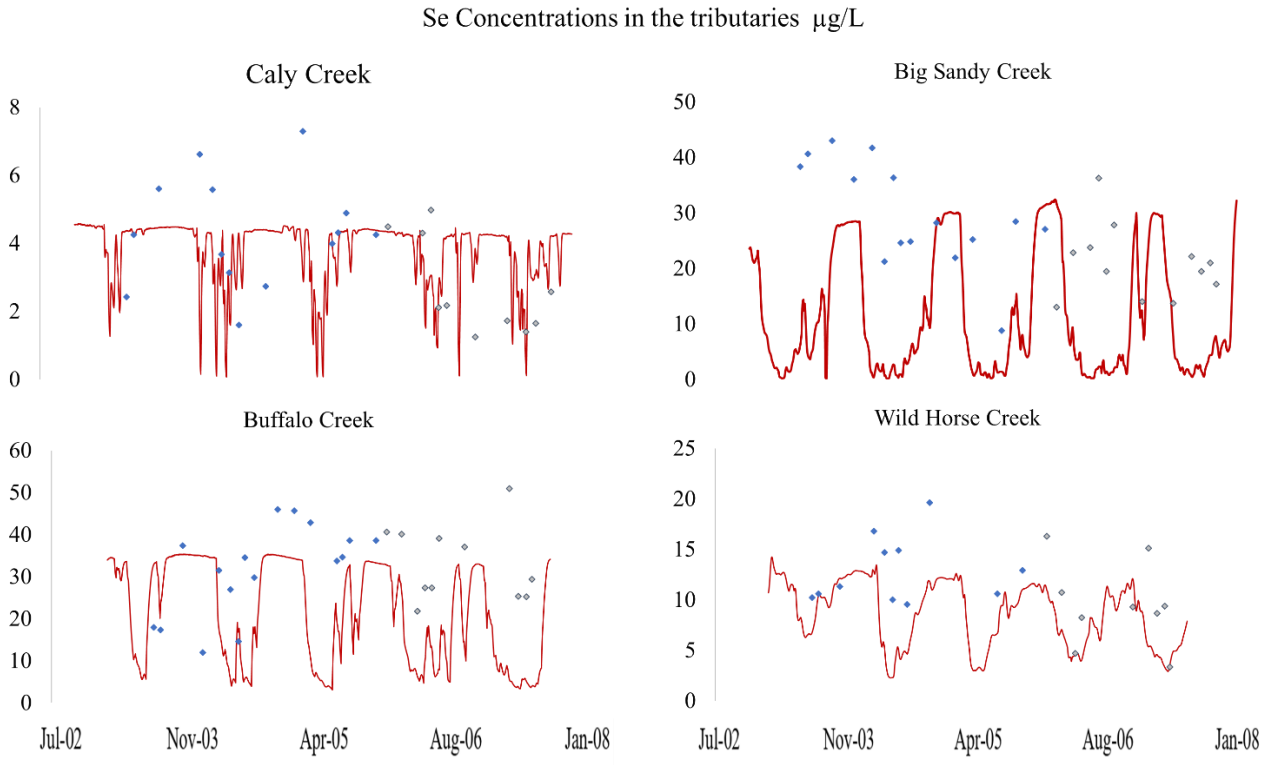

Figure 26: Simulated tributaries calibration for Se

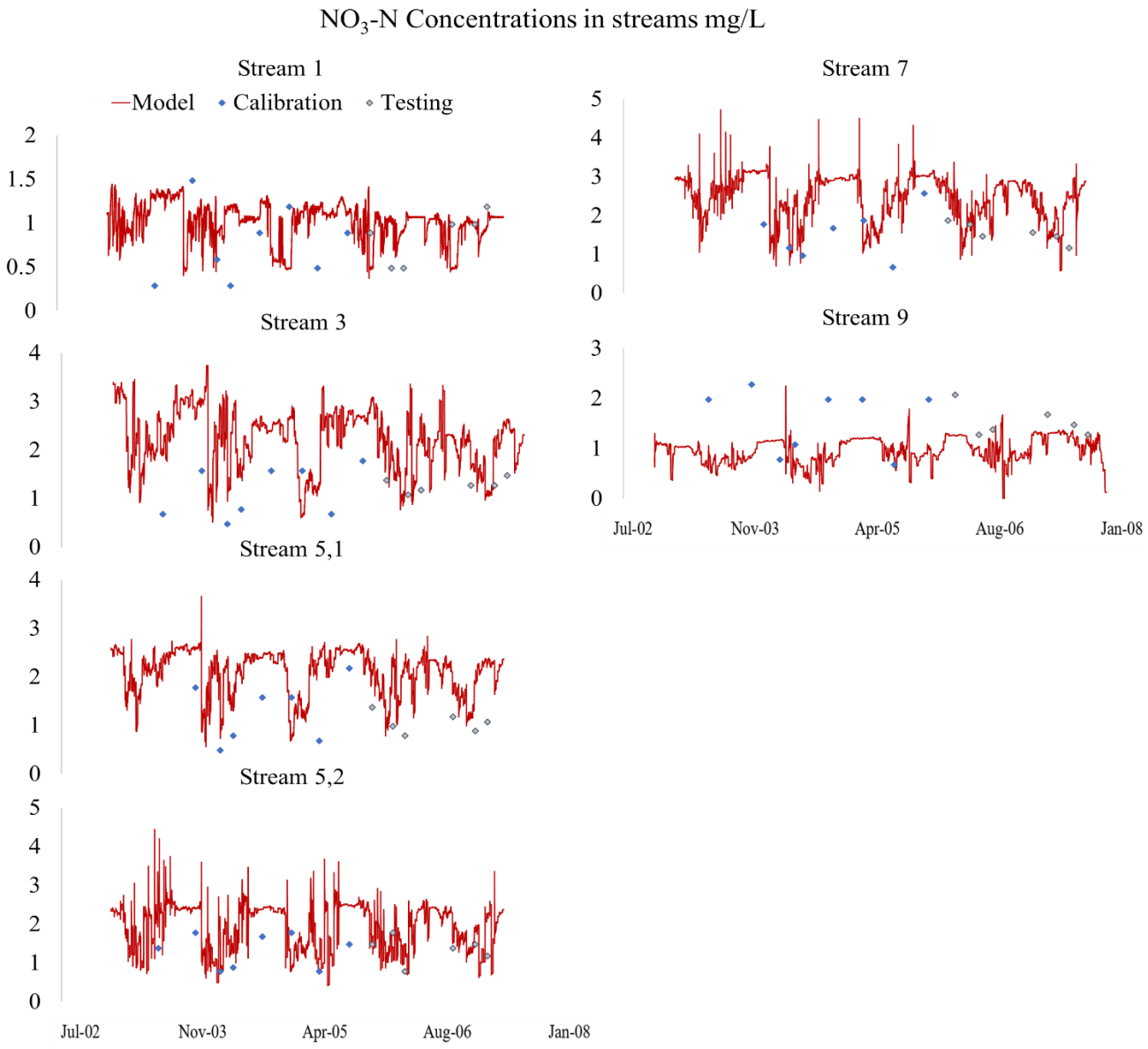

Figure 27 Simulated in streams calibration for NO_3-N

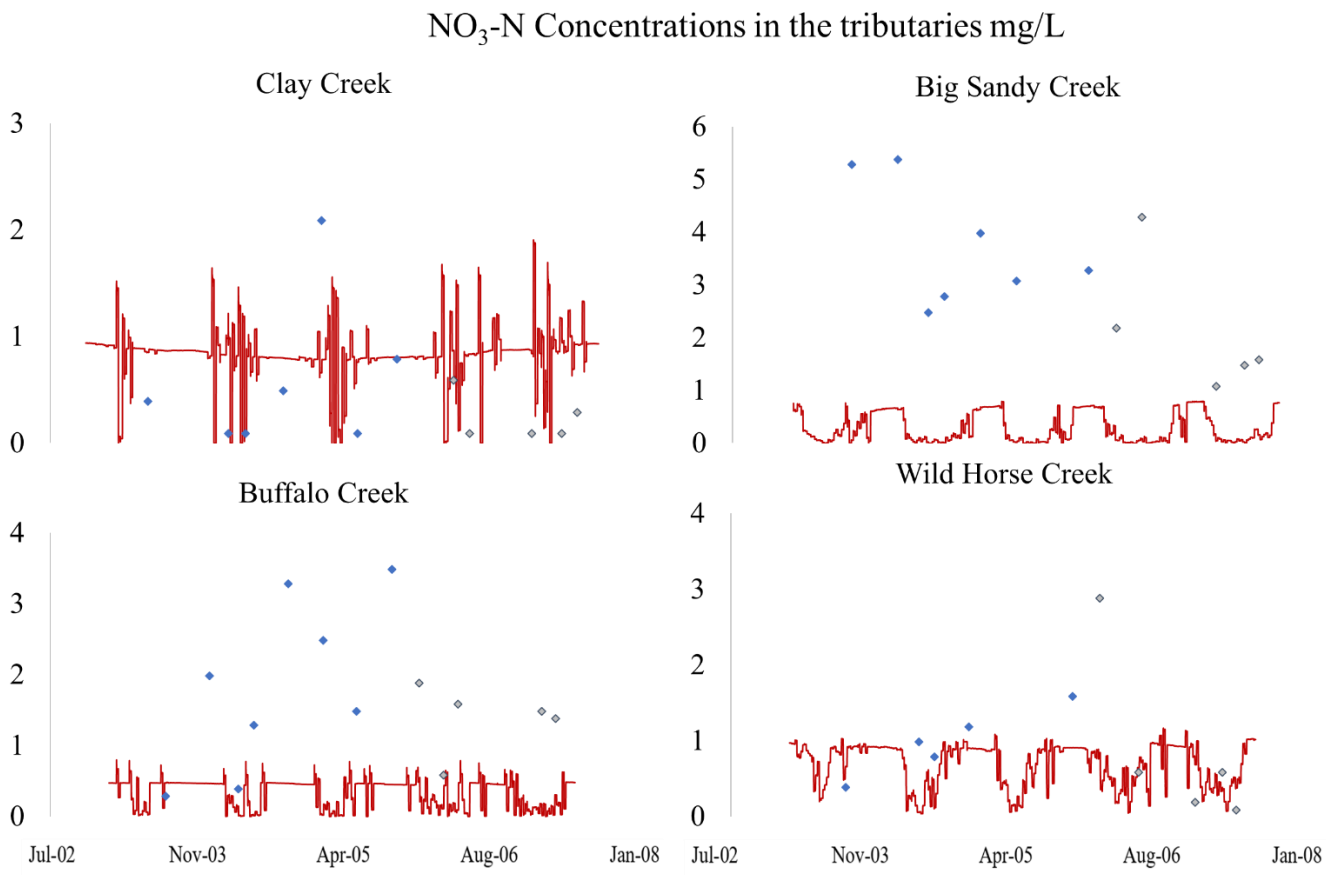

Figure 28: Simulated tributaries calibration for NO_3-N

Finally, the final streams and tributaries calibration have been compared with the Colorado Department of Public Health and Environment (CDPHE) standard for Se and total NO_3-N (NO_2-N + NO_3-N + NH_4-N) with values of 4.6 µg/L and 2 mg/L, respectively. Figure (29) shows the final calibration with the standard. Also, the results show that Se is mostly higher than the CDPHE standard for all streams and tributaries for both the model and the observations. For NO_3-N, both the model and observed values are higher than the standard, except for some tributaries, such as Big Sandy and Buffalo Creeks.

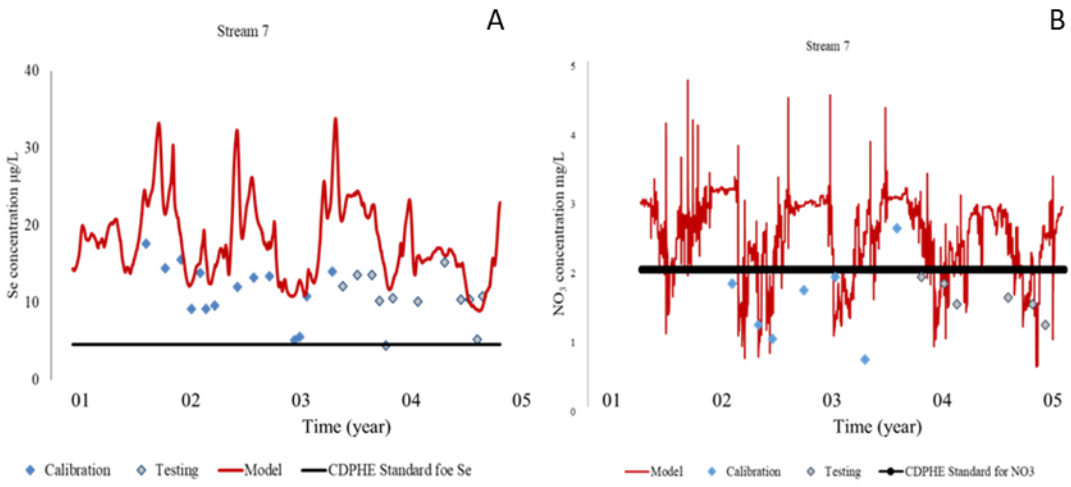

Figure 29 Streams calibration in comparison with the CDPHE standard for (A) Se and (B)NO_3-N

4.2.1 Baseline Result

The calibrated model that has been described in section 4.2 is used as baseline model to investigate the BMPs that decrease the concentrations of Se and NO_3 in groundwater, stream, and the mass loading that return to the Arkansas River. Figures 30-33 show results of the Baseline simulation. Figure 34 shows the temporal average concentrations of Se and NO_3 over the last 5 years of the 40-year simulation. The Se concentrations vary form 0 µg/L to 3760 µg/L, with an average of 61.3 µg/L. Where, the overall 85% of the observed value of Se is 52 µg/L which is above the USEPA groundwater standard of 50 µg/L. For NO_3, the concentration varies from 0 mg/L to 685 mg/L with an average of 9.7 mg/L. Where, the overall 85% of the observed value of NO_3 is 8.2 µg/L which is below the USEPA groundwater standard of 10 mg/L.

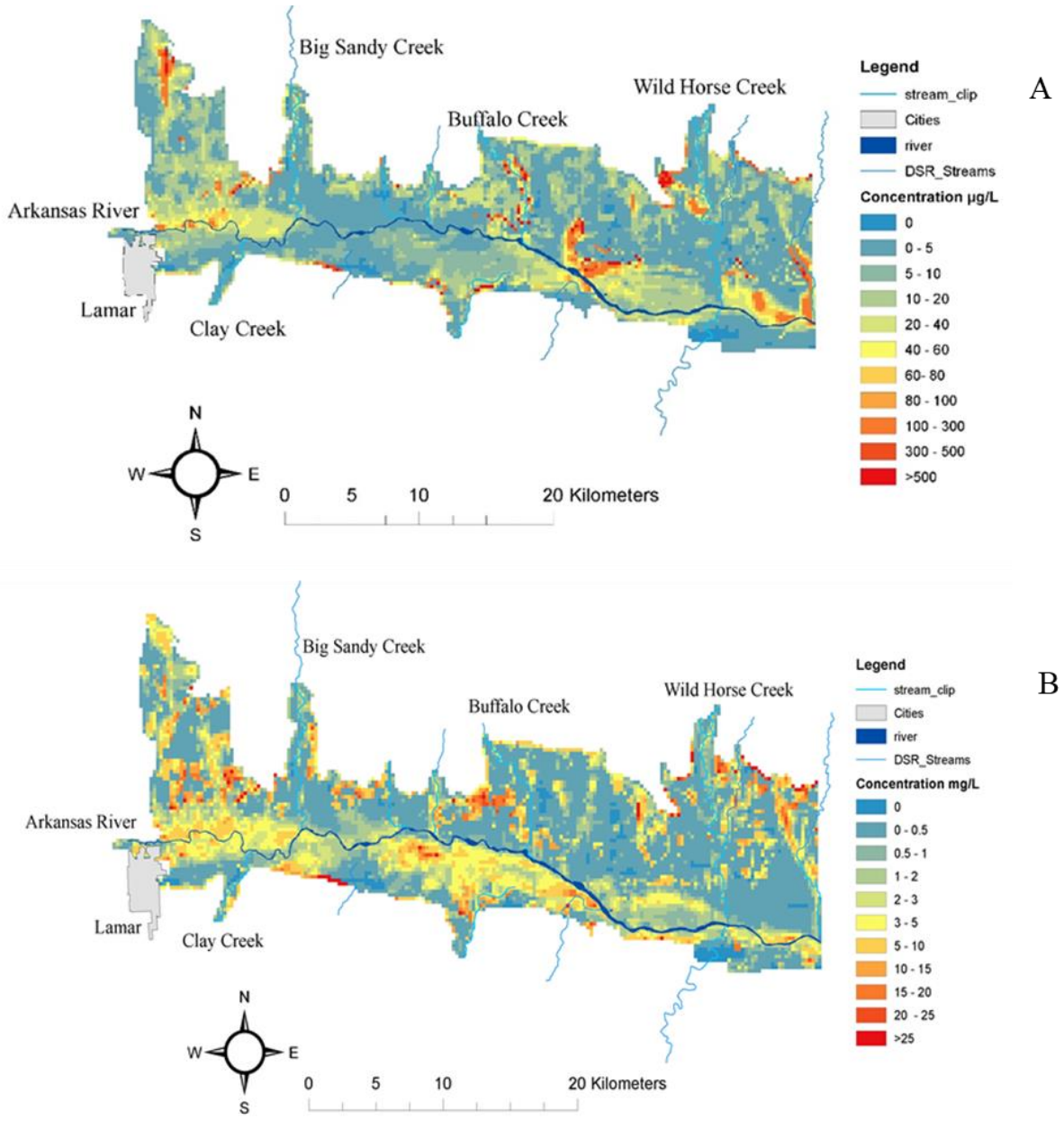

Figure 30 Simulated average groundwater concentrations over last 5-years of baseline condition (A) Se and (B) NO_3

Figure (31) illustrates the total mass loading to the Arkansas River for each day of the period, for (A) Se and (B) NO3. Figure (32) shows the daily volume of the groundwater return flow to the Arkansas River over the 40 years of the baseline simulation. Finally, Figure (33) shows stream concentrations of the average daily 85th percentile of simulated Se concentrations

and the average concentrations of the NO_3-N over the last 5 years of the baseline simulation. The CDPHE standards are shown on the plots for context.

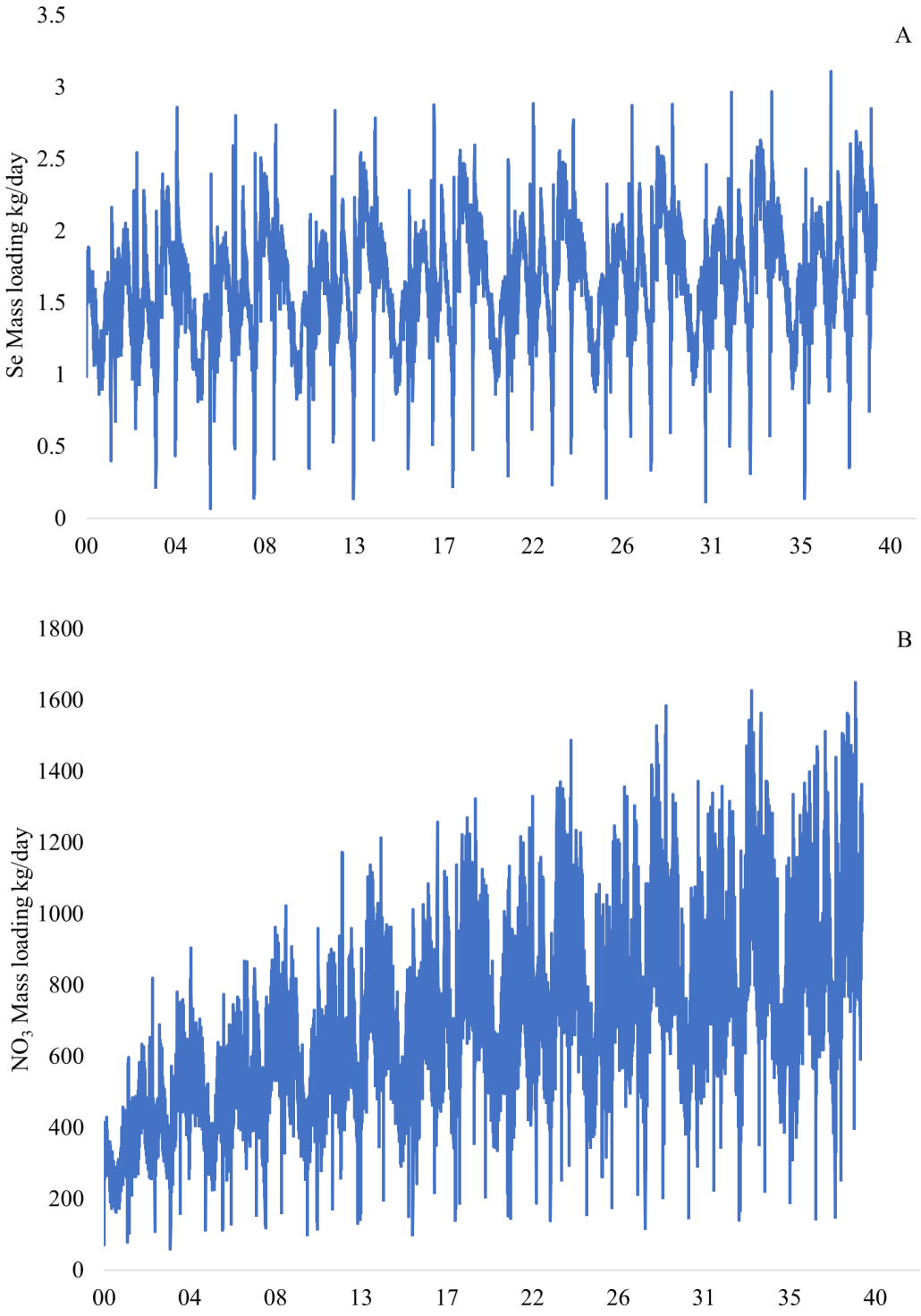

Figure 31 Simulated mass loading over the 40-years of baseline condition (A) Se mass loading and (B) NO_3 mass loading

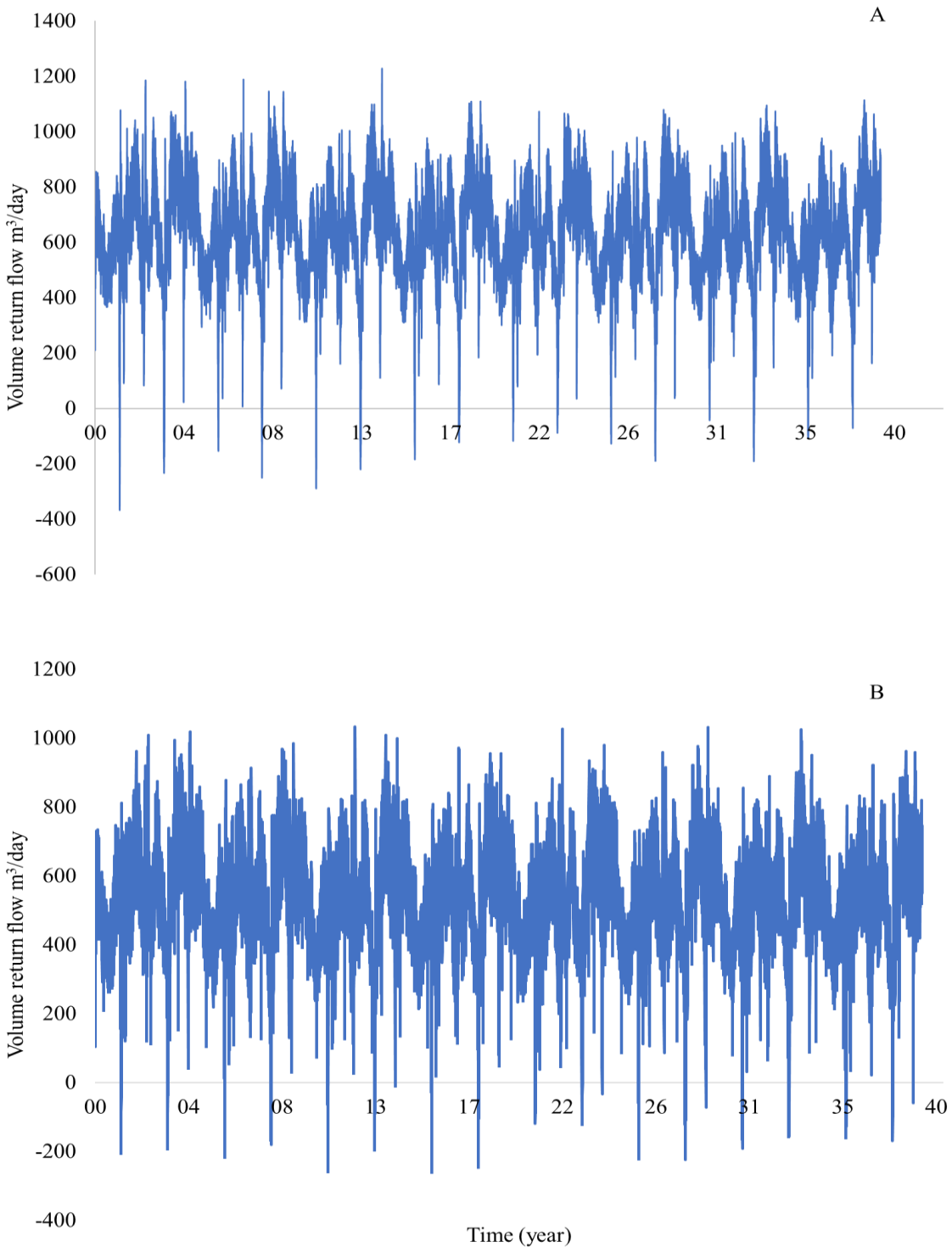

Figure 32 Simulated total return flow volume over the 40-years of baseline condition (A) Se and (B) NO_3

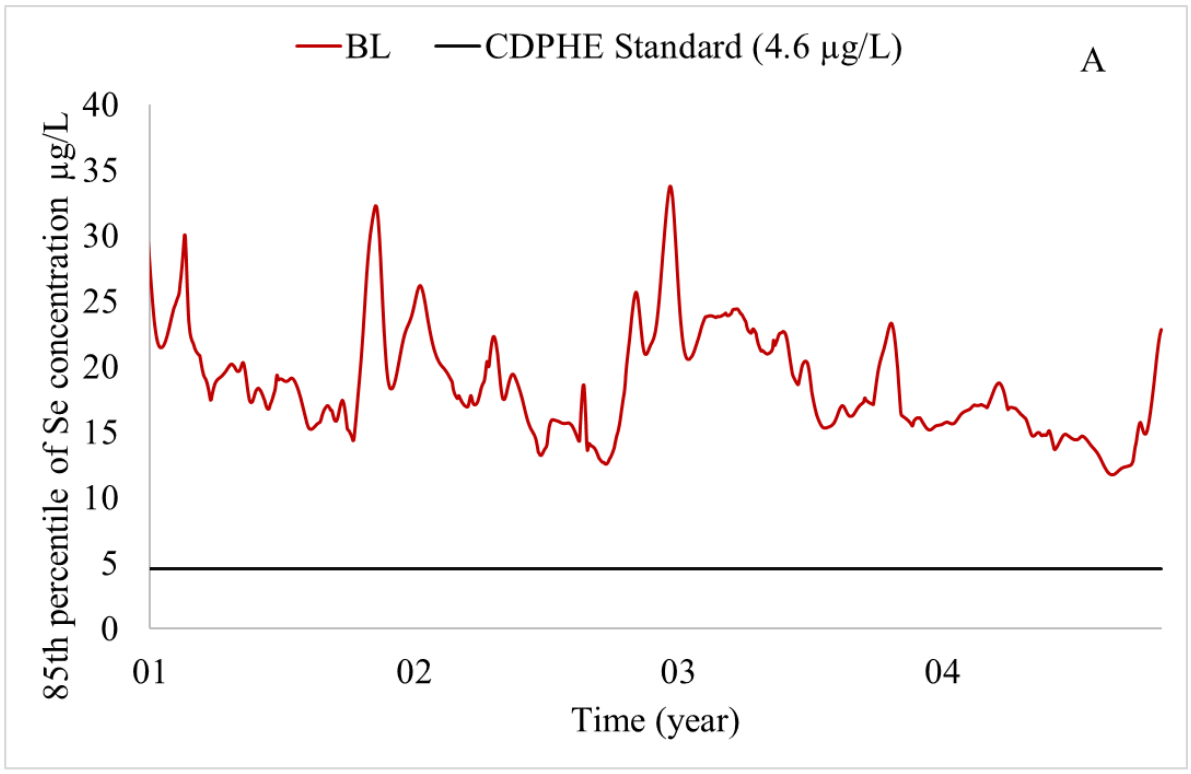

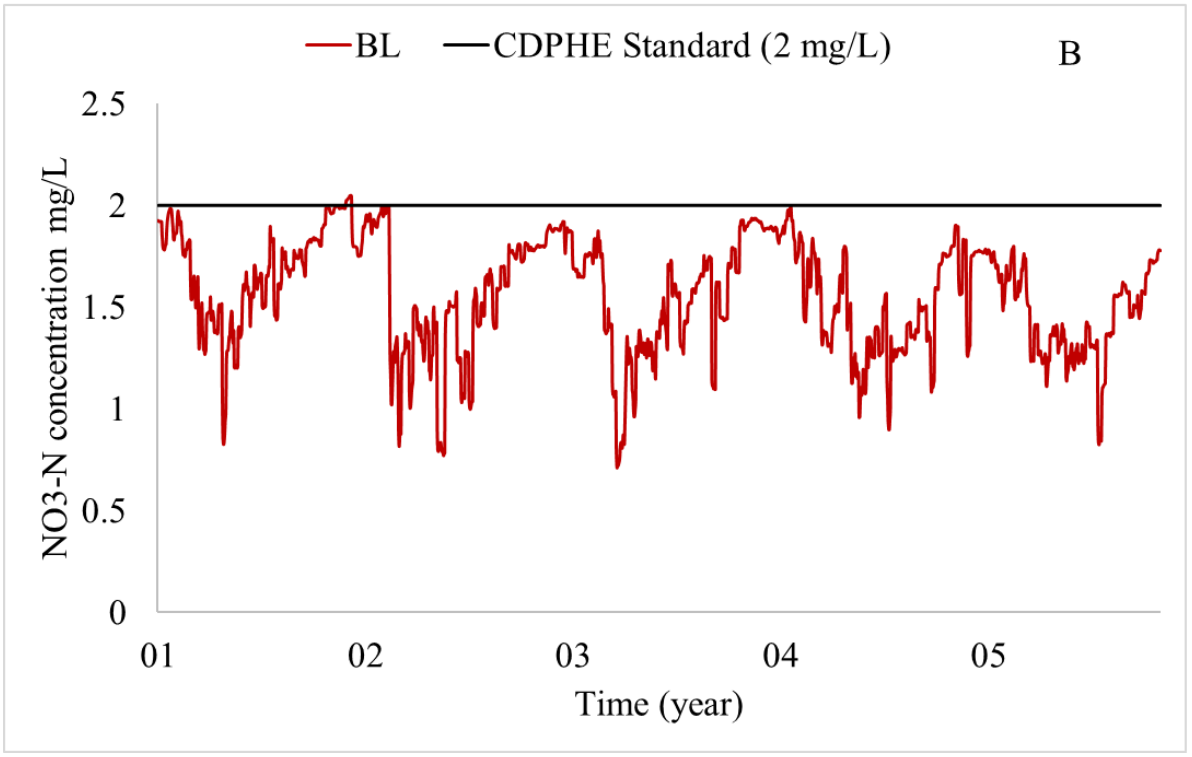

Figure 33 Simulated average surface water concentrations along the Arkansas River over the last 5-years of baseline condition (A) Se and (B) NO_3-N

4.3 Effect of Reduced Irrigation, Land Fallowing, and Canal Sealing BMPs

4.3.1 Groundwater Se and NO_3

9 different water management BMPs have been applied over the 40 years of simulation in order to investigate whether the concentrations of the Se and NO_3 contamination have been reduced. In addition, each of these BMPs were tested for three different levels, which were basic, intermediate, and aggressive implementations. Also, these BMPs was tested and compared against the baseline condition.

The effect of all 9 BMPs have been compared against the Baseline simulation over the 40-years of the simulation. Additionally, the BMPs have been tested against each of the 15 sub-regions that have been discussed in section 3.8, for both Se and NO_3. Figure (34 - 35) represents the temporarily average groundwater concentration decrease for Se and NO_3 for the last 5 years of the simulation. The average has been taken by factoring in the difference between the baseline and all the most aggressive level for each BMPs implemented in the area. Moreover, the blue colors that represent the reduction in the groundwater concentration occurred due to the BMPs implementation. However, the red color represented the increase in the groundwater concentration. As such, the concentration has been reduced mostly for all areas, except for when there are some net values that show high concentrations, particularly at the upper part of the study region (Fort Lyon canal) and the area between the Buffalo canal. Overall, the Figure showed that the implementation of the BMPs had a high impact in reducing the concentration, and some areas had high reductions while other areas had significantly increases. On the other hand, similar to the Se analysis, Figure (35) shows the average groundwater concentration of NO_3 has been reduced over the area, which meant the implementation of the BMPs had been affected for the study area. In addition, there are some areas that had net negative values and

other areas that had net positive values. Figure (34) show that there is a significate decrease of the concentration. Likely, Figure (35) show the difference of NO_3 groundwater concentrations between the baseline condition and each BMPs that implemented under the aggressive scenario, and at Figure (34.C) is shows a significate decrease of the concentration near stream.

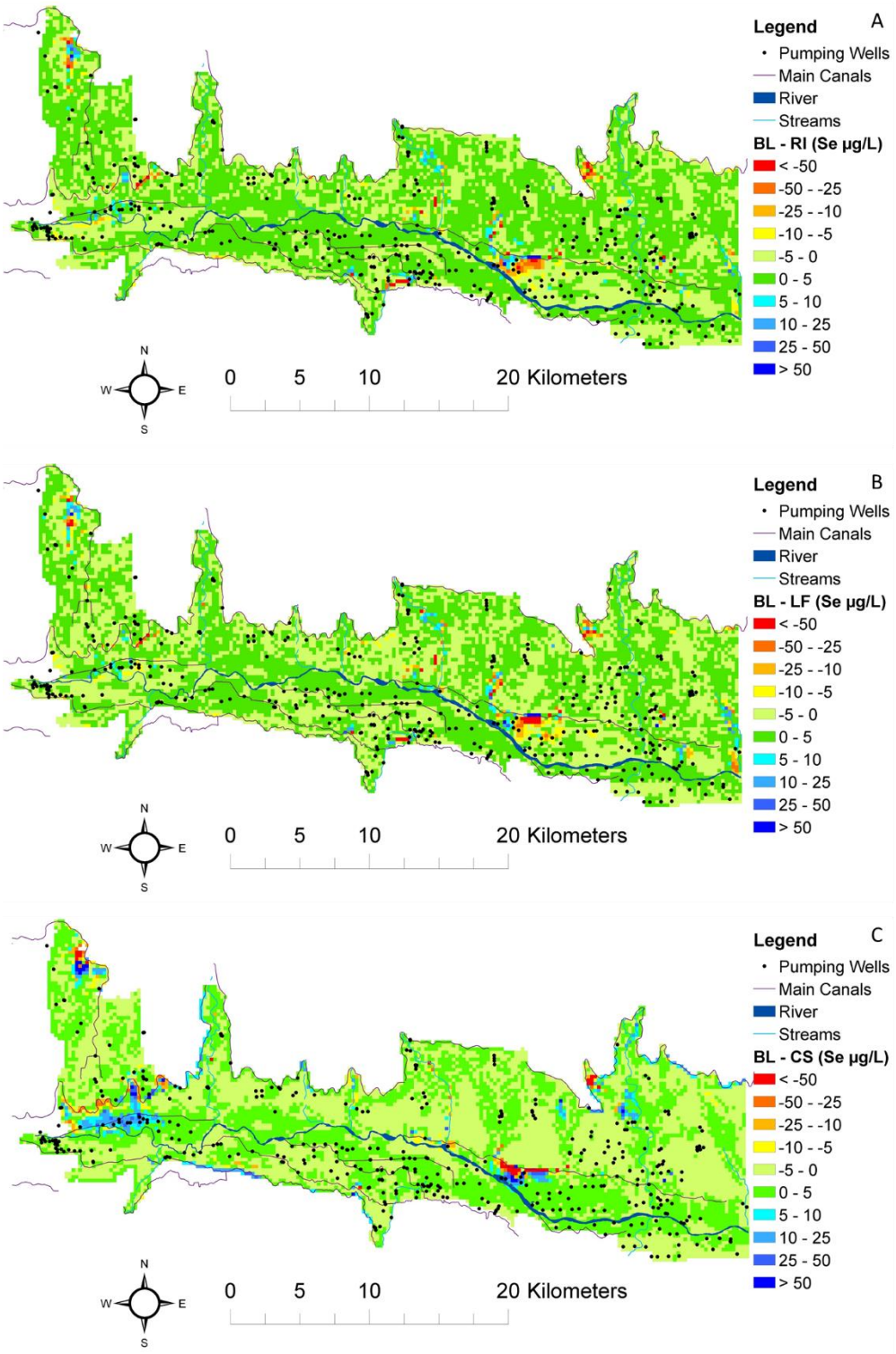

Figure 34 Difference in Se concentration between the Baseline and each BMPs (A) RI 30, (B) LF 30, and (C) CS 90, for the last 5 years of the 40-year simulation.

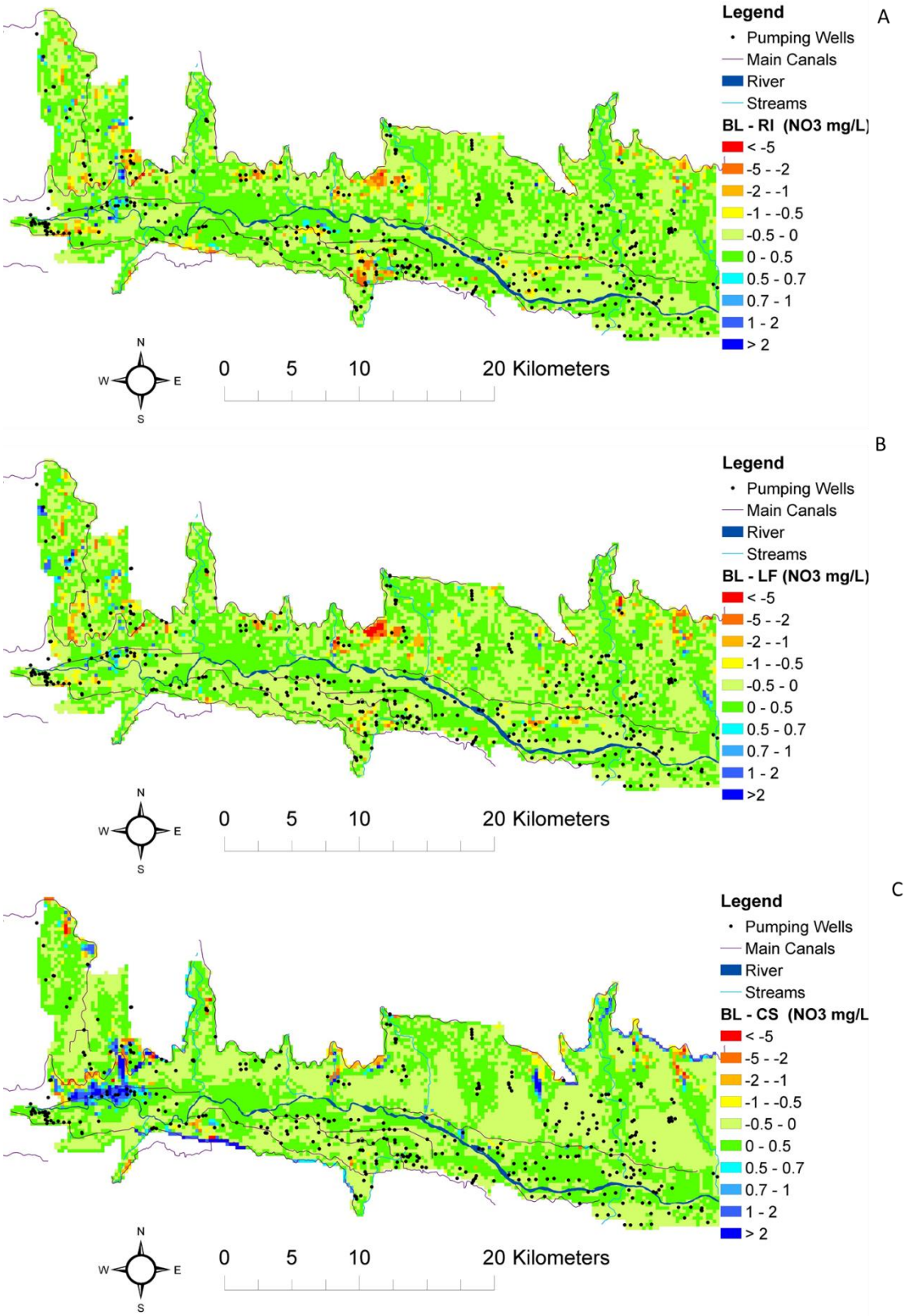

Figure 35 Difference in NO_3 concentration between the Baseline and each BMPs (A) RI 30, (B) LF 30, and (C) CS 90 for the last 5 years of the 40-year simulation.

The overall percentage reduction of the Se and NO_3 over the 40 years simulation has been accomplished by taking the difference between the baseline condition. The positive values mean that there is a reduction for the implementation. However, the negative values mean that there is an increased in the BMPs.

Figure (36) illustrates the total reduction of the Se along the 40 years simulation for all 9 BMPs for all the three scenarios: basic, intermediate, and aggressive. For Figure (36.A) the percent of reduced irrigation has been increased, which means the implementation of the reduced irrigation is not affecting the area in appropriate condition for the long simulation, especially for the aggressive scenario, where the percentage increased to 15%. Similarly, for Figure (36.B), the percentage of lease fallowing has been increased. This means that implementation was not affecting the area for the long simulation, especially for the aggressive scenario where the percent increased to 10%. However, both reduced irrigation and the lease fallowing showed that there was some reduction of the Se that reached 24% and 25%, respectively. On the other hand, Figure (36.C) shows the canal sealing had the most effective reduction of the groundwater and the reduction reached up to 40% under the aggressive scenario. This significant decreases of Se is mainly due to the sealing of the canals from the interaction between the groundwater and the direct contact with shale, thus leading to a high concentration of Se. Unlike the reduced irrigation and the lease fallowing implementations, the groundwater concentration has been increased and as such, this due to the slowing if the return flows that cause delineation in the water table, so the groundwater head gradient has been lowered. Then the reaction of the NO_3 and the DO will start again by interacting with the shale layer and the seleno-pyrite.

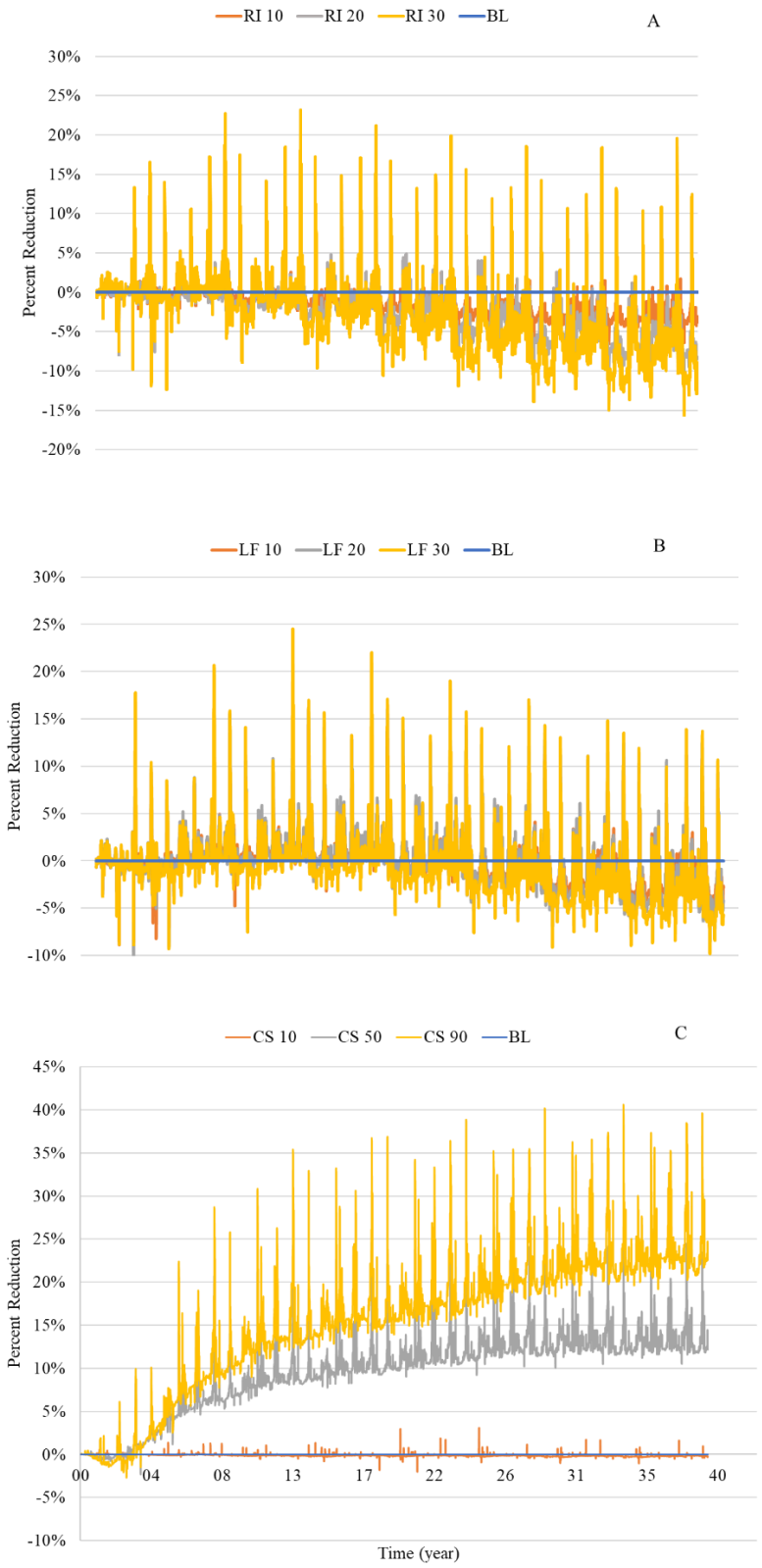

Figure 36 Groundwater concentration reduction for Se over the 40-years simulation (A) reduced irrigation, (B) lease fallowing, and (C) canal sealing compared with the baseline condition

Figures (37) shows that difference of depth to water table under the aggressive level for each BMP. Negative values indicate that the depth to water table has increased due to the BMP, i.e. a lower groundwater level results. Positive values indicate the depth to the water table has decreased, i.e. a high groundwater level results. Figures (37.A-37.B) illustrate that the water table has been lowered significantly along the agricultural areas of the study region (north side of the Arkansas River) and at the Buffalo Creek area under the RI and LF aggressive scenarios. The average depth to water table under the RI and LF are -0.8 m and -0.9, respectively. Figure (37.C) shows that the water table has been lowered mainly within the vicinity of the irrigation canals, within average depth to water table -1.8 m under the CS. Figure (38) shows the explanation of lowering or raising the water table under the BMP scenarios.

The concentrations of Se and NO_3 are entering the aquifer throughout the irrigated water and from the ET or the upflux that allow leaching Se and NO_3 to the crop root zone. In addition, RI and LF BMPs lead to less water being applied to the root zone, leading to a lowered water content in the soil profile and therefore a higher concentration of Se and NO_3. The lowering of the water table reduces upflux from the saturated zone, thereby preventing movement of Se and NO_3 mass into the soil profile. Furthermore, the LF applied at the area by assuming that the irrigation is removed from the fallowed land and the ET is reformed to represent the absence of the crop demand (Morway et al., 2013). Sealing the earthen irrigation canals decreases seepage, leading to a lowering of the water table. In contract to the RI and LF scenarios, this reduction in soil profile flushing occurs only within the vicinity of the canals, with typical irrigation practices occurring throughout the remainder of the cultivated region in the model domain. Therefore, elevated concentrations do not occur in the shallow groundwater zone, and a lowering of the

water table results in less Se and NO_3 mass entering the Arkansas River via groundwater mass loading.

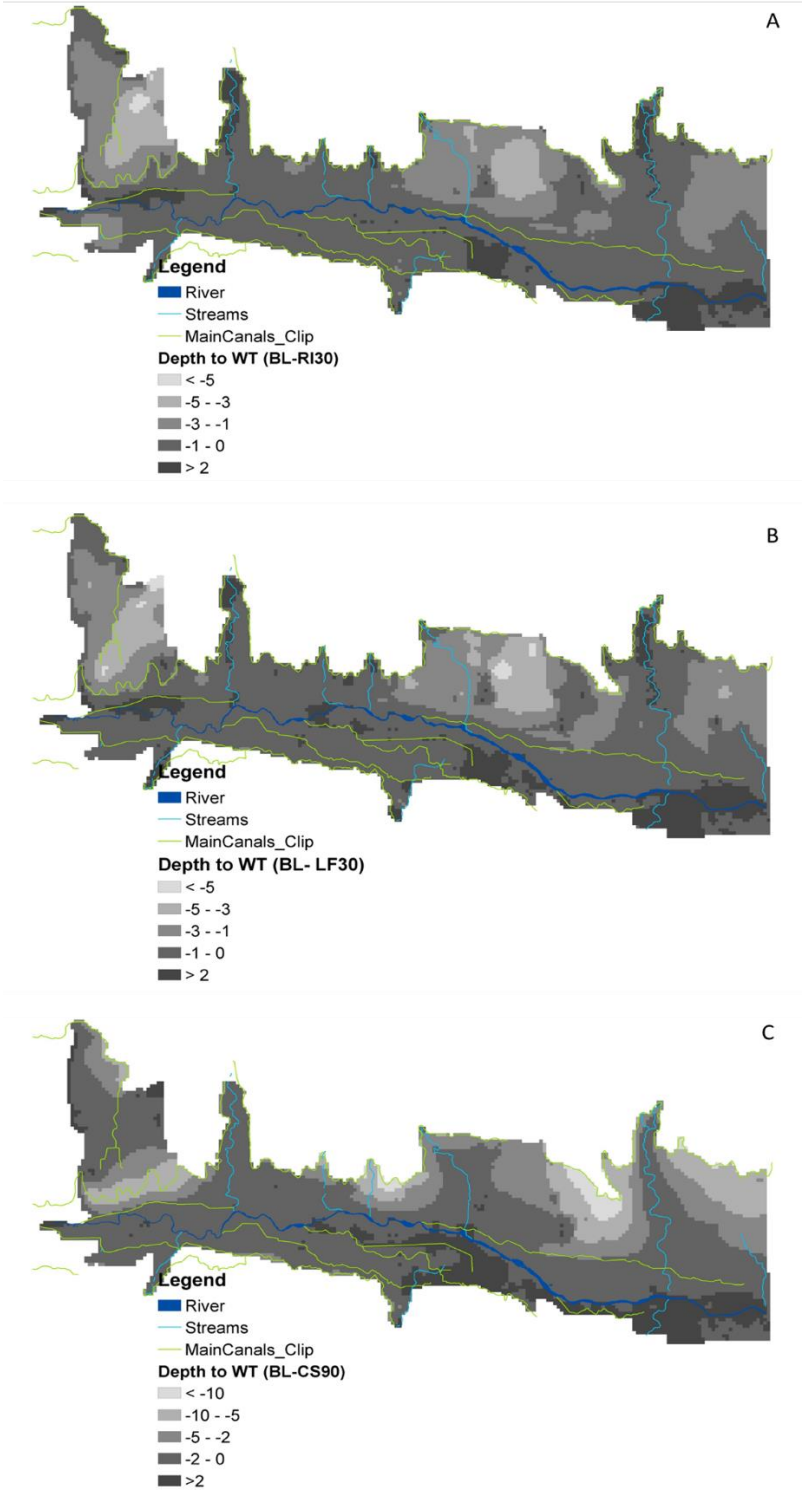

Figure 37: Difference depth to water table (A) RI 30, (B) LF 30, and (C) CS 90

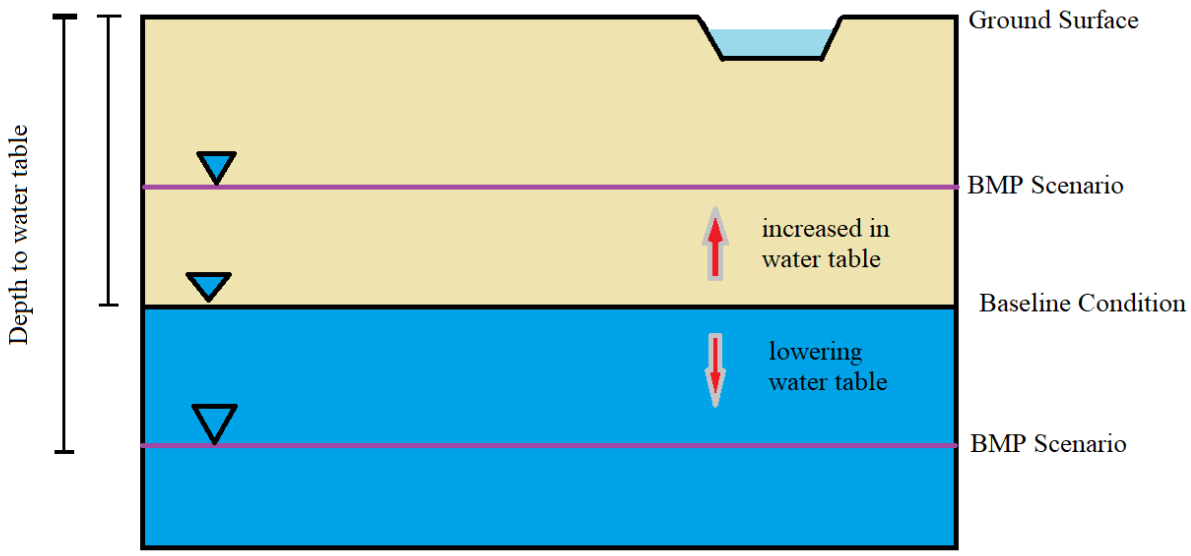

Figure 38: Comparison water table between the baseline and BMPs implementation

Figure 39 Groundwater concentration reduction for NO_3 over the 40-years simulation (A) reduced irrigation, (B) lease fallowing, and (C) canal sealing compared with the baseline condition

For NO_3 concentration, the results show in Figure (39) that the groundwater concentration has increased with the reduced irrigation and lease fallowing strategies by 7% and 11%, respectively, under the aggressive conditions. It had also shown that the groundwater concentration has been reduced by 20% and 15%, respectively, under the aggressive scenario. The values would have increased due to the lowering the water table. Once the irrigation is reduced, so would the leaching of Se and DO that react with NO_3, leading to increases of the concentration under these strategies. However, the canal sealing strategy represents a reduction of 40% in the concentration over the long simulation period. This is due to the isolating of the canals to prevent interaction with all marine shale in that area.

4.3.2 Groundwater Mass Loading of Se and N to the Arkansas River

The reduction of Se and NO_3 mass loading to the Arkansas River for groundwater has been estimated for the 40-years simulation for all 9 BMPs. The results are represented in Figure (40) for Se and Figure (41) NO_3. For Se, its shows that it is mainly the mass load that has been reduced for the RI and LF scenarios, with an exception for some years that might a drought year, which increased by 10%. The maximum reduction percentage under the aggressive condition reached 100% for RI and 100% for the LF strategies, where the average mass loading to the Arkansas River is 9% for the RI and 8% for the LF. For the CS strategy, the results show high reduction along the 40 years period and its reaches 100% under the aggressive scenario, where the average is 24%. On the other hand, the NO_3 results show a 90% reduction mainly in the RI, where the average is 7%. However, the LF shows high fluctuation between the reduction and the increases in the total mass loading, with reductions reaching 60% and increasing to 22%, with an average of 2%. Finally, for the CS, the reduction reached 60% under the aggressive scenario, where the average is 11%. These results of Se and NO_3 were shown to occur due to the total

return flow to the river that has less concentration in the surface water. In addition, both the concentrations and mass loading results have some high fluctuation, which is due either to the assumption of the taking off the riparian zone that occurred mostly in the denitrification and the heterophonic on it. Otherwise, this could have occurred due to the canal sealing, especially at the Buffalo canal, with the groundwater leaching to the stream.

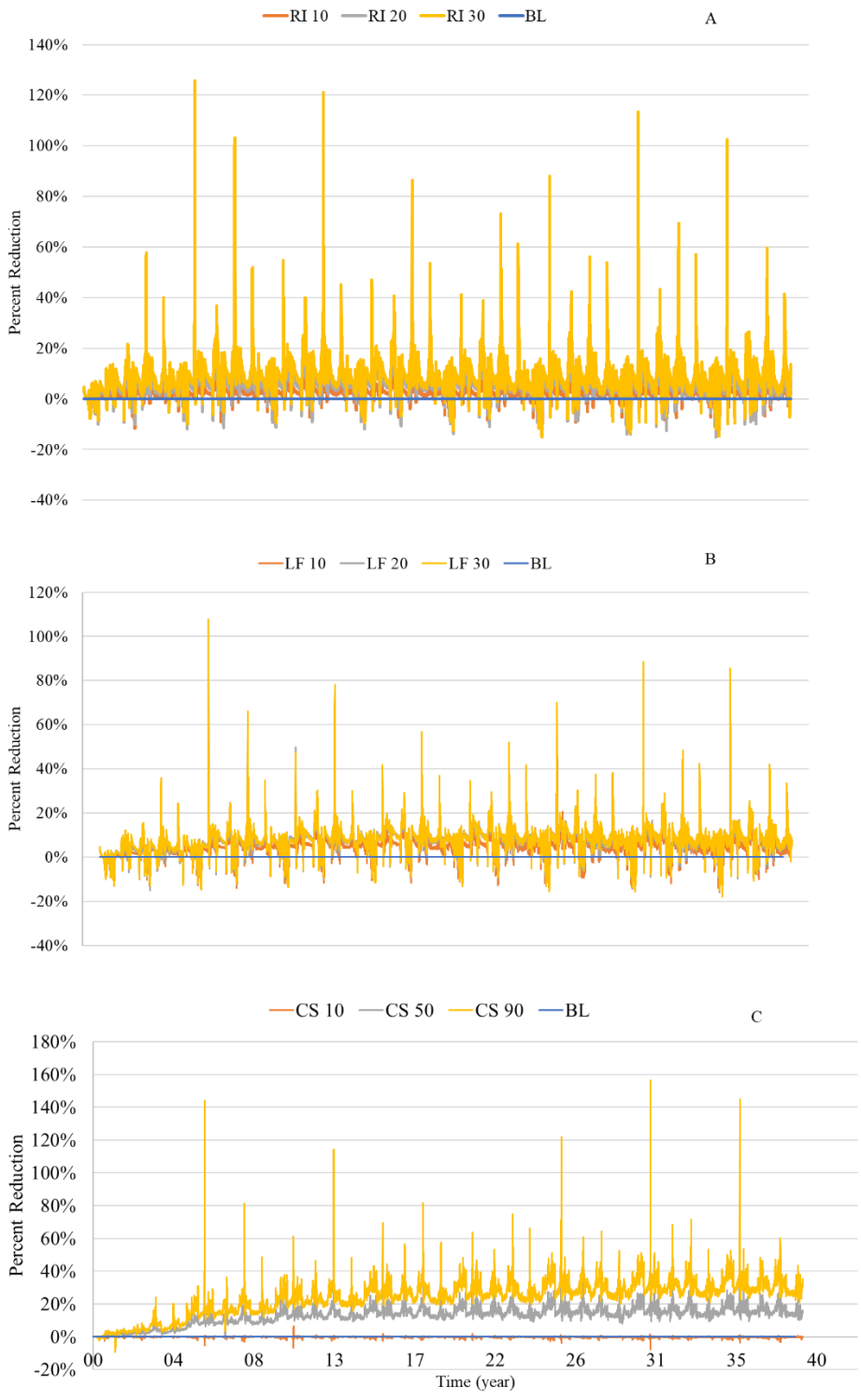

Figure 40 Mass loading reduction for Se over the 40-years simulation (A) reduced irrigation, (B) lease fallowing, and (C) canal sealing compared with baseline condition

Figure 41 Mass loading reduction for NO_3 over the 40-years simulation - (A) reduced irrigation, (B) lease fallowing, and (C) canal sealing compared with baseline condition.

Moreover, the groundwater concentrations, return flow, and total mass loading to the river of Se and NO_3 were tested against the baseline condition by applying the 9 BMPs over the last 5-years of the simulation, and by taking the average difference of the last 5 years of the simulation. The results are shown in Figure (42) for Se, and Figure (43) for NO_3. Also, the results show a high reduction of Se in all 9 BMPs under all conditions: basic, intermediate, and aggressive. This is due to the volume return flow that is shown in the Figure (32) which has a high impact at reducing the concentration. It is likely that the NO_3 was reduced in all BMPs scenarios under the basic, intermediate, and aggressive scenarios due to the return flow.

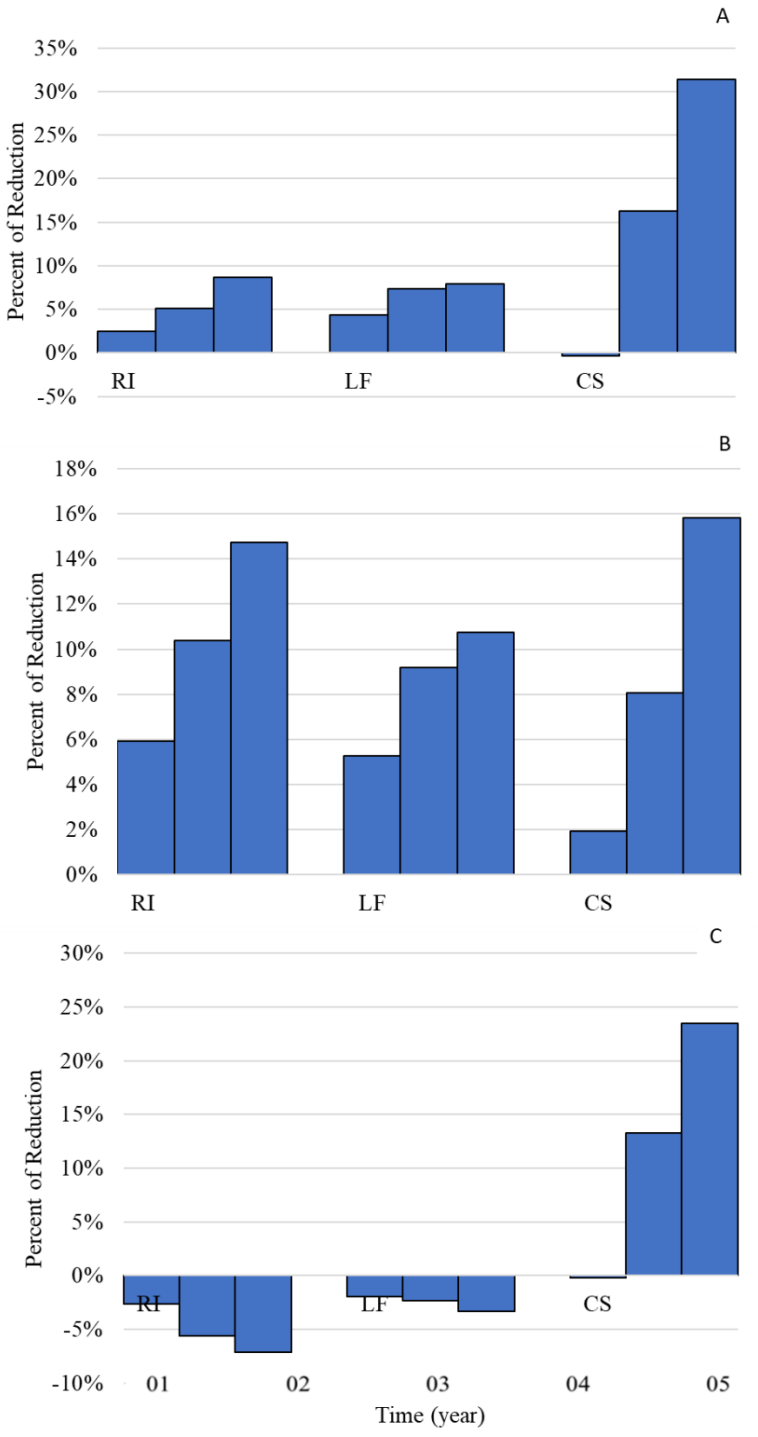

Figure 42 Average Se simulated (A) mass loading, (B) return flow, and (C) groundwater concentration over the last 5 years compared with the baseline

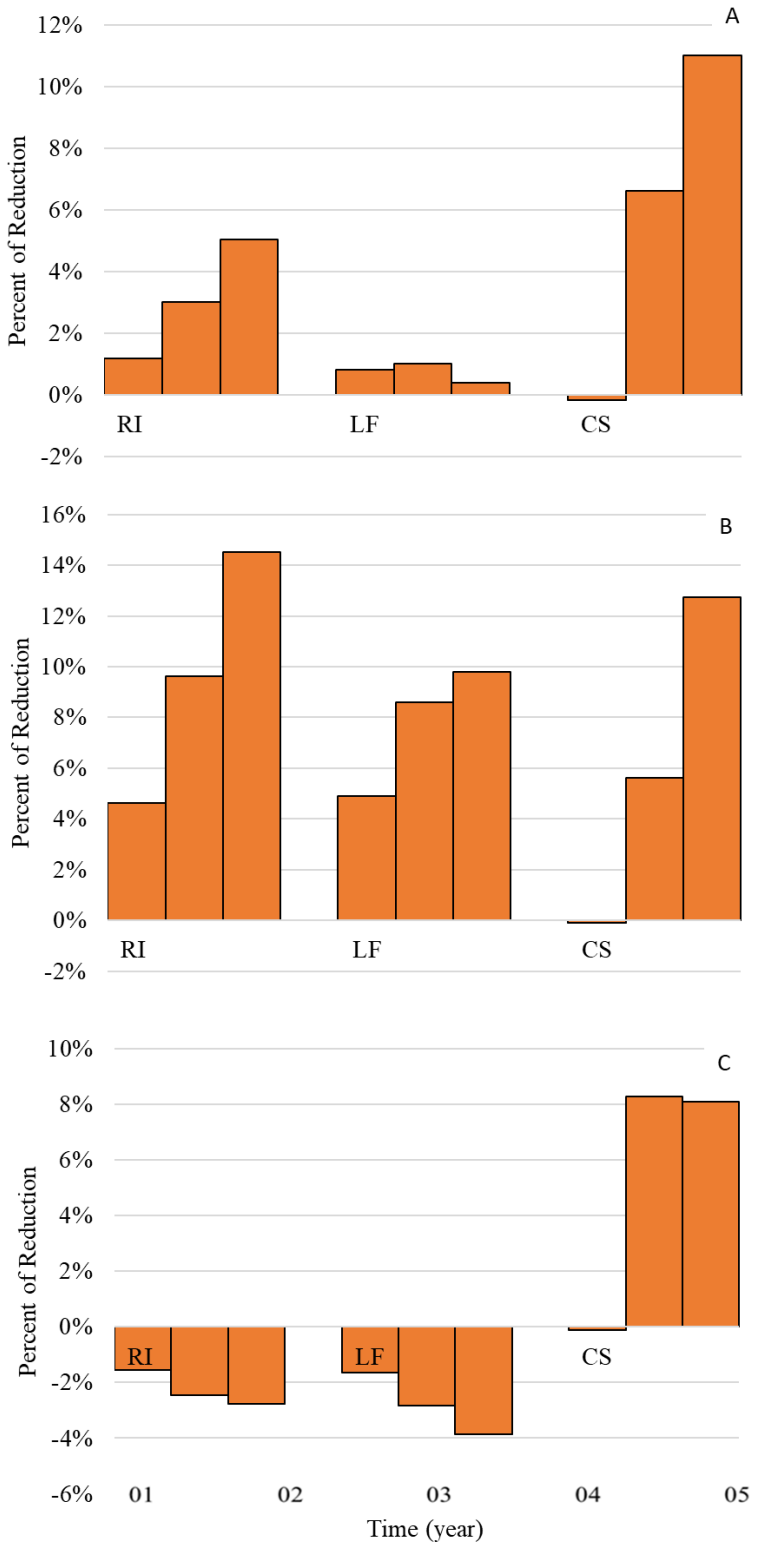

Figure 43 Average NO_3 simulated (A) mass loading, (B) return flow, and (C) groundwater concentration over the last 5 years compared with the baseline

Finally, the implementations of the BMPs were applied into the 15 sub-regions that were discussed in section 3.8 for the Se and NO_3, in order to figure out how the BMPs affect the groundwater concentrations in each sub-region over the 40-years simulation period. The result was obtained by taking the average groundwater concentrations of each sub-region of the 40 years of the simulation. Figure (44) showed the groundwater concentration in each sub-region for each species, and it is showed that in some regions the reduction goes up to 48% for Se and 38% for the NO_3. However, it showed a significant increase in some regions, going up to 25% and 41%, respectively. Figure (44.A) showed, under the aggressive CS scenario, that the concentration of Se had been reduced in most of the sub-regions and that was done mainly by isolating the irrigated canals from interacting with the marine shale that in the stream. However, the concentration of Se increased at the sub-regions 8, 11, and 14 under all the 9 MBPs scenarios. This might occur because of the delineation of the water table led to reduced irrigation being applied and that lead to oxidized with DO and NO_3. Another reason was that at sub-region 8, the groundwater was leaching to the irrigated canals (Buffalo canal), instead of leaching to the groundwater. Moreover, these four sub regions are affected directly by the shale layer that in the unsaturated zone as seen the Figure (45). On the other hand, Figure (44.B) showed that at all the 15 sub-regions, and under the aggressive CS scenario, the NO_3 groundwater concentration has been reduced by a maximum of 38%. However, under RI and LF, the concentrations mainly increased in most of the sub-regions, especially in sub region number 8, reaching 41%, and was due the same reason of the Se.

The results show that under the CS scenario the concentrations of both Se and NO_3 decreased in the study region. Also, the RI and LF was useful in some periods of the simulation before it increased. So, based into this analysis targeting BMPs in some of the regions instead of

applying BMPs for the entire study region is one of the future work that will focus on it. Finally, these BMPs could be applied in regions that had similar conditions.

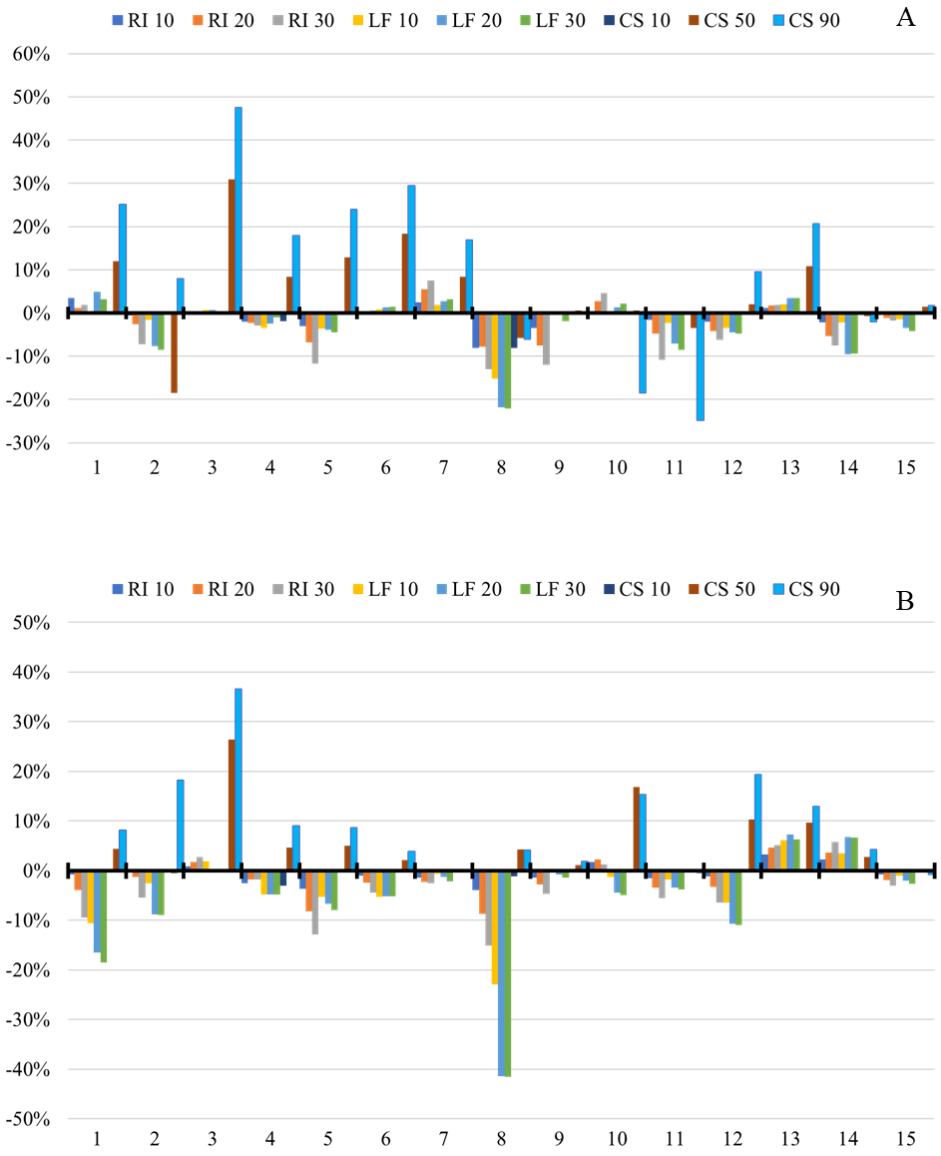

Figure 44 Groundwater concentration averaged over the simulation period within each sub-region (A) Se and (B) NO_3

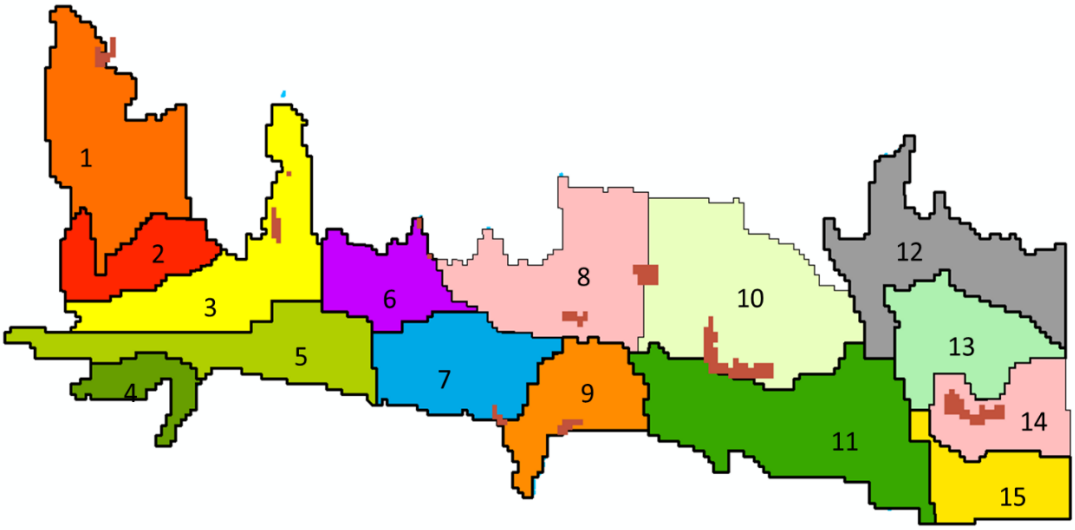

Figure 45: Shale location at each sub region

4.3.3 Streams Se and N

The reduction of Se and NO_3-N concentrations along the Arkansas River has been measured for the 40-years simulation for all 9 BMPs. The results are represented in Figure (46) for Se and Figure (47) NO_3. Thus, for Se, its shows that it is mainly the stream concentration has increased in some regions for the RI and LF scenarios, with an exception for some regions, which decrease by 25% under the RI and 15 % LF. This increase is mainly due to the high groundwater concentration that represented in Figures (42,43) which has impact to the return flow. Moreover, the RI and LF BMPs impact the river by increasing the concentrations that return to the stream from the groundwater which result a net increase in the stream concentrations. For the CS strategy, the results show significant decrease along the 40 years period and its reaches 30% under the aggressive scenario, and this is the most effective strategy. On the other hand, the NO_3-N results show a 30% increase in both RI and LF, and mainly this increases due to the low groundwater return flow concentration. Furthermore, the groundwater return flow concentration of NO_3 is lower than the stream concentration that leads to dilute the stream water. Thus, once the return flow reduced under the RI and LF the and less stream

dilution, higher concentration in the stream will occur. Finally, for the CS, the reduction reached 40% under the aggressive scenario. These results of Se and NO_3 were shown that the CS scenario is the most effective strategy to reduce the surface water concentration.

In addition, Figure (48) shows the last 5 years of the simulation for all water management BMPs and that compared with the CHPDE standard for both Se and NO_3. For Se, Figure (48.A) shows that the average daily 85^{th} percentile of the simulated data and it is impossible to reduce the stream concentration under the CHPDE standard which is 4.6 µg/L, however, its shows that under the CS the concentration reduced by around 66% from the baseline condition. On the other hand, Figure (48.B) shows the NO_3-N stream concentration over the last 5 years, it is shows that under the CS scenario the concentration has been reduce under the CHPDE standard which is 2 mg/L. That conclude the CS is the most effective BMP for the surface water.

Figure 46 Stream concertation for Se over the last 5 years (A) RI, (B) LF, and (C) CS.

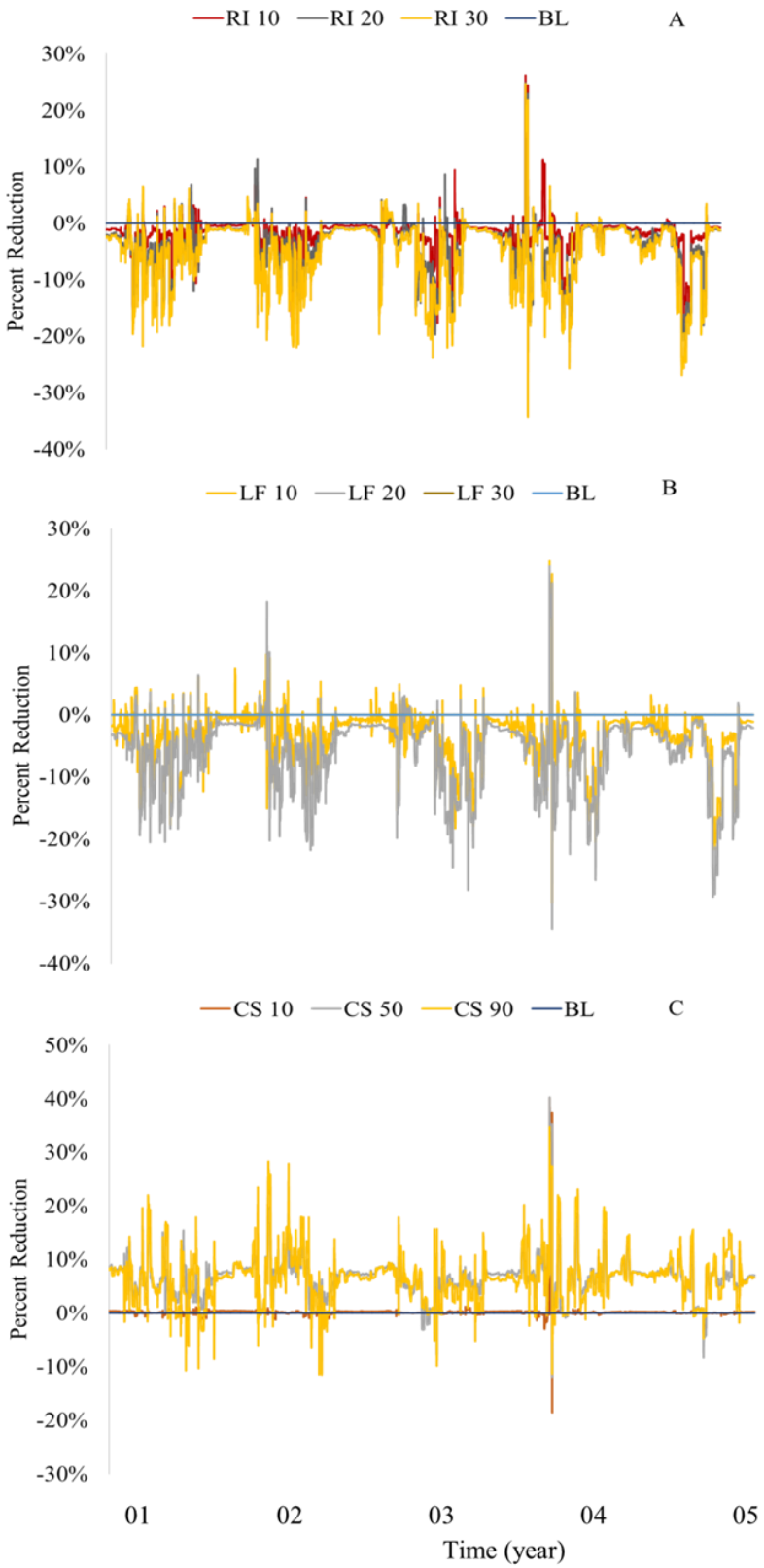

Figure 47 Stream concertation for NO_3 over the last 5 years (A) RI, (B) LF, and (C) CS.

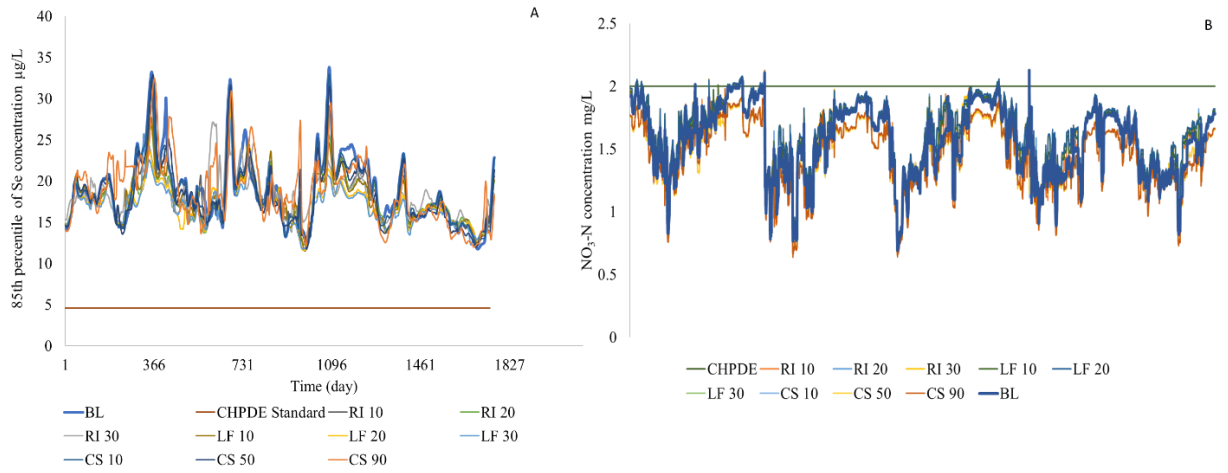

Figure 48 All BMPs comparison with the baseline and the CHPDE standard (A) 85th percentile of Se and (B) NO_3-N

4.3.4 Comparison Between the Downstream and Upstream Study Regions

A comparison between the DSR and the USR was made to see how the models and the BMPs implementations are similar or different in term of reduced to contamination of Se and NO3 in the groundwater and along the Arkansas River. Shultz (2017) implemented the water and land management BMPs and the combination of water management BMPs and land management in the USR under three level of the implementation: basic, intermediate, and aggressive. However, due to the limitation of time only water management BMPs have been applied in the DSR in this thesis. The results of implementing single water management BMPs for the USR are mostly the same that have been applied for the DSR. Both RI and LF have a negative impact in the groundwater concentrations that lead to increase in the Se and NO3 concentrations. Moreover, the Se concentration under RI and LF has been increased in the USR maximum by 13% and 16%, respectively. Similar Se increases at the DSR under the RI and LF with an increase of 15% and 10%, respectively. On the other hand, it is found that the best water management BMPs that lead to decrease the Se concentration in both USR and DSR was the canal sealing implementation with a maximum decrease of 18.3% in the USR and 40% in the

DSR. For the NO_3 concentration, it is found that CS is most effective water management strategy in the USR with a reduction of 11% and this is like the DSR with maximum reduction of 40%.

Furthermore, the implementation of the BMPs in the USR and DSR could not meet the Colorado chronic standard for Se concentration in the stream which 4.6 µg/L. However, CS implementation shows the most effective Se reduction in stream for both studies regions. On the other hand, the NO_3-N concentration in stream is below the Colorado Interim Standard for total N concentration which is 2 mg/L, and the concentration below the standard for the NO3-N only without including other N species.

In conclusion, the USR and DSR show a similar result of the implementation of water management BMPs. It is also illustrated that the models that applied in both region are capable to use for such a region that have similar condition. Moreover, there are some differences in the concentration of Se and NO_3, at the DSR it is always shows higher concentration than the USR. This is due to the shale marine layer that affects the DSR which keep producing high concentrations as going the downstream and these concentrations are kept getting the load from the Arkansas River as moving to the downstream.

CHAPTER 5: CONCLUSION AND FUTURE WORK

Irrigation and agriculture are one of the important sources of the sustainable food chain. This is especially the case in the future, when the increasing world population is expected to reach 9.7 billion people by 2050. Food and water sustainability are the main concerns for humans and livestock. Since the extensive irrigation practices at the LARV have lasted 100 years, serious issues occur which is declining crop land, high water table, waterlogging, saline soil, and high concentrations of Se and NO_3. High concentrations of Se and NO_3 lead to water quality issue, human health problems, and death and deformation for both fish and waterfowls. The area was studied and monitored by the Colorado State University over the last decade in order to investigate best strategies to sustain the food chain and to reduce the groundwater contaminations.

In this thesis, groundwater modeling techniques to simulate the fate and transport of Selenium and Nitrogen species in the stream-aquifer system of the Downstream Study Region of the Lower Arkansas River Valley between the town of Lamar, CO and the Colorado-Kansas state line, with the final goal of assessing the effectiveness of various best management practices on mitigating Se and N contamination in the aquifer and the Arkansas River. In addition, NO_3 occur due to the applied Fertilizer to the cropland to achieve high yields, that can lead to polluted groundwater sources, then can be transported to surface water. Where, Se is found mainly in the geological area, it occurs by oxidative weathering of pyrite in bedrock and outcrop shale areas.

The MODFLOW and RT3D-OTIS models were applied to simulate the groundwater flow and the solute transport in the study area. The SFR2 package has been added to the MODFLOW in order to simulate the interaction between the groundwater and surface water.

The RT3D model was coupled with OTIS and QUAL2E to simulate Se and N chemical transport in the Arkansas River network. Both MODFLOW and RT3D were calibrated manually and automatically against observation data (groundwater head, streamflow, groundwater concentration of Se and NO_3, surface water concentration of Se and NO_3). PEST was used to calibrate the species parameter for Se and NO_3 to match the groundwater and surface water model with the observation data. The calibrated model used to investigate the water management BMPs in the DSR at the LARV.

The 40 years calibrated model was used as a baseline in order to draw a comparison with the applied BMPs. The multi-decadal simulation applied in order to investigate the accurate impact of the mass loading that return to the Arkansas River, since the groundwater movement is too slow. So, several water management BMPs were applied in the study region. This included reduced irrigation (RI), lease fallowing (LF), and canal sealing (CS), under three different scenarios basic, intermediate, and aggressive. These implementations were applied in the calibrated model in order to figure out how the model will act with the BMPs in future.

The results show that the canal sealing strategy had the most effective results at reducing the amount of Se and NO_3 in the DSR. The maximum reduction of Se and NO_3 was 40% and 38%, respectively. Moreover, the mass loading to the Arkansas River has been reduced under the CS by 100% for Se, and 60% for NO_3. In contrast, the RI and LF application showed an increase in Se and NO_3 rates, which could be due to return flow decrease. Also, the concentrations of Se and NO_3 are entering the aquifer by the irrigated water and from the ET or the upflux that allow leaching Se and NO_3 to the crop root zone. In addition, the lowering of the water table reduces upflux from the saturated zone, thereby preventing movement of Se and NO3 mass into the soil profile. Furthermore, the LF applied at the area showed that the irrigation is removed from the

fallowed land and the ET is reformed to represent the absence of the crop demand. Finally, the results show the effect of implementing BMPs into each groundwater sub-region, assisting in identifying sub-regions that could be targeted for localized BMP implementation.

In conclusion, the results show that it was not possible to reduce the concentration of Se in streams to go below the Colorado State standard, which is 4.6 µg/L. However, the work was done by a calibrated the model against the observation data and it also suggests some strategies that can reduce the contaminations of Se and NO_3. For future work, there are some recommendations that could give a better understanding for the study area. These are:

1. Study the area that is outside the domain of the DSR region, in order to investigate the effect of the geology outside the domain and see how it interacts with Se and NO_3 in the study region. That also means extending the domain, so it will include the area from the John Martin Reservoir, instead of starting from the City of Lamar.
2. Implement land management BMPs, such as reduced fertilizer and enhance riparian buffer zone.
3. Consider a combined water BMPs and combined land and water BMPs that could affect a reduction of the contamination of Se and NO_3.
4. Apply the same strategies for the uranium and salt minerals to understand the extent of contamination relation and improve the water quality.

REFERENCES

Afzal, S., Younas, M., & Ali, K. (2000). Selenium Speciation Studies from Soan-Sakesar Valley, Salt Range, Pakistan. *Water International*, *25*(3), 425–436. https://doi.org/10.1080/02508060008686850

Alemi, M. H., Goldhamer, D. A., & Nielsen, D. R. (1988). Selenate transport in steady-state, water-saturated soil columns. *Journal of Environment Quality*, *17*(4), 608. Retrieved from https://www.agronomy.org/publications/jeq/abstracts/17/4/JEQ0170040608

Alemi, M. H., Goldhamer, D. A., & Nielsen, D. R. (1991). Modeling selenium transport in steady-state, unsaturated soil columns. *J Environ Qual*, *20*(1), 89–95. https://doi.org/10.2134/jeq1991.00472425002000010014x

Alfthan, G., Wang, D., Aro, A., & Soveri, J. (1995). The geochemistry of selenium in groundwaters in Finland. *Science of the Total Environment*, *162*(2–3), 93–103. https://doi.org/10.1016/0048-9697(95)04436-5

Allen, A., & Chapman, D. (2001). Impacts of afforestation on groundwater resources and quality. *Hydrogeology Journal*, *9*(4), 390–400. https://doi.org/10.1007/s100400100148

Bailey, R. T., Gates, T. K., & Ahmadi, M. (2014). Simulating reactive transport of selenium coupled with nitrogen in a regional-scale irrigated groundwater system. *Journal of Hydrology*, *515*, 29–46. https://doi.org/10.1016/j.jhydrol.2014.04.039

Bailey, R. T., Gates, T. K., & Halvorson, A. D. (2013). Simulating variably-saturated reactive transport of selenium and nitrogen in agricultural groundwater systems. *Journal of*

Contaminant Hydrology, *149*, 27–45. https://doi.org/10.1016/j.jconhyd.2013.03.001

Bailey, R. T., Gates, T. K., & Romero, E. C. (2015). Assessing the effectiveness of land and water management practices on nonpoint source nitrate levels in an alluvial stream-aquifer system. *Journal of Contaminant Hydrology*, *179*(3), 102–115. https://doi.org/10.1016/j.jconhyd.2015.05.009

Bailey, R. T., Hunter, W. J., & Gates, T. K. (2012). The Influence of Nitrate on Selenium in Irrigated Agricultural Groundwater Systems. *Journal of Environment Quality*, *41*(3), 783. https://doi.org/10.2134/jeq2011.0311

Bailey, R. T., Morway, E. D., Niswonger, R. G., & Gates, T. K. (2013). Modeling variably saturated multispecies reactive groundwater solute transport with MODFLOW-UZF and RT3D. *Groundwater*, *51*(5), 752–761. https://doi.org/10.1111/j.1745-6584.2012.01009.x

Bailey, R. T., Romero, E. C., & Gates, T. K. (2015). Assessing best management practices for remediation of selenium loading in groundwater to streams in an irrigated region. *Journal of Hydrology*, *521*, 341–359. https://doi.org/10.1016/j.jhydrol.2014.11.079

Bern, C. R., & Stogner, R. W. (2017). The Niobrara Formation as a challenge to water quality in the Arkansas River, Colorado, USA. *Journal of Hydrology: Regional Studies*, *12*(April), 181–195. https://doi.org/10.1016/j.ejrh.2017.05.001

Boon, D. Y. (1989). Potential selenium problems in Great Plains soils. *Symp. Selenium in Agriculture and the Environment, SSSA Speci*(Madison, Wisconsin, USA), 107–121.

Brätter, P., Negretti De Brätter, V. E., Recknagel, S., & Brunetto, R. (1997). Maternal selenium status influences the concentration and binding pattern of zinc in human milk. *Journal of*

Trace Elements in Medicine and Biology, *11*(4), 203–209. https://doi.org/10.1016/S0946-672X(97)80014-4

Brunner, P., & Simmons Craig. (2011). HydroGeoSphere: A Fully Integrated, Physically Based Hydrological Model. *Groundwater*, *50*(2), 170–176. https://doi.org/10.1111/j.1745-6584.2011.00882.x

Bye, R., & Lund, W. (1982). Determination of selenium in pyrite by the atomic absorption-hydride generation technique. *Fresenius' Zeitschrift Für Analytische Chemie*, *313*(3), 211–212. https://doi.org/10.1007/BF00488858

Calder, I. R., Reid, I., Nisbet, T. R., & Green, J. C. (2003). Impact of lowland forests in England on water resources: Application of the Hydrological Land Use Change (HYLUC) model. *Water Resources Research*, *39*(11), 1–10. https://doi.org/10.1029/2003WR002042

Chen, J. (2012). An original discovery: Selenium deficiency and Keshan disease (an endemic heart disease). *Asia Pacific Journal of Clinical Nutrition*, *21*(3), 320–326.

Clement, T. P. (1997). Rt3D, 1–59.

Colaizzi. (2009). Irrigation in the Texas High Plains: a brief history and potential reductions in demand. *Irrigation and Drainage*, *58*(3), 257–274. https://doi.org/10.1002/ird.418

Darton. (1906). Geology and underground waters, *52*(52).

De Pascale, S., & Barbieri, G. (1995). Effects of soil salinity from long-term irrigation with saline-sodic water on yield and quality of winter vegetable crops. *Scientia Horticulturae*, *64*(3), 145–157. https://doi.org/10.1016/0304-4238(95)00823-3

Dhillon, K. S., & Dhillon, S. K. (2003). Quality of underground water and its contribution towards selenium enrichment of the soil-plant system for a seleniferous region of northwest India. *Journal of Hydrology*, *272*(1–4), 120–130. https://doi.org/10.1016/S0022-1694(02)00259-7

Dinnes, D. L., Karlen, D. L., Jaynes, D. B., Kaspar, T. C., Hatfield, J. L., Colvin, T. S., & Cambardella, C. A. (2002). Nitrogen Management Strategies to Reduce Nitrate Leaching in Tile-Drained Midwestern Soils. *Agronomy Journal*, *94*, 153–171. https://doi.org/10.2134/agronj2002.1530

Dougherty, T. C., Hall, A. W., & Food and Agriculture Organization of the United Nations. (1995). *Environmental impact assessment of irrigation and drainage projects*. Food and Agriculture Organization of the United Nations. Retrieved from http://www.fao.org/docrep/V8350E/V8350E00.htm

Elrashidi, M. A., West, L. T., Seybold, C. A., Wysocki, D. A., Benham, E., Ferguson, R., & Peaslee, S. D. (2009). Nonpoint source of nitrogen contamination from land management practices in lost river basin, west Virginia. *Soil Science*, *174*(3), 180–192. https://doi.org/10.1097/SSL.0b013e31819869b8

Fan, A. M., & Steinberg, V. E. (1996). Health implications of nitrate and nitrite in drinking water: An update on methemoglobinemia occurrence and reproductive and developmental toxicity. *Regulatory Toxicology and Pharmacology*, *23*(1 I), 35–43. https://doi.org/10.1006/rtph.1996.0006

Feltz, H., Engberg, R., & Sylvester, M. (1990). Investigations of water quality, bottom sediment, and biota associated with irrigation drainage in the western United States. *... Symposium on*

the Hydrologic Basis for Water …, (197), 119–130. Retrieved from http://scholar.google.com/scholar?hl=en&btnG=Search&q=intitle:Investigations+of+water+quality+,+bottom+sediment+,+and+biota+associated+with+irrigation+drainage+in+the+western+United+States#0

Fernández-Martínez, A., & Charlet, L. (2009). Selenium environmental cycling and bioavailability: A structural chemist point of view. *Reviews in Environmental Science and Biotechnology*, *8*(1), 81–110. https://doi.org/10.1007/s11157-009-9145-3

Gates, B. T. K., Garcia, L. a, Hemphill, R. a, Morway, E. D., & Elhaddad, A. (2008). Irrigation Practices , Water Consumption , & Return Flows in Colorado ' s Lower Arkansas River Valley Final Report of Field and Model Investigations. *Water*, (000), 0–119.

Gates, T. K., Cody, B. M., Donnelly, J. P., Herting, A. W., Bailey, R. T., & Mueller Price, J. (2009). Assessing Selenium Contamination in the Irrigated Stream–Aquifer System of the Arkansas River, Colorado. *Journal of Environment Quality*, *38*(6), 2344. https://doi.org/10.2134/jeq2008.0499

Gates, T. K., Garcia, L. A., & Labadie, J. W. (2006). Toward Optimal Water Management in Colorado's Lower Arkansas River Valley: Monitoring and Modeling to Enhance Agriculture and Environment Colorado Agricultural Experiment Station. Retrieved from http://www.csuarkriver.colostate.edu/OptimalWaterManagementLowerArkansasRiverValley.pdf

Hamilton, S. J. (2004). Review of selenium toxicity in the aquatic food chain. *Science of the Total Environment*, *326*(1–3), 1–31. https://doi.org/10.1016/j.scitotenv.2004.01.019

Hamilton, S. J., & Weston, L. K. (2005). Selenium impactson razorback sucker , Colorado River , Colorado I . Adults.

Hill, A. R. (1996). Nitrate Removal in Stream Riparian Zones. *Journal of Environment Quality*, *25*(4), 743. https://doi.org/10.2134/jeq1996.00472425002500040014x

Hoffman, G. J., Evans, R. G., Jensen, M. E., Martin, D. L., & Elliott, R. L. (n.d.). Design and Operation of Farm Irrigation Systems 2nd edition. Retrieved from http://irrigationtoolbox.com/IrrigationToolBox/Section 2 - Irrigation System Planning/ASABE DesignandOperationofFarmIrrigationSystems/Preface.pdf

Hudak, P. F. (2010). Archive of SID Nitrate , Arsenic and Selenium Concentrations in The Pecos Archive of SID, *4*(2), 229–236.

Jacobs, L. W., McNeal, J. M., & Balistrieri, L. S. (1989). Geochemistry and Occurrence of Selenium: An Overview, (23), 1–13. https://doi.org/10.2136/sssaspecpub23.c1

Johnson, Bonrud, Dosch, & et al. (1987). Fatal outcome of methemoglobinemia in an infant. *JAMA*, *257*(20), 2796–2797. https://doi.org/10.1001/jama.1987.03390200136029

Kramer, S. B., Reganold, J. P., Glover, J. D., Bohannan, B. J. M., & Mooney, H. A. (2006). Reduced nitrate leaching and enhanced denitrifier activity and efficiency in organically fertilized soils. *Proceedings of the National Academy of Sciences*, *103*(12), 4522–4527. https://doi.org/10.1073/pnas.0600359103

Kulp, T. R., & Pratt, L. M. (2004). Speciation and weathering of selenium in upper cretaceous chalk and shale from South Dakota and Wyoming, USA. *Geochimica et Cosmochimica Acta*, *68*(18), 3687–3701. https://doi.org/10.1016/J.GCA.2004.03.008

Kumar, A. R., & Riyazuddin, P. (2011). Speciation of selenium in groundwater: Seasonal variations and redox transformations. *Journal of Hazardous Materials*, *192*(1), 263–269. https://doi.org/10.1016/j.jhazmat.2011.05.013

Large, R. R., Halpin, J. A., Danyushevsky, L. V., Maslennikov, V. V., Bull, S. W., Long, J. A., … Calver, C. R. (2014). Trace element content of sedimentary pyrite as a new proxy for deep-time ocean–atmosphere evolution. *Earth and Planetary Science Letters*, *389*, 209–220. https://doi.org/10.1016/J.EPSL.2013.12.020

Levander, O. A., & Burk, R. F. (2006). Update of human dietary standards for selenium. In D. L. Hatfield, M. J. Berry, & V. N. Gladyshev (Eds.), *Selenium: Its Molecular Biology and Role in Human Health* (pp. 399–410). Boston, MA: Springer US. https://doi.org/10.1007/0-387-33827-6_35

Lin, Z.-Q., & Terry, N. (2003). Selenium Removal by Constructed Wetlands: Quantitative Importance of Biological Volatilization in the Treatment of Selenium-Laden Agricultural Drainage Water. *Environmental Science & Technology*, *37*(3), 606–615. https://doi.org/10.1021/es0260216

List of Counties and cities in Colorado. (2018).

Lorenzen, M. W. (1979). By, *3*(41 5).

Miller, L. D., Watts, K. R., Ortiz, R. F., & Ivahnenko, T. (2010). Occurrence and distribution of dissolved solids, selenium, and uranium in groundwater and surface water in the Arkansas river basin from the headwaters to Coolidge, Kansas, 1970 – 2009, 1–60.

Mizutani, T., & Kanaya, K. (2001). Map of Selenium Content in Soil in Japan, *47*(4), 407–413.

https://doi.org/10.1248/jhs.47.407

Morway, E. D., Gates, T. K., & Niswonger, R. G. (2013). Morway, E. D., Gates, T. K., & Niswonger, R. G. (2013). Appraising options to reduce shallow groundwater tables and enhance flow conditions over regional scales in an irrigated alluvial aquifer system. Journal of Hydrology, 495, 216–237. https://doi.org/1. *Journal of Hydrology*, *495*, 216–237. https://doi.org/10.1016/j.jhydrol.2013.04.047

Mueller, D. K., Hamilton, P. a, Helsel, D. R., Hitt, K. J., & Ruddy, B. C. (1995). Nutrients in Ground Water and Surface Water of the United States An Analysis of Data Through 1992 Water-Resources Investigations Report 95-4031. *USGS Report 95-4031*.

Musick, J. T., Pringle, F. B., Harman, W. L., & Stewart, B. A. (1990). Long-term irrigation trends. Texas High Plains. *Applied Engineering in Agriculture*, *6*(6), 717–724. https://doi.org/10.13031/2013.26454

Myers, T. (2013). Remediation scenarios for selenium contamination, Blackfoot watershed, southeast Idaho, USA. *Hydrogeology Journal*, *21*(3), 655–671. https://doi.org/10.1007/s10040-013-0953-8

Nash, J. E., & Sutcliffe, J. V. (1970). River flow forecasting through conceptual models part I — A discussion of principles. *Journal of Hydrology*, *10*(3), 282–290. https://doi.org/https://doi.org/10.1016/0022-1694(70)90255-6

Navarro-Alarcón, M., & López-Martínez, M. C. (2000). Essentiality of selenium in the human body: Relationship with different diseases. *Science of the Total Environment*, *249*(1–3), 347–371. https://doi.org/10.1016/S0048-9697(99)00526-4

Neitsch, S. L., Arnold, J. G., Kiniry, J. R., & Williams., J. R. (2005). Soil and Water Assessment Tool User's Manual Version 2005. *Diffuse Pollution Conference Dublin*, 494.

Nielsen, E., & Lee, L. (1987). The magnitude and costs of groundwater contamination from agricultural chemicals. *Econ. Res. Ser. A National Perspective,*. Retrieved from http://naldc.nal.usda.gov/download/CAT88907300/

Niswonger, R. G., Panday, S., & Motomu, I. (2011). MODFLOW-NWT , A Newton Formulation for MODFLOW-2005. *USGS Reports*, 44.

Niswonger, R. G., Prudic, D. E., & Regan, S. R. (2006). Documentation of the Unsaturated-Zone Flow (UZF1) Package for Modeling Unsaturated Flow Between the Land Surface and the Water Table with MODFLOW-2005. *U.S. Geological Survey Techniques and Methods*, 71.

Ohlendorf, H. M. (2002). The birds of Kesterson Reservoir: A historical perspective. *Aquatic Toxicology*, *57*(1–2), 1–10. https://doi.org/10.1016/S0166-445X(01)00266-1

Ohlendorf, H. M. (2011). *Wildlife Ecotoxicology* (Vol. 3). https://doi.org/10.1007/978-0-387-89432-4

Oremland, R. S., Steinberg, N. A., Maest, A. S., Miller, L. G., & Hollibaugh, J. T. (1990). Measurement of in Situ Rates of Selenate Removal by Dissimilatory Bacterial Reduction in Sediments. *Environmental Science and Technology*, *24*(8), 1157–1164. https://doi.org/10.1021/es00078a001

Presser, T. S., Sylvester, M. A., & Low, W. H. (1994). Bioaccumulation of selenium from natural geologic sources in western states and its potential consequences. *Environmental Management*, *18*(3), 423–436. https://doi.org/10.1007/BF02393871

R. C. SEVERSON, SCOTT E. FISHER, JAMES R. Herring, And L.P. GOUGH, E. (1992). Proceeding of the 1990 Billings Land Reclamation symposium on Selenium in Arid and Semiarid Environments, Western United States. *US Geological Survey Circular, Volumes 1064*, 146p. Retrieved from https://books.google.com/books?id=aQolAQAAIAAJ&pgis=1

Ranalli, A. J., & Macalady, D. L. (2010). The importance of the riparian zone and in-stream processes in nitrate attenuation in undisturbed and agricultural watersheds - A review of the scientific literature. *Journal of Hydrology*, *389*(3–4), 406–415. https://doi.org/10.1016/j.jhydrol.2010.05.045

Rosegrant, M. W., Cai, X., & Cline, S. (2002). *World Water and Food to 2025: Dealing with Scarcity*. *Food Policy*. https://doi.org/10.1098/rstb.2005.1744

Runkel, R. L., & Broshears, R. E. (1991). One-Dimensional Transport with Inflow and Storage (OTIS): A Solute Transport Model for Small Streams CENTER FOR ADVANCED DECISION SUPPORT FOR WATER AND ENVIRONMENTAL SYSTEMS Acknowledgments.

Seiler, R. L. (1995). Prediction of Areas Where Irrigation Drainage May Induce Selenium Contamination of Water. *Journal of Environmental Quality*, *24*(5), 973–979.

Seiler, R., Skorupa, J., & Peltz, L. (1999). Areas Susceptible to Irrigation-Induced Selenium Contamination of Water and Biota in the Western United States. *US Geological Survey*, *1180*. Retrieved from http://books.google.com/books?hl=en&lr=&id=If4kAQAAIAAJ&oi=fnd&pg=PA1&dq=Areas+Susceptible+to+Irrigation-Induced+Selenium+Contamination+of+Water+and+Biota+in+the+Western+United+States

&ots=-Oxwy84vEN&sig=NhLeiBBq5tbY9ehARdYk3M9dty4

Sharps, J. A. (1976). Geologic map of the Lamar quadrangle, Colorado and Kansas. Retrieved from https://ngmdb.usgs.gov/Prodesc/proddesc_9832.htm

Shultz. (2017). Submitted by.

Shultz, C. D., Bailey, R. T., Gates, T. K., Heesemann, B. E., & Morway, E. D. (2018). Simulating Selenium and Nitrogen Fate and Transport in Coupled Stream-Aquifer Systems of Irrigated Regions. *Journal of Hydrology*. https://doi.org/10.1016/j.jhydrol.2018.02.027

Sposito, G., Yang, A., Neal, R. H., & Mackzum, A. (1991). Selenate reduction in an alluvial soil. *Soil Science Society of America Journal*, *55*(6), 1597–1602. https://doi.org/10.2136/sssaj1991.03615995005500060016x

Stillings, L. L., & Amacher, M. C. (2010). Kinetics of selenium release in mine waste from the Meade Peak Phosphatic Shale, Phosphoria Formation, Wooley Valley, Idaho, USA. *Chemical Geology*, *269*(1–2), 113–123. https://doi.org/10.1016/j.chemgeo.2009.10.011

Tayfur, G., Tanji, K. K., & Baba, A. (2010). Two-dimensional finite elements model for selenium transport in saturated and unsaturated zones. *Environmental Monitoring and Assessment*, *169*(1–4), 509–518. https://doi.org/10.1007/s10661-009-1193-1

Tummalapenta, R. K. T. (2015). Investigating Best Management Practices To Reduce Selenium and Nitrate Contamination in a Regional Scale Irrigated Agricultural Groundwater System: Lower Arkansas River Valley, Southeastern Colorado.

UNESCO-WWAP. (2003). *Water for People Water for Life. The United Nations World Water Development Report. Water*. https://doi.org/10.1017/CBO9781107415324.004

Voss, C. I., & Provost, A. M. (2010). SUTRA: a model for saturated-unsaturated, variable-density ground-water flow with solute or energy transport. *Water-Resources Investigations Report 02-4231, 2010*, 300 p. Retrieved from http://scholar.google.com/scholar?hl=en&btnG=Search&q=intitle:SUTRA+A+Model+for+Saturated-Unsaturated,+Variable-Density+Ground-Water+Flow+with+Solute+or+Energy+Transport#2

Wright, W. G. (1999). Oxidation and Mobilization of Selenium by Nitrate in Irrigation Drainage. *Journal of Environmental Quality*, *28*(June 1998), 1182–1187. https://doi.org/10.2134/jeq1999.00472425002800040019x

Yamagata, K., Butts, M. B., Grooss, J., Clausen, T. H., Graham, D. N., Clausnitzer, V., … Monninkhoff, B. (2012). OpenMI coupling of FEFLOW and MIKE SHE. *Hwrs 2012*, 52–59.

Yang, R., & Wang, X. (2011). Effects of nitrogen fertilizer and irrigation rate on nitrate present in the profile of a sandy farmland in northwest China. *Procedia Environmental Sciences*, *11*(PART B), 726–732. https://doi.org/10.1016/j.proenv.2011.12.113

Zhang, H. H., Wu, Z. F., Yang, C. L., Xia, B., Xu, D. R., & Yuan, H. X. (2008). Spatial Distributions and Potential Risk Analysis of Total Soil Selenium in Guangdong Province, China All rights reserved. No part of this periodical may be reproduced or transmitted in any form or by any means, electronic or mechanical, including photoco. *Journal of Environmental Quality*, *37*, 780–787. https://doi.org/10.2134/jeq2007.0154